The geochemical composition of the Scioto River, Ohio: influence of urbanization and seasonal changes in agricultural inputs

Thesis

Presented in Partial Fulfillment of the Requirements for the Degree of Master of Science in the Graduate School of The Ohio State University

By

Connor Wichterich, B.S.

Graduate Program in Earth Sciences

The Ohio State University

2022

Thesis Committee:

Dr. W. Berry Lyons, Advisor

Dr. Nicholas Basta

Dr. Thomas Darrah

Dr. Susan Welch

ABSTRACT

Despite efforts to mitigate and reduce contamination of surface water resources, water quality remains impaired in many places worldwide. Primary causes of pollution are nonpoint source pollutants, as point source pollution has been heavily regulated. Agriculture and urbanization are leading sources of impairment of surface water quality, as they both introduce excess sediment and nutrients, various types of chemicals, and more to surface waters. The Scioto River in the Upper Scioto River Basin in central Ohio was studied in order to assess the influence of large-scale agriculture and urbanization/suburbanization on river geochemistry. The Scioto River has its headwaters in land dominated by row-crop agriculture, then flows through the expanding metropolitan Columbus area. After flowing through the city, the Scioto River again flows through suburbs and agricultural land before exiting the Upper Scioto River Basin. Additionally, the river is dammed in two places, providing another means of assessing how modification of natural river systems impacts river geochemistry.

The Scioto River was sampled in five locations with varying degrees of surrounding agricultural and urban land use. Samples were collected weekly at three locations from February 2021 to August 2021, then monthly through December 2021. The other two locations were sampled monthly for the entire study period. The most upstream location was located in an area dominated by agriculture; the second location also in an area dominated by agriculture but at the beginning of the northernmost reservoir; the third location in a suburb northwest of Columbus and in the southernmost reservoir; the fourth in downtown Columbus; the fifth south of Columbus in an area influenced by both agriculture and urbanization. Samples were analyzed for major ions, nutrients, select trace elements, and stable water isotopes. Results revealed that concentrations of many analytes were highest at the most upstream location, decreased until downtown Columbus, and increased at the location furthest

downstream. The same trend was observed in discharge-weighted yields for the same analytes. Because much of the study area is underlain by carbonate bedrock, correlations with Ca and/or Mg were thought to indicate a primarily geogenic source of the solute. Elements with moderate to strong positive correlations with Ca and/or Mg included Na, HCO_3, Cl, SO_4 F, Br, Li, U, Ni, Rb, Mo, Ba, and Sr. Additionally, many of these elements had moderate to strong negative correlations with NO_3+NO_2, which is primarily from agricultural inputs.

Further, log C – log Q relationships of these data revealed chemostatic to weak dilution of analytes that positively correlated with Ca/Mg, suggesting a geogenic source of these elements that was weakly diluted with increasing discharge. In contrast, NO_3+NO_2 and Cu displayed slight mobilization behavior, indicated by positive log C – log Q slopes. Discharge-weighted yields of Cu and NO_3+NO_2 decreased from upstream agricultural sample locations until downtown Columbus, where yields of both increased before decreasing at the location furthest downstream. This suggests an urban input of NO_3+NO_2 in addition to agricultural input upstream, and an influx of Cu from metropolitan Columbus, potentially from impermeable surface runoff that collects contamination from vehicle wear, motor fluids, and vehicle emissions.

Lastly, the influences of extended water residence time and hydrologic modification from damming of the river was evident in these data. Correlations between elements were weakest at the suburban and urban sampling locations, those closest to the reservoirs, and log C – log Q relationships were closest to chemostatic at these locations for most analytes. The damming of rivers has been shown to promote uptake of dissolved Si by diatoms behind dams, leading to lower concentrations downstream of reservoirs. The lowest dissolved Si concentrations measured in this study were at both locations within reservoirs and in downtown Columbus, a few kilometers downstream of a reservoir. Releases of deep-water from the upstream reservoir also resulted in elevated NH_4 concentrations and

isotopically enriched water measured in the downstream reservoir, most evident in late summer into the fall when river flows were lowest.

These data reveal both urban and agricultural controls on the river's chemistry that vary due to hydroclimatic conditions and surrounding land use. Frequent sampling of the Scioto River during relatively higher flows allowed for a more nuanced understanding of sources of solutes to the river. Continued water quality monitoring is imperative to maintain and protect water quality resources, especially as urban populations are predicted to grow significantly in the next century.

ACKNOWLEDGMENTS

I would like to thank the Ohio State University Graduate School for funding in the form of a fellowship and the Friends of Orton Hall fund through the School of Earth Sciences for financial support for sample analysis and to attend conferences.

I would like to express my great gratitude and appreciation for my advisor, Dr. Berry Lyons, for guidance and constant support through my research journey. I would also like to thank members of my committee including Dr. Sue Welch, Dr. Tom Darrah, and Dr. Nick Basta for their assistance in evaluating and reviewing this work. Additionally, I thank Dr. Sue Welch, Dr. Chris Gardner, and Devin Smith for assistance with sample analysis and their willingness to examine and discuss data with me. I would like to thank Anthony Lutton of the Ohio State University Trace Element Research Lab for assistance with ICP-MS analyses. I would like to further thank Dr. Lyons and Devin Smith for their help in sample collection.

I thank all other faculty and staff in the School of Earth Sciences for their support in both classes and research. Likewise, I would like to thank my fellow graduate students in the School of Earth Sciences for their camaraderie during my graduate school experience. Last, I wish to express my utmost appreciation to my friends and family for their endless support and encouragement, without which none of this would have been possible.

VITA

2020 ..... B.S. Geology, Texas A&M University

2020 to Present..... University Fellow, Graduate Teaching Associate
The Ohio State University

Fields of Study

Major Field: Earth Sciences

TABLE OF CONTENTS

LIST OF TABLES

LIST OF FIGURES

1. INTRODUCTION

1.1 Rationale for Work

Riverine geochemistry is highly variable as it is influenced by both natural and anthropogenic processes and activities (Berner & Berner, 1987). Natural variability in solute chemistry is influenced by factors such as climate, watershed lithology, vegetation, and hydrological conditions. Anthropogenic contamination from agriculture and urbanization are two of the biggest threats to surface water quality, as they can introduce large volumes of sediment, excess nutrients, numerous types of chemicals, and other potential contaminants to receiving waters (Carpenter et al., 1998; Kaushal et al., 2005; Sañudo-Wilhelmy & Gill, 1999; Steuer et al., 1997). Despite efforts like the Clean Water Act meant to improve water quality, many surface waters are still impaired worldwide. In the U.S., this is largely due to nonpoint source pollution, as point source pollution has been heavily regulated and reduced since the 1970s (Carpenter et al., 1998; Sañudo-Wilhelmy & Gill, 1999). Poor surface water quality has implications for drinking water resources and ecosystem health. This water quality degradation has human health implications because of the reliance on surface water for human use. In 2015, 74% of water used in the U.S. was from surface water sources (Dieter et al., 2018). Of this, 10% was used for public supply or domestic use, and this percentage will increase as human populations and population densities grow. By 2050, 68% of the global population is projected to live in urban areas where water needs will be exacerbated (United Nations, 2018). In North America, 90% of the population is estimated to be urban by 2050. As population continues to grow, strain on surface water resources by withdrawal and anthropogenic pollution will be exasperated. The 2008-2009 National Rivers and Streams Assessment from the U.S. EPA found that 46% of U.S. rivers and streams are in poor biological condition, citing low pH, high salinity, excess sediments and nutrients as causes (U.S. EPA, 2017). The primary

causes of this pollution were pathogens, sediment, and excess nutrients, and the most common sources of these pollutants were agriculture, atmospheric deposition, and hydrologic modifications.

The Midwest is dominated by agricultural land use, and elevated levels of nitrate and phosphate are regularly found in surface waters due to fertilizer runoff (Carpenter et al., 1998; David et al., 1997; Pease et al., 2018; Royer et al., 2006; Stets et al., 2015). Excess levels of nitrate and phosphate can lead to algal blooms, eutrophication, and potentially hypoxia, as seen in Lake Erie and the reoccurring Gulf of Mexico dead zone (Burns et al., 2005; Michalak et al., 2013; U.S. EPA, 2011). In 2002, 65% of fixed nitrogen in the U.S. environment came from agricultural sources including fertilizer application and biological nitrogen fixation which has grown significantly as a result of the large-scale cultivation of nitrogen-fixing crops like soybeans and alfalfa (U.S. EPA, 2011). Overuse of fertilizer causes excess nutrients to run off during precipitation events, leach into groundwater, volatilize, or flow through subsurface tile drains (Byrnes et al., 2020; Davidson et al., 2012; Royer et al., 2006). Tile drainage prevents nutrient rich water from flowing through soil via natural recharge processes which aid in elemental removal. This results in shallow flow that is high in nutrients which is then discharged to surface waters (Blann et al., 2009; Macrae et al., 2007; Pease et al., 2018). Overland flow is an important contributor of both dissolved and particulate phosphorus to aquatic systems, while subsurface drainage mainly transports dissolved phosphorus (Van Esbroeck et al., 2016; Pease et al., 2018; Royer et al., 2006). Royer et al. (2006) showed that more than 80% of phosphorus and 50% of nitrate annual export from an agricultural watershed in Illinois occurred at greater than 90th percentile discharge. Although a large proportion of nitrate and total phosphorus are transported during high flow events, groundwater discharge is also a significant source of nitrate to surface waters, especially during baseflow conditions (Johnson & Stets, 2020). Legacy nitrate in groundwater is likely a significant contributor to sustained elevated nitrate concentrations in surface waters despite efforts to reduce nonpoint source nitrogen

pollution in the U.S. (Stets et al., 2015). Although agricultural “best” management practices like conservation tillage and cover crop rotation have been implemented to reduce nutrient pollution, surface water quality remains impaired in many areas (Stets et al., 2015).

While agriculture is a dominant source of surface water pollution, urban and suburban areas can also have profound effects on surface water quality, thus compounding pollution from agricultural activity. As with agriculture, nonpoint source pollution in urban and suburban areas is difficult to regulate and also perpetuates poor surface water quality despite mitigation efforts (Sañudo-Wilhelmy & Gill, 1999). Pollution from urban and suburban areas primarily enters surface waters from stormwater overflow, wastewater discharges, atmospheric deposition, interaction with legacy contaminants, and overland flow which is enhanced due to the high concentration of impervious surfaces. Impervious surfaces in urban areas cause “flashiness” of streams and rivers, elevated nutrient and contaminant concentrations, and a shift in aquatic biotic assemblages; these effects are termed the ‘urban stream syndrome’ (Meyer et al., 2005; C. J. Walsh et al., 2005). Heavy metals from automobile/tire wear and fossil fuel exhaust settle and concentrate on impervious surfaces and are later transported into receiving waters during precipitation events (Bannerman et al., 1993; Fitzpatrick et al., 2007; Sansalone & Buchberger, 1997). Vehicle wear, motor fluids, and emissions are primary or secondary sources of many trace metals found in runoff from impervious surfaces; these metals include (but are not limited to) Cd, Cu, Fe, Pb, Ni, V, Mo, and Zn (Huber et al., 2016; Kaushal et al., 2020; Sansalone & Buchberger, 1997). Application of road deicing salt has increasing salinization of fresh waters for decades, threatening drinking water resources and aquatic life (Hintz et al., 2022). Urban infrastructure dissolution contributes significant Ca, Mg, HCO_3, CO_3, and SO_4 to surface waters through runoff, and in some cases can overwhelm natural sources of these constituents (Connor et al., 2014; Kaushal et al., 2020). In addition to runoff from impervious surfaces, wastewater discharge is often enriched in nutrients, certain

major ions, and trace elements relative to receiving waters. Wastewater treatment plant effluent typically has high concentrations of NO_3, PO_4, NH_4, Ca, Mg, Na, K, Cl, SO_4, HCO_3, CO_3, As, Mo, Li, Rb, Ni, Cu, and Zn relative to natural waters (Kaushal et al., 2020; Meybeck, 1998; Sañudo-Wilhelmy & Gill, 1999).

The damming of river systems for water collection and flood control is a common feature of many rivers in the U.S. (Graf, 1999). Surface water reservoirs provide drinking water resources, flood control, and recreational services to the surrounding population, but are susceptible to anthropogenic pollution and climatic changes. The presence of reservoirs is shown to alter the chemical and physical characteristics of river systems (Chalise et al., 2021; Ferrazzi et al., 2021; Poff et al., 2007). Dams trap sediment, promoting sediment buildup behind them and disrupting sediment flow downstream (Vorosmarty et al., 1997). These sediments can act as important sinks for hydrophobic synthetic organic compounds as well as trace metals (Karbassi et al., 2011). Ferrazzi et al. (2020) analyzed discharge data above and below dams across the Central and Eastern U.S. in relation to the primary hydrologic function of the impoundment. They found that flood control dams dampened climatic signatures in downstream flow patterns, while urban water supply reservoirs nearly eliminated this relationship downstream of dams, completely regulating flow and homogenizing regional flow patterns. Extended residence times in reservoirs promotes the loss of dissolved nutrients through biological activity and/or sediment adsorption (Ittekkot et al., 2000; Jossette et al., 1999). This effect has implications for nutrient ratios (i.e. N:P:Si) further downstream, shifting algal species distribution (Admiraal et al., 1990; Humborg, 1997). Additionally, evaporative water loss from reservoirs can threaten water resources as temperatures increase globally and precipitation events become more erratic (Adeloye et al., 1999).

1.2 Research Objectives

The determination of water quality criteria is often based on samples collected infrequently, on a roughly monthly basis (Loftis & Ward, 1980; Vilmin et al., 2018). However, many analytes that affect water quality, like those introduced from agricultural and impervious surface runoff, can vary significantly on a short temporal scale due to weather conditions, variations in runoff, and biological activity (Bernard-Michel & de Fouquet, 2005; Loftis & Ward, 1980). The importance of collecting samples at high flows and on a more frequent basis has become apparent in order to better understand the biogeochemical dynamics in fluvial systems (Halliday et al., 2014). As discussed previously, overland flow, especially from agricultural fields and urban areas, is an important source of many pollutants found in surface waters. Sampling at higher flows and during, or soon after, storm events can better capture the chemistry of this runoff. Vilmin et al. (2018) showed that in order to capture the true behavior of highly variable elements and compounds, like those introduced in wastewater effluent, sampling should be done weekly or more frequently. Frequent and strategic sampling will aid in regulatory water quality monitoring and protection of surface water resources.

The goal of this study was to compare the role of agriculture, which makes up much of the land use in the headwaters and upper sections of the Scioto River, and urbanization/suburbanization, as the river flows through the growing metropolitan Columbus, Ohio area, on the biogeochemistry of the river. The Scioto River in the Upper Scioto River basin provides an ideal setting for this study, as much of the basin is dominated by agriculture, but there are significant urban and suburban areas that the river flows through as well. To achieve this, the Scioto River was sampled weekly to monthly at five locations that vary in agricultural-urban influence. Through the text, when referring to the Scioto River, this indicates only the portion of the river in the Upper Scioto River Basin (39.61^{o}N-40.80^{o}N).

As discussed previously, agriculture and urbanization pose threats to surface water quality worldwide. Studying the anthropogenic influence on a river in conjunction with natural hydroclimatic changes in the river's chemistry is important in protecting and managing water resources in the future. Additionally, the Scioto River is dammed in two places in the study area to form reservoirs used primarily for urban water supply. Effects of land use, hydrologic modifications, and weather conditions will be compared through the analysis of major cations and anions, nutrients, select trace metals, and stable water isotopes.

1.3 Study Area

Ohio, like much of the Eastern Corn Belt in the midwestern U.S., is dominated by row-crop agriculture, with agriculture/pastureland making up 49% of land cover in the state (MRLC, 2019). Soybeans and corn are the primary crops grown in Ohio. Developed (urban/suburban) areas make up about 15% of land in Ohio, while 32% of the state is forested (Figure 1) (MRLC, 2019). Roughly 87% of all water used in Ohio (water-use categories include public supply, domestic, irrigation, livestock, aquaculture, industrial, mining, and thermoelectric (Dieter et al., 2018) comes from surface water resources, and 15% of surface water withdrawn is for public supply and domestic uses (Dieter et al., 2018). The Upper Scioto River Basin is located in Central Ohio, with its headwaters near Roundhead (40.560, -83.835) and its southernmost point near Circleville (39.590, -82.972). From there, the river flows south until it joins the Ohio River at Portsmouth. The Upper Scioto River flows through agricultural landscape from its headwaters until it nears metropolitan Columbus (Figure 1), passing through sprawling suburbs north and west of downtown and eventually flowing through downtown Columbus. South of Columbus, the river flows again through suburbs then again predominately agricultural lands. Land use in the Upper Scioto River Basin is similar to that of the state of Ohio, with 56% of land used for

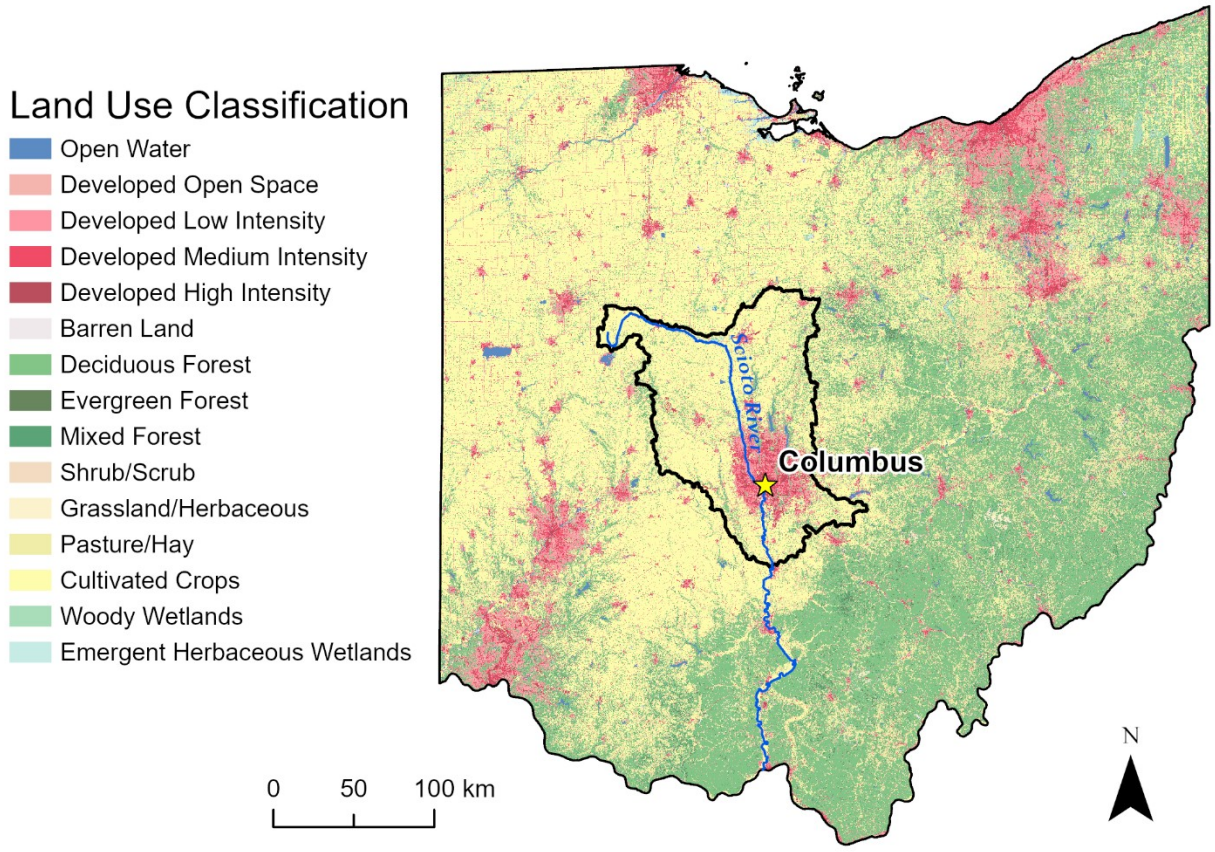

Figure 1. Land use in Ohio and the Upper Scioto River Basin (MRLC, 2019).

agriculture, 21% classified as developed, and only 12% classified as forested (MRLC, 2019) (Figure 1). Tile drainage underlies 30% of the Upper Scioto River Basin (Valayamkunnath et al., 2020).

The Scioto River Basin is primarily underlain by Silurian age dolomites in the western half and Devonian age limestone and shale in the east (Figure 2) (Ohio Division of Geological Survey, 2006). The transition from carbonate to shale is along a roughly north-south line through Columbus (Schiefer, 2002). There is a small percent of Mississippian age interbedded shale, siltstone, and sandstone along the eastern boundary of the watershed (Figure 2). The Scioto River cuts through Quaternary surface

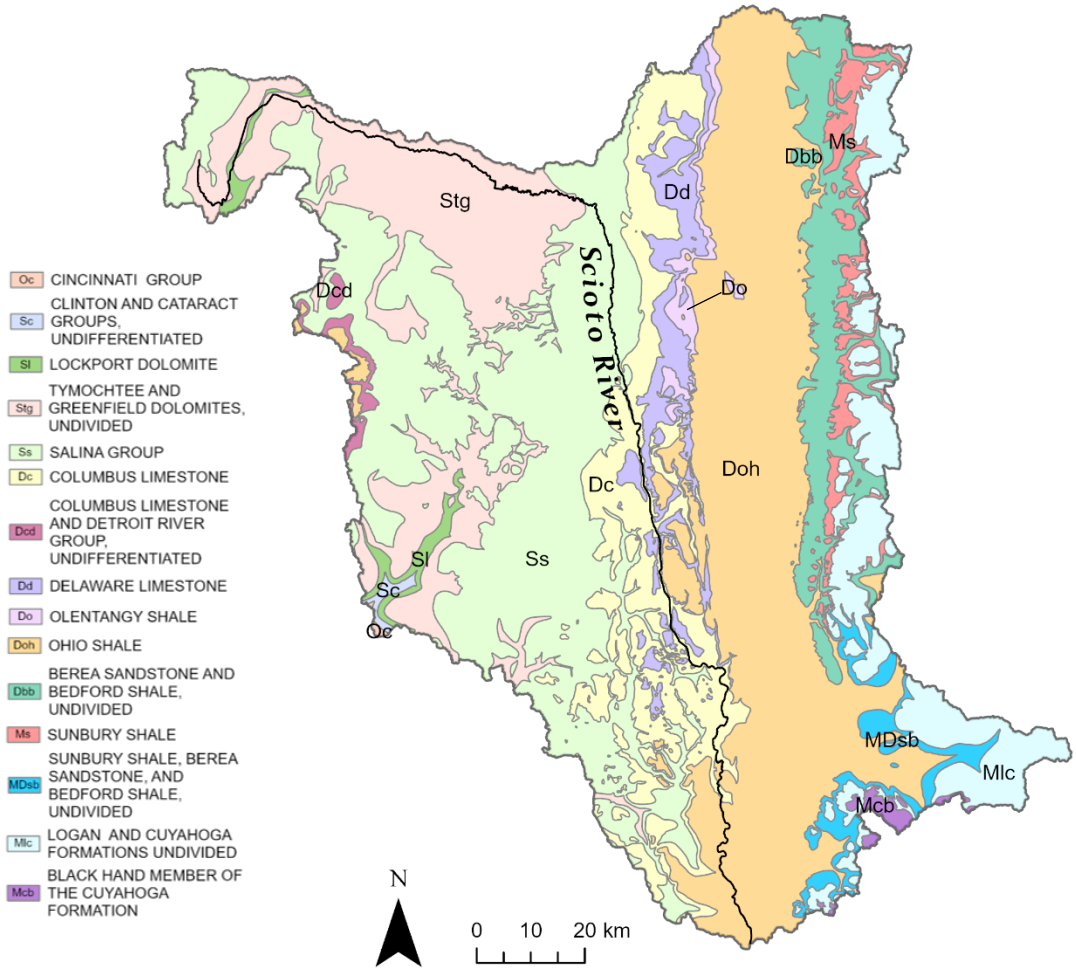

Figure 2. Bedrock geology of the Upper Scioto River Basin (Ohio Department of Natural Resources).

deposits into the underlying Salina Group dolomites while smaller tributaries do not cut through to bedrock (Swinford & Slucher, 1995). North of Columbus, the river flows through a narrow gorge at a gradient of 0.76 m/km. South of Columbus, the river widens and shallows, flowing south at a slope of 0.32 m/km (Schiefer, 2002).

The Upper Scioto River Basin is north of the glacial boundary representing glacial extent during the Wisconsinan and Illinoian ice ages. Because of this, much of the Upper Scioto River Basin is relatively

flat to gently rolling, with swampy depressional areas near the Scioto River headwaters (Ohio EPA, 1999; Schiefer, 2002). Glacial drift covers the landscape and can reach 60 meters in thickness in some areas (Curtis & Stueber, 1973; Hubbard et al., 1914). Glacial till around Columbus is primarily derived from the local bedrock, with more than 80% of pebbles in till made up of dolomite (Schmidt & Goldthwait, 1958). These glacial deposits store large quantities of water and can significantly affect streamflow in the basin (Schiefer, 2002). Soils are primarily glacially derived with low permeability (Ohio EPA, 1997; Schiefer, 2002).

Central Ohio and the Upper Scioto River Basin are characterized by a humid continental climate (Ohio EPA, 1999). Hot, humid summers and cold winters are typical of this area. Summer temperatures average 23 ^{o}C (74 ^{o}F) and winter temperatures average 0 ^{o}C (32 ^{o}F) (CFAES, n.d.). Average annual precipitation is 38 inches (96 cm), with most precipitation falling from February to July (CFAES, n.d.; Ohio EPA, 1999). Analysis of central Ohio precipitation data revealed that increases in monthly average precipitation were greatest in late winter (February-March) and late summer (August-September) when comparing 2000-2020 monthly averages to 1948-2020 monthly averages (NOAA, 2021).

The Upper Scioto River serves as the main drinking water source for Columbus. The population of Columbus has grown from 125,500 in 1900 to 905,000 in 2020 and is now the 14th largest city in the U.S. (United States Census Bureau, 1920; United States Census Bureau 2021). The Upper Scioto River is dammed in two locations, forming two reservoirs. Griggs Reservoir was constructed in 1905 and is located in suburbs north of Columbus (City of Columbus, n.d.) (Figure 3A). O'Shaughnessy Reservoir was constructed north of Griggs Reservoir in 1925 to support the growing Columbus metropolitan population. Both reservoirs are considered to be riverine in character, with maximum depths of 6 m in Griggs and 12 m in O'Shaughnessy, and shorter residence time of 26 days (O'Shaughnessy) relative to lacustrine reservoirs (Allen, 2011). Together, the two reservoirs hold 6.2 billion gallons of water

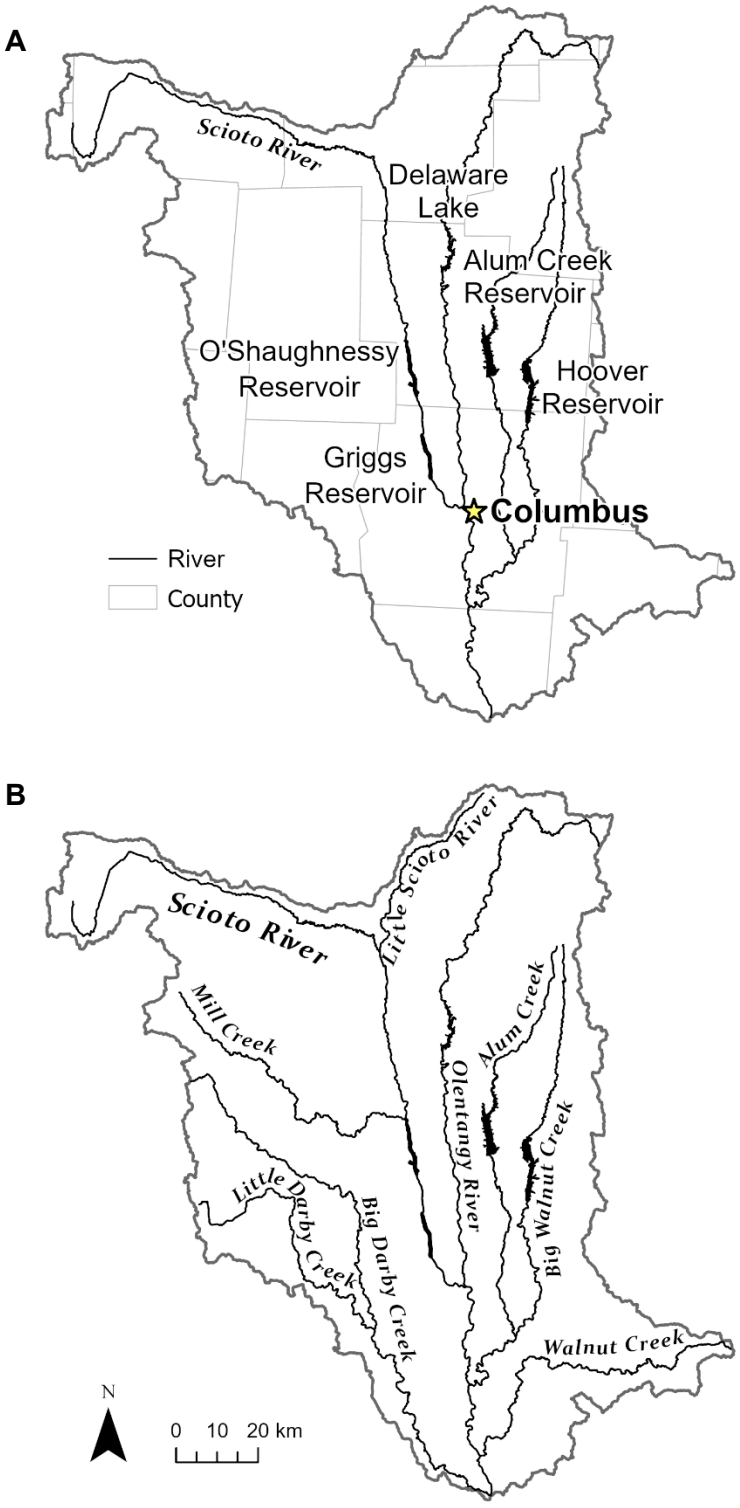

Figure 3. Reservoirs and major tributaries in the Upper Scioto River Basin. Figure 3A. Reservoirs in the Upper Scioto River Basin. Figure 3B. Major tributaries of the Scioto River in the Upper Scioto River Basin.

(City of Columbus, n.d.). Hoover, Alum Creek, and Delaware Lake reservoirs are in tributaries northeast of the Scioto River and are more lacustrine in character (Figure 3A). These reservoirs have greater depths and longer residence times than Griggs and O'Shaughnessy Reservoirs, with an average residence time of 152 days in Hoover Reservoir (Allen, 2011). Griggs and O'Shaughnessy Reservoirs provide water for downtown, west, and northwest Franklin County, where Columbus is located, while Hoover Reservoir provides water for the northeast portion of Franklin County (City of Columbus, n.d.). These three reservoirs provide 90% of the water used in Franklin County, with the rest supplied by wellfields in southern Franklin County (City of Columbus, n.d.).

1.4 Sample Locations

Sampling locations for this study are shown in Figure 4. Sample locations were chosen to represent land uses/types that differentiate portions of the watershed and may be contributing solutes to the river. Land use surrounding the river transitions from primarily rural-agricultural upstream to suburban and urban towards Columbus, then back to rural south of Columbus. The contributing watersheds of the Prospect and Bellepoint sampling locations are dominated by agriculture, with 79% and 75% of land cover classified as agricultural (Table 1). The Bellepoint sampling location is at the north end of O'Shaughnessy Reservoir where the river begins to widen into the reservoir. The Prospect and Bellepoint sample locations were chosen to represent the agricultural portion of the river, as development increases south of these locations. However, the Bellepoint sampling location is located in Delaware County which was the fastest growing county in Ohio from 2000-2019 (United States Census Bureau, 2019). It was hypothesized that any influence from the expanding suburbs was expected to be observed by measurable differences in geochemistry between the Prospect and Bellepoint sample locations. Griggs Reservoir is located north of Columbus, and land draining to Griggs Reservoir is 13%

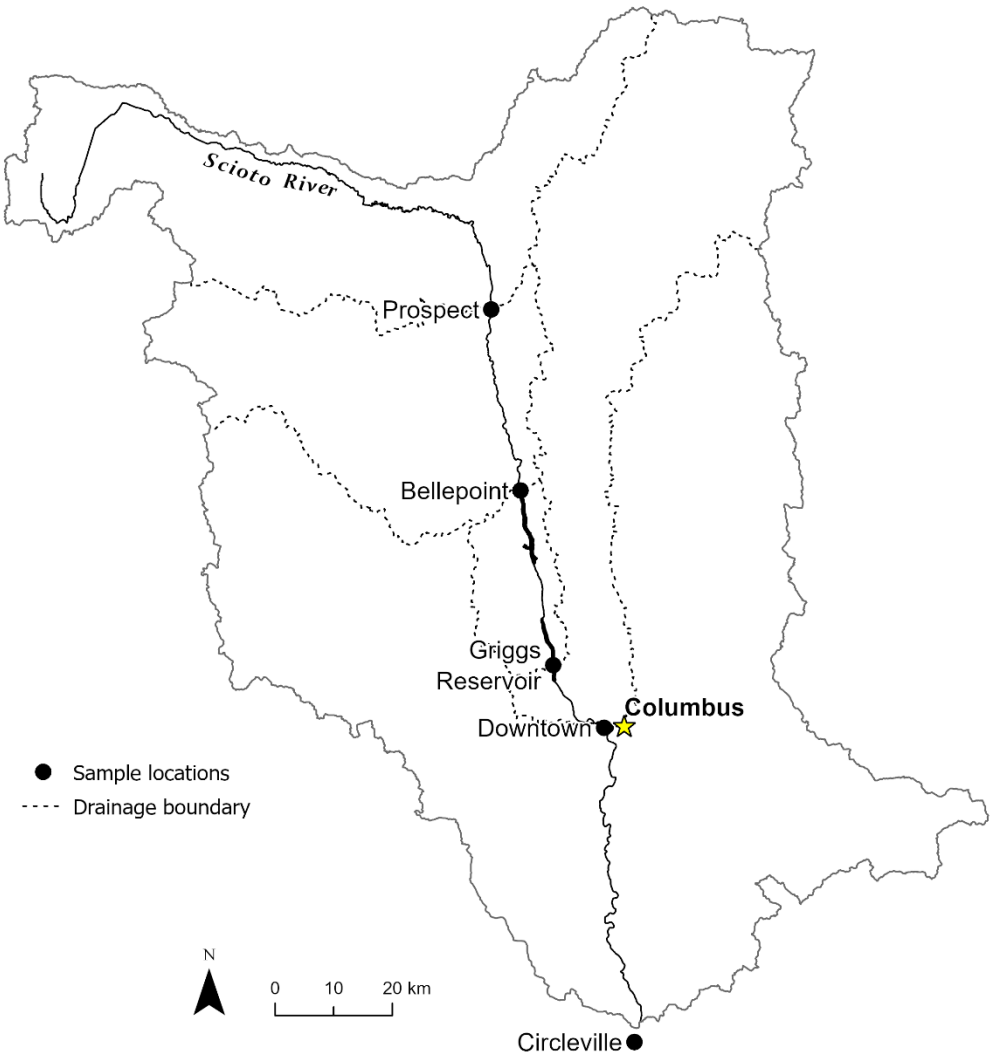

Figure 4. Sample locations. Dashed lines indicate upstream drainage area of sampling points. Circleville location drains entire Upper Scioto River Basin.

developed (Table 1). The downtown sample location represents the urban end member of the river and is about 1.5 km south of where the Olentangy River joins the Scioto. This location was chosen to capture the influence of downtown Columbus on the river and will include influences of the Olentangy River's input to the Scioto. The Circleville sampling location is about 6.5 km south of the boundary of the Upper Scioto River basin and will include the input of a number of other tributaries from both the east and

west of the mainstem of the river. Big Walnut Creek is a major tributary of the Scioto River that joins the river just before Circleville and includes contributions from Alum Creek which passes through the east side of Columbus (Figure 3B). It drains much of the eastern half of the Upper Scioto River Basin, a portion of which is underlain by shale and sandstone, in contrast with the high concentration of carbonates in the western part of the Upper Scioto River Basin. The Big Darby is another major tributary of the Scioto, entering the river from the west just north of Circleville. Circleville is also south of the city's wastewater treatment plants, so a signal from wastewater input may be visible here.

	Drainage Area (km^2)	Agriculture	Developed	Forested	Other
Prospect	1,386	79%	8%	7%	2%
Bellepoint	2,453	75%	9%	9%	2%
Griggs Reservoir	2,686	70%	13%	9%	2%
Downtown	4,149	64%	18%	10%	2%
Circleville	8,265	56%	21%	12%	2%
Upper Scioto River Basin	8,265	56%	21%	12%	2%
Ohio	116,096	36%	15%	32%	4%

Table 1. Land use in the Upper Scioto River Basin and drainage areas of sampling points (MRLC, 2019).

2. METHODS

2.1 Sampling Frequency

Sampling frequency varied throughout the study duration. Samples were collected weekly at the Bellepoint, Griggs Reservoir, and downtown locations beginning at the end of February through July 2021. Samples were collected biweekly starting in August, then monthly from October to December. Sampling frequency decreased starting in August because river flows were lowest during this period, so baseflow geochemistry was expected to dominate flow conditions. Long-term precipitation records suggest that this is the time of lower rainfall (CFAES, n.d.). Additionally, samples were collected at these three locations after precipitation events. Samples at Prospect and Circleville were collected monthly throughout the sampling period. Table A.1 summarizes dates and locations of samples collected during the study period.

2.2 Cleaning

For each sample collected, a new 250 mL LDPE bottle was used for bulk sample collection. Prior to sampling, these bottles were rinsed then soaked with 18.2 MΩ deionized (DI) water overnight. After collection, each sample was filtered into three bottles for analysis: one new 60 mL HDPE bottle that was cleaned in the same manner as the bulk sampling bottle, and two new 60 mL HDPE bottles that were soaked in 10% HCl overnight, rinsing twice with DI water before and after the acid soak. Samples for isotopic analysis were collected in new 20 mL plastic vials that were not precleaned prior to collection. Two DI-precleaned 60 mL HDPE bottles were filled with DI water in the lab for use as field blanks.

2.3 Collection

The majority of river water samples were collected from riverbanks using a 1-liter HDPE bottle attached to a 1-meter PVC pole. Precleaned sample bottles were transported to and from the field in new LDPE bags, one for each sample location. One person collected the sample using the sampling device and did not touch the final bulk sample bottle or storage bag. The second person wearing new nitrile gloves handled the 250 mL DI-precleaned bottles. The sampling device was submerged completely and rinsed twice with river water prior to collection of the sample. The 250 mL bulk sampling bottle was rinsed three times with river water from the collection device before filling completely. When collecting samples by hand (fewer than 10 samples), the 250 mL LDPE bottle was submerged and rinsed twice with river water by the collector wearing new nitrile gloves before collecting the final bulk sample. Samples were collected for isotopic analysis by filling 20 mL plastic vials with river water. Isotope samples were filled to the top of the container to reduce any influence of evaporation. All samples were stored in the dark in a closed cooler until return to the lab, less than four hours from sample collection. Field blanks were collected during most sampling expeditions at one of the locations sampled (Appendix A). DI-filled bottles for field blanks were each opened for one minute at the chosen sample location then closed and stored with samples.

2.4 Processing

Upon return to the lab, samples were filtered through new 0.45 µm pore-size Whatman polypropylene filters using 30 mL polypropylene Luer Lock syringes (polyethylene plunger) within four hours of collection. As noted previously, each sample was filtered into three different bottles: two acid-precleaned bottles (one for trace element analysis and one for major cation analysis), and one DI-precleaned bottle (for nutrient and major anion analysis). Before filling these bottles, 5-10 mL of sample

were passed through the filter into the collection bottle; the bottle was then capped, shaken, and then the water was discarded. Each bottle was then filled with the filtered sample water and refrigerated in the dark at 4°C until analysis, which was done within two months of collection. Blanks were filtered into one 60 mL acid-precleaned bottle (for trace element analysis) and one 60 mL DI-precleaned bottle (for major cation, anion, and nutrient analysis) and stored as samples until analysis. Samples collected for stable water isotopic analysis were not filtered or opened until analysis.

2.5 Analysis

All samples were prepared and analyzed at The Ohio State University. Major ion analysis was done by ion chromatography using the methods of Welch et al. (2010). Cation (Ca, Mg, Na, K, Li) analysis was performed on a Dionex-DX120 Ion Chromatograph, and anion (F, Cl, Br, SO_4) analysis was done on a Dionex-ICS-2100. HCO_3 was calculated as the difference between cation (Ca, Mg, Na, K) and anion (Cl, SO_4, NO_3+NO_2) equivalents (Σ cations – Σ anions = HCO_3^-). Welch et al. (2010) demonstrated that the error associated with this approach was generally within 5% of alkalinity measured by titration. Accuracy of laboratory measurements for cations was determined by round robin analysis of USGS Standard Reference Sample (Major Ion Constituents) in the Lyons lab from 2011-2015 (Table 2). Accuracy of anion analysis was determined by analysis of a 100x dilution of SPEX® CertiPrep Ion Chromatograph Instrument Check Standard 3. This check standard was run at the start of every anion analysis. Precision of major ion analysis is calculated as the percent difference between analysis of duplicate samples (Table 2). One duplicate sample was run between every 10 samples. Detection limits were calculated as three times the standard deviation of a low concentration standard.

Nutrient (NO_3+NO_2, PO_4, NH_4) and H_4SiO_4 analysis was done using a Skalar SAN++ Continuous Flow Analyzer. Concentrations are reported as NO_3+NO_2 as N, PO_4 as P, NH_4 as N, and H_4SiO_4 as Si.

Accuracy was determined by comparing calibration standard concentrations across runs and comparing calibration standards made on different days and from different stock solutions to ensure accuracy of serially diluted standard solutions (Table 3). Precision of nutrient analysis is calculated as the percent difference between analysis of duplicate samples. One duplicate sample was run between every 10 samples. Precision of nutrient analyses were generally between 1-5%, except when duplicates were

	Average % difference (%)	Range (%)	Average accuracy (%)	Accuracy range (%)	Detection limit (μM)
Ca	3	1-5	11	6-24	2.8
Mg	4	0-9	7	2-15	0.62
Na	2	0-11	3	0-8	1.4
K	<1	0-3	3	0-9	0.30
Li	10	0-44	17	8-23	0.08
Cl	<1	0-1	4	2-6	2.1
SO_4	<1	0-0.4	4	3-4	1.4
F	5	0-22	7	5-10	1.3
Br	4	0-12	6	1-10	0.28

Table 2. Precision and accuracy of cation and anion analysis. Precision denoted by average % difference between duplicate samples. Cation accuracy calculated from round-robin analysis of USGS Standard Reference Sample Major Ion Constituents. Anion accuracy calculated as the difference between the measured and certified values of external standard. Detection limit calculated as three times the standard deviation of replicates of low concentration calibration standards.

analyzed after samples with exceptionally high concentrations and concentrations in samples were relatively low (<0.48 μM PO_4, <1.1 μM NH_4). Detection limits were calculated as three times the standard deviation of replicates of a low concentration standard (Table 3).

Trace element samples were acidified prior to analysis to 2% v/v HNO_3 using Fisher TraceMetal™ Grade HNO_3 that was distilled in-lab after purchase. Field blanks and method blanks were run as samples to determine field and method contamination. Trace elements were analyzed on a SciEx ICPMS

Elan DRC II in the Trace Element Research Lab (TERL) at The Ohio State University. Dilutions of CPI International Peak Performance™ and Inorganic Ventures™ single element stock solutions were done to produce a six-point calibration curve comprising the range of analyte concentrations. Standards were also acidified to 2% v/v HNO_3. Accuracy was determined by analyzing the National Institute of Standards and Technology (NIST) Standard Reference Material 1643e/1643f (Trace Elements in Water) and Environment Canada TMDA 64.2 (Trace Elements in Water). External standards were run after instrument calibration was complete and prior to sample analysis. Calibration standards were run between every 8-10 samples to determine precision of instrument and relative standard deviation for each element. Precision of trace element analysis is calculated as the percent difference between concentrations of these check standards (Table 4). Accuracy of trace element analysis was generally within 15%, except for Cu on the last sample run, where accuracy was 30% (Appendix B). The absolute difference between the external standard certified value and measured value was 0.78 μg/L or 12 nM. This only affected 15 samples (collected in November and December 2021) that range from 13-25 nM Cu. Concentration means by sample location for Cu changed by 1 nM or less when these samples were removed from calculations. Precision was within 10% for all analytes except for U in the last analysis. These data along with the MDLs (method detection limit) are summarized in Table 4. Method detection limits were calculated according to the USEPA Method Detection Limit procedure. Three method blanks were analyzed at the start of runs 2, 3, and 4. MDL was calculated by

$$MDL_b = \bar{X} + t_{(n-1,1-\alpha=0.99)} s_b$$

where MDL_b is the method detection limit based on method blanks, $\bar{X}$ is the mean of blank concentrations (replaced with 0 if mean was negative), $t_{(n-1,1-\alpha=0.99)}$ is Student's t-value for n-1

degrees freedom (n=9 for this study) and α=0.01, and s_b was the standard deviation of the blanks (US EPA Office of Water, 2016). Detailed accuracy and precision are provided in Appendix B.

Stable water isotope analysis was done using a Picarro Model L2130-i using the methods of Smith et al. (2021). Data correction was performed using internal laboratory standards calibrated to VSMOW at the Institute of Arctic and Alpine Research (INSTAAR) at University of Colorado Boulder. Accuracy was calculated by duplicate analysis of samples (Table 5). Precision was calculated by analysis of 150 injections of DI water. Means of every 6 samples were calculated, and the standard deviation of those means was reported as instrument precision. Detailed methods are explained in Appendix B and in Smith et al. (2021).

	Average % difference (%)	Range (%)	Average accuracy (%)	Accuracy range (%)	Detection limit (µM)
H_4SiO_4	3	0-19	4	0-14	0.25
NO_3+NO_2	3	0-12	4	0-22	0.18
PO_4	14	0-51	3	0-21	0.13
NH_4	14	0-92	8	0-22	1.3

Table 3. Precision and accuracy of nutrient analysis. Precision denoted by average % difference between duplicate samples. Accuracy measured from comparison of sets of calibration standards across runs and standards made on different days and from different stock solutions. Detection limit calculated as three times the standard deviation of replicates of low concentration calibration standards.

	Average RSD (%)	RSD Range (%)	Average accuracy (%)	Accuracy range (%)	MDL (nM)
U	7	2-13	11	8-15	0.85
Ni	8	6-9	7	2-14	0.94
Cu	7	5-9	11	1-30	1.7
Rb	6	3-9	8	3-12	0.29
Mo	6	4-8	10	2-17	1.9
Ba	6	4-8	3	1-6	2.6
Sr	5	3-10	2	0-4	420

Table 4. Precision and accuracy of trace element analysis. Precision denoted by average RSD of check standards. Accuracy reported as an average and range of calculated differences from external standard. MDL (method detection limit) calculated from replicate analysis of method blanks according to the US EPA MDL procedure (US EPA Office of Water, 2016).

	In-run accuracy (average of all runs) (%)	In-run accuracy (greatest measured) (%)	Precision (‰)
$\delta^{18}O$	<1	1	0.028
δD	<1	3	0.42

Table 5. Precision and accuracy of stable water isotope analysis.

3. RESULTS

3.1 Field Blanks

Field blanks were measured for each analyte except for $\delta^{18}O$ and δD. Mean concentrations of major ions and nutrients in field blanks were below the detection limit for most analytes. Concentrations of Na, Cl, SO_4, Br, PO_4, Li, U, Cu, Rb, Mo, Ba, and Sr in all field blanks were below the MDL. For those field blanks with concentrations above detection limits, concentrations were still well below concentrations measured in many samples, with a few exceptions that will discussed in the text. Geochemical data for all field blanks can be found in Appendix C.

3.2 Climate and Hydrology

Average monthly temperature and precipitation data from the Upper Scioto River Basin during the study period are shown in Figure 5. Much of the year had lower than average precipitation, except for July, August, and December. Deviations from average monthly precipitation range from 6.7 cm below average in May to 3.9 cm above average in August. Temperature anomalies range from about 3^{o}C below average in February to 5^{o}C above average in December. Average temperatures from April-September were about 1^{o}C or less different from the 25-year average.

Daily precipitation data were taken from two locations: the first about 50 kilometers northwest of downtown Columbus in Marysville, and the second from Ohio State University's campus (CFAES source discussed previously) (Figure 6). This was done to provide a clearer picture of precipitation in the study area, as pop-up storms frequently occurred during the study period and only affected certain portions of the study area.

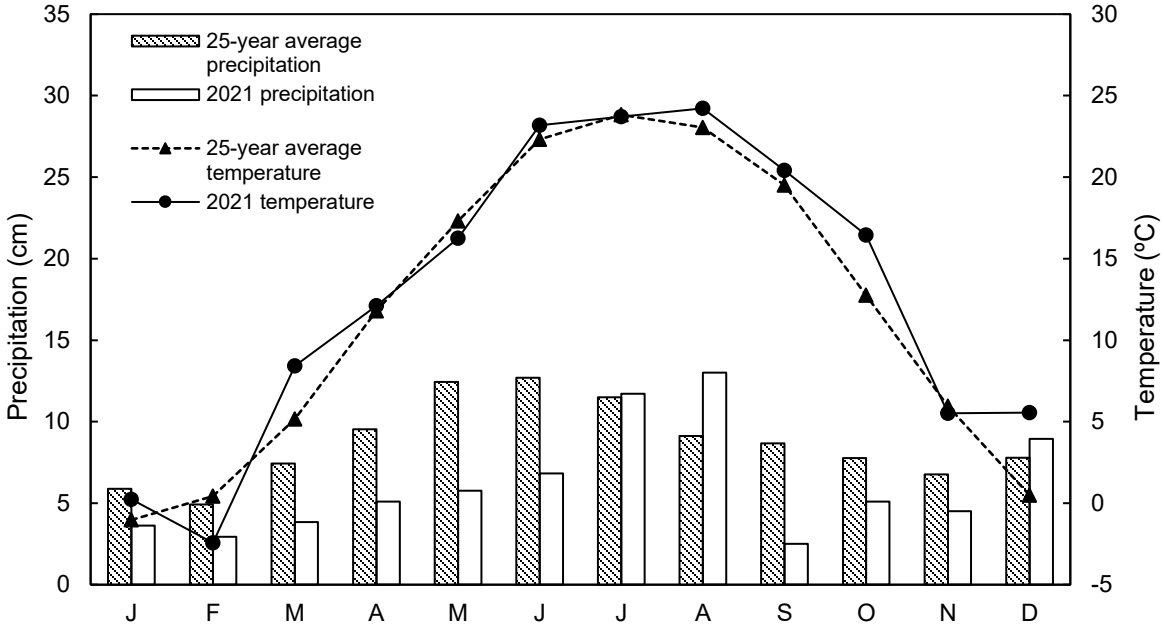

Figure 5. Monthly average temperature and precipitation totals in central Ohio in 2021. Data from Columbus (40.0112, -83.0442) collected by the College of Food, Agricultural, and Environmental Sciences (CFAES) at Ohio State University and can be found at https://weather.cfaes.osu.edu/stationinfo.asp?id=14.

Discharge data were compiled from USGS gages (Figure 7). Details for the gages that were used for each sample location are provided in Appendix B. River discharge increased significantly from downtown to Circleville as three major tributaries join the Scioto River between Columbus and Circleville. Timing and magnitude of high flow events were similar at Prospect and Bellepoint but appear more subdued at Griggs Reservoir as a result of the damming and creation of the reservoir. More frequent high flow events were evident at downtown and Circleville locations which could be due to the confluence of the Olentangy River just north of the downtown site and Big Darby Creek and Big Walnut Creek north of Circleville. The higher percentage of impermeable surfaces in the drainage areas of the

Scioto River at downtown Columbus and of Big Walnut Creek (18% and 37% developed) also could have increased the flashiness of discharge as well.

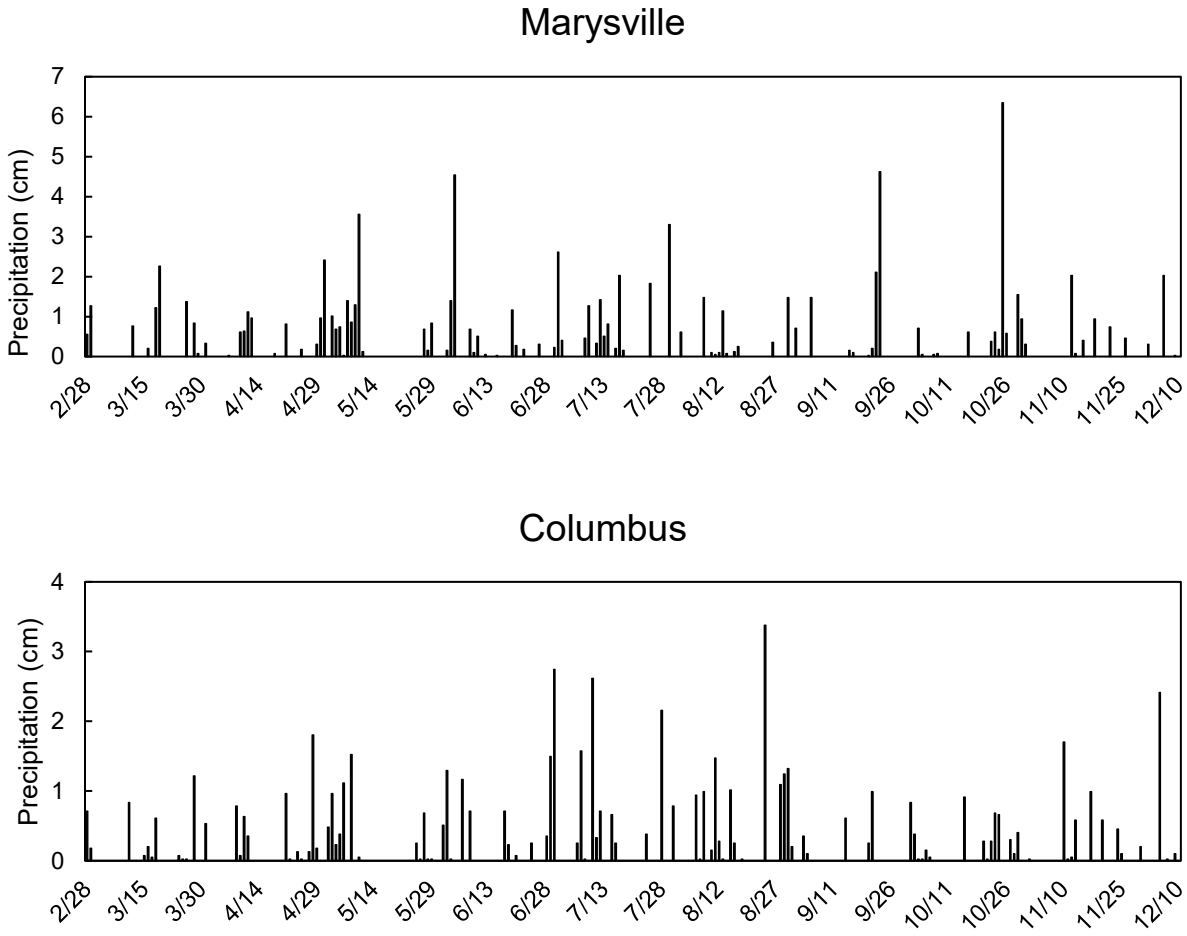

Figure 6. Daily precipitation totals during study period from two locations. Marysville station located west of O'Shaughnessy Reservoir (40.1938, -83.2675). Columbus station discussed in caption of Figure 5.

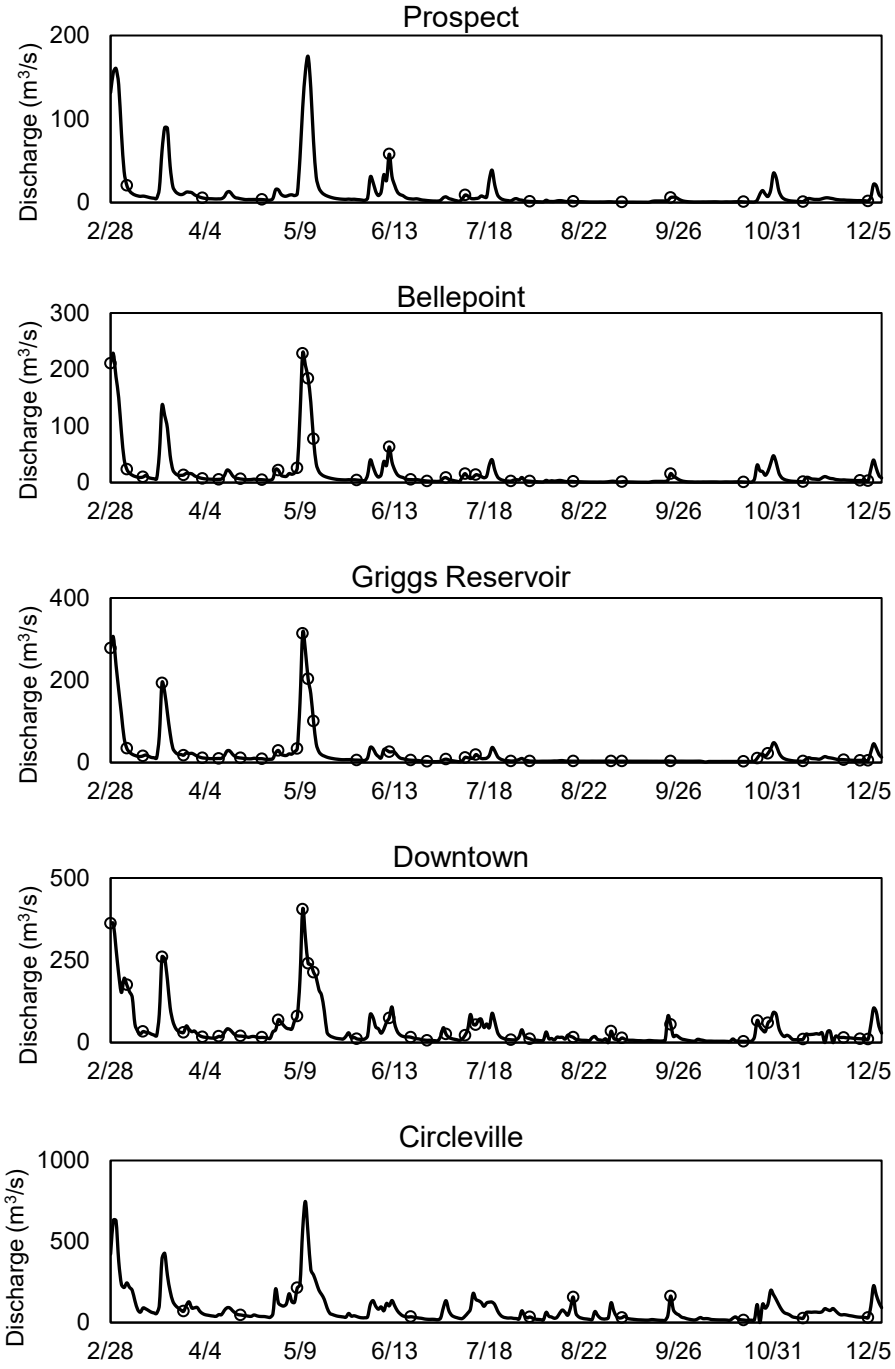

Figure 7. Discharge data for each sample location. USGS gage metadata provided in Appendix B. Open circles indicate sample collection.

3.3 Average Analyte Concentrations

All results are included in Appendix C. Table 6 summarizes analyte concentrations at each location and includes geochemical data for the Mississippi River, major Irish rivers (Lyons et al., 2021), and "unpolluted" world rivers (Meybeck, 1979).

Before discussing the results of geochemical analyses, it should be noted that two samples collected at Prospect had significantly higher concentrations of PO_4 and NH_4 relative to concentrations in the rest of the dataset (Appendix C). These samples were collected on 9/23/2021 and 10/20/2021. Phosphate concentrations in these samples were 5-8 times greater than the average of the rest of the samples collected at Prospect. Ammonium concentrations in these samples were 5-10 times greater than concentrations measured at any sample location. It is not clear what the cause of these extraordinarily high values were. Concentrations of analytes in field blanks collected on these days were negligible. Although there is no direct evidence of sample contamination, it cannot be completely ruled out. On the other hand, these high values could reflect input from a local source that dominated these low value conditions. Means, yields, and correlation coefficients were calculated including and excluding these data, and both results are reported.

Total dissolved solids (TDS) ranged from 171 mg/L to 648 mg/L with an average of 415 $\pm$ 106 mg/L across all sample locations. Average TDS was highest at Prospect and Circleville (481 mg/L and 452 mg/L), followed by Bellepoint (442 mg/L), and lowest at Griggs Reservoir and downtown (390 mg/L and 382 mg/L respectively). This downstream trend in mean TDS is reflected in many of the major ions analyzed, discussed below.

Major cation chemistry was dominated by Ca and Na, with mean concentrations of 1317 μM (RSD= 23%) and 1327 μM (RSD= 43%) respectively. Calcium, Mg (mean=968 μM; RSD=34%), and H_4SiO_4

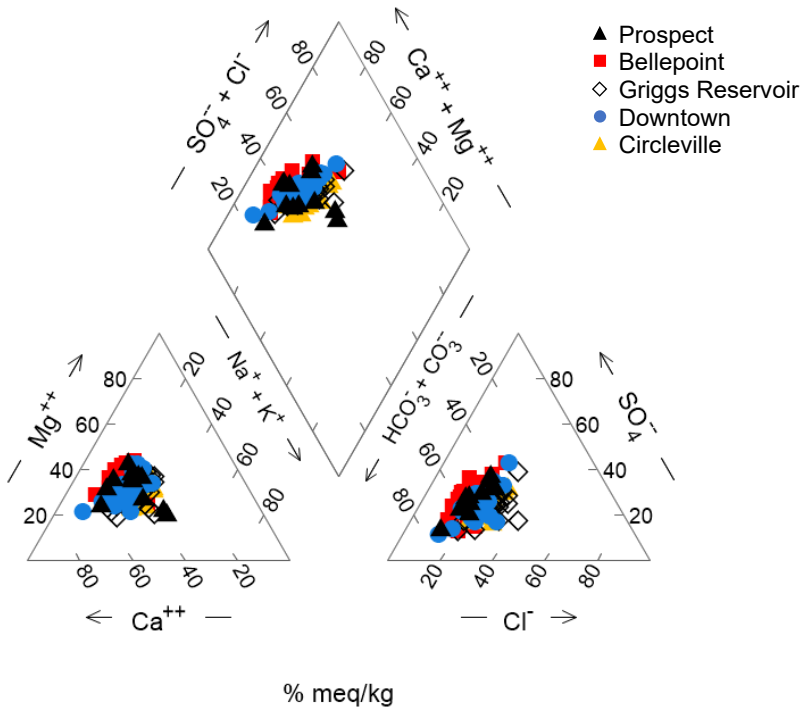

Figure 8. Piper diagram of all samples.

(mean= 87 µM; RSD= 40%) exhibited the same spatial pattern as TDS: concentrations were highest upstream at Prospect and Bellepoint and decreased until Circleville, where concentrations increased again. Mean Na concentrations decreased from Prospect to Griggs Reservoir, then increased and peaked at Circleville. Potassium (mean= 124 µM; RSD= 30%) concentrations stayed relatively constant, ranging from 114 µM at the downtown site to 158 µM at Prospect. Calcium, Mg, Na, and K mean concentrations were all higher in this study than values for the Mississippi River and "unpolluted" world rivers, though Ca concentrations were similar to those measured in major Irish rivers Lyons et al. (2021), another watershed dominated by carbonate bedrock. Dissolved Si concentrations were slightly lower than the Mississippi River, but twice that in major Irish rivers.

Major anion chemistry was dominated by HCO_3 (mean= 2999 μM; RSD= 29%), with more than twice the mean of Cl. Bicarbonate, Cl, and SO_4 were high at all locations compared to concentrations in world rivers, with a mean Cl concentration of 1334 μM (RSD = 34%) and mean SO_4 concentration of 761 μM (RSD = 44%) for all samples. Chloride concentrations had a similar pattern to that of Na but were lowest at Bellepoint and increased downstream, reaching a maximum at Circleville. Bicarbonate, SO_4, F (mean=19 μM; RSD= 39%), and Br (mean= 0.64 μM; RSD= 121%) all had the same downstream pattern as Ca, Mg, and H_4SiO_4. Major anion concentrations were higher than average concentrations in the Mississippi River and world rivers, but HCO_3 mean concentrations were similar to that measured in Irish rivers. Thirty-three samples had Br concentrations below the detection limit, so concentrations were set to half the detection limit.

Nitrate mean concentrations were highest at Bellepoint (mean=259 μM; RSD=55%) and lowest at downtown (mean= 180 μM; RSD=59%). Nitrate concentrations displayed a pattern similar to Ca, Mg, H_4SiO_4, HCO_3, SO_4, F, and Br, with relatively higher concentrations at Prospect and Bellepoint, a decrease at Griggs Reservoir and downtown, then increased at Circleville. Excluding the two anomalous NH_4 concentrations measured at Prospect, NH_4 was highest at Griggs Reservoir, with an average of 7.6 μM (RSD=89%), and lowest at Circleville (mean=2.4 μM; RSD=117%) and Prospect (mean=2.8 μM; RSD= 110%). Phosphate concentrations displayed nearly the opposite trend compared to NH_4, with the highest concentrations at Prospect (mean=14 μM; RSD=117%) and Circleville (mean=7.0 μM; RSD=77%) and lowest at downtown (mean= 1.9 μM; RSD= 65%) and Griggs Reservoir (mean=2.1 μM; RSD=83%). Dissolved NO_3+NO_2 mean concentrations in this study were nearly twice that measured in the Lower Mississippi River in 1991-92 by Shiller (1997), while PO_4 mean concentrations were only 40% greater. Two samples had PO_4 concentrations below the detection limit and 40 samples had NH_4 concentrations below the detection limit, so concentrations were set to half the detection limit.

		Prospect		Bellepoint		Griggs Reservoir		Downtown		Circleville		All		Mississippi River[a]	Major Irish Rivers[b]	"Unpolluted" World Rivers[a]
		n=12		n=29		n=34		n=34		n=11		n=116				
	Analyte	Mean	RSD	Mean	RSD	Mean	RSD	Mean	RSD	Mean	RSD	Mean	RSD	Mean	Mean	Mean
µM	Ca	1455	22%	1448	24%	1260	21%	1201	19%	1356	24%	1317	23%	975	1436	335
	Mg	1109	32%	1091	34%	926	33%	850	33%	986	26%	968	34%	440	251	140
	Na	1625	61%	1175	54%	1166	32%	1362	31%	1789	25%	1327	43%	739	519	226
	K	158	50%	127	31%	121	19%	114	14%	123	25%	124	30%	72	74	33
	H_4SiO_4	111	31%	93	39%	82	46%	78	39%	91	30%	87	40%	105[c]	42	
	HCO_3	3431	23%	3363	35%	2830	25%	2653	23%	3165	19%	2999	29%	1934	3067	852
	Cl	1338	39%	1149	37%	1229	27%	1469	31%	1731	24%	1334	34%	544	583	164
	SO_4	959	41%	911	48%	694	39%	638	31%	736	35%	761	44%	524	111	86
	F	26	46%	21	41%	16	27%	16	23%	20	25%	19	39%		3.6	
	Br	1.4	114%	0.81	119%	0.44	67%	0.41	53%	0.67	47%	0.64	121%		0.40	
	NO_3+NO_2 (as N)	222	41%	259	55%	210	64%	180	59%	228	35%	216	57%	115[c]	93	
	PO_4 (as P)	14 (7.8)	117% (67%)	4.2	49%	2.1	83%	1.9	65%	7.0	77%	4.2 (3.5)	157% (95%)	3.0[c]	<0.1	
	NH_4 (as N)	21 (2.8)	203% (110%)	5.7	120%	7.6	89%	4.3	114%	2.4	117%	7.1 (5.3)	211% (112%)		0.6	
	Sr	29.4	43%	23.9	45%	18.1	36%	14.1	31%	14.5	33%	19.2	49%		2.78	0.69
nM	Li	996	40%	947	47%	647	38%	642	35%	824	32%	767	45%			
	U	8.7	53%	9.2	44%	7.2	32%	6.8	33%	5.8	33%	7.6	42%	4.8[c]	4.2	0.78[d]
	Ni	116	57%	99	57%	75	27%	66	20%	62	24%	81	50%	26[c]		13[e]
	Cu	18	30%	21	48%	23	47%	24	41%	18	23%	22	44%	24[c]	19	23[e]
	Rb	18	77%	12	40%	10	22%	12	23%	20	33%	13	50%	13[c]	22	19[e]
	Mo	89	48%	108	85%	64	36%	61	29%	70	23%	77	69%	24[c]	3.6	8[f]
	Ba	322	19%	321	21%	318	15%	320	16%	390	18%	326	18%	475[c]	242	167[e]

Table 6. Mean concentration for dissolved major ions, nutrients, and trace elements by sample location.
a. Meybeck (1979). b. Lyons et al. (2021). c. Shiller (1997). d. Palmer & Edmond (1993). e. Gaillardet et al. (2003). f. Miller et al. (2011). Values in parentheses indicate mean concentrations and RSDs of PO_4 and NH_4 when 2 outliers from Prospect were removed.

Lithium (mean=767 nM; RSD= 45%), Mo (mean= 77 nM; RSD= 69%), and Sr (mean= 19.2 μM; RSD=49%) all exhibited the same downstream trend in mean concentrations as Ca, Mg, H_4SiO_4, HCO_3, SO_4, and F, although Sr had a minimal increase from downtown to Circleville. Uranium (mean=7.6 nM; RSD= 42%) and Ni (mean= 81 nM; RSD= 50%) both had higher means at Prospect or Bellepoint and decreased downstream, reaching a minimum at Circleville, though U means by location did not vary as much as Ni. Rubidium (mean= 13 μM; RSD= 50%) was highest at Prospect (mean=18 nM; RSD= 77%) and Circleville (mean=20 nM; RSD=33%), and stayed nearly constant between 10-12 nM at Bellepoint, Griggs Reservoir, and downtown. Barium (mean= 326 μM; RSD=18%) stayed nearly constant from Prospect through downtown (318-322 nM) and increased to an average of 390 nM at Circleville. Copper was the only trace element where the lowest mean concentration was at Prospect and Circleville (18 nM) with higher concentrations at Bellepoint, Griggs Reservoir, and downtown (21-24 nM). Mean U concentrations measured in the Scioto River were 40-50% greater than averages in the Mississippi River and major Irish rivers, and an order of magnitude greater than world rivers. Ni and Mo mean concentrations were roughly 3 times greater than concentrations in the Mississippi River and almost 10 times greater than world river concentrations (Mo only). Mean Cu concentrations were within 15% of averages of the Mississippi River, major Irish rivers, and world rivers. Rubidium mean concentrations in the Scioto River were equal to the Mississippi River, and between 60-80% less than Irish and world rivers. Mean Ba concentrations were 45% less in the Scioto River than the Mississippi River, but 25-50% higher than Irish and world rivers. Strontium concentrations in the Scioto River were roughly 7 times greater than Irish rivers and 28 times greater than world rivers.

3.4 Geochemical Temporal Trends

Calcium, Mg, and Na concentrations (except K) at all locations generally increased from the start of the study period to mid to late April, where concentrations decreased through May, coinciding with a major precipitation event in early May (Figure 9). Concentrations then began to slightly increase again until reaching another peak in late summer to early fall, then decreased slightly through the end of the study period. Dissolved Si concentrations decreased from March through early May, reaching a low a few weeks earlier than Ca, Mg, and Na concentrations. Dissolved Si concentrations then generally increased through the summer and decreased again in the fall. Potassium concentrations stayed nearly constant for the entire study period, ranging from 80-190 μM, with the exception of an increase in late September and October, also observed in Na concentrations (Figure 9).

Major anion concentrations showed similar trends as cations (Figure 10). Concentrations of all major anions were similar in Griggs Reservoir and downtown samples, with the exception of Cl. Chloride concentrations were generally higher at downtown than at Griggs Reservoir (and other sample locations) from February to late April (Figure 10C), which could indicate the influence of road salt runoff in winter that is more concentrated downtown than upstream, further from Columbus. The peak in Na and K in September and October occurred in F, Br, and HCO_3 concentrations as well (Figure 10).

Nitrate concentrations were high in mid-May, during a heavy precipitation event from 5/1 to 5/10 (Figure 11). Nitrate, PO_4, and NH_4 concentrations increased with the rising limb of the hydrograph during this event, though the magnitude of increase and peak timing varied among these three analytes. Concentrations of all three analytes then decreased from mid-May to the end of May, as flow returned to lower values at the end of May. Concentrations of NO_3+NO_2 and PO_4 were highest at Bellepoint, Prospect, and Circleville for the second half of the study period (July-December). Nutrient concentrations were similar at Griggs Reservoir and downtown for much of the study period, except for

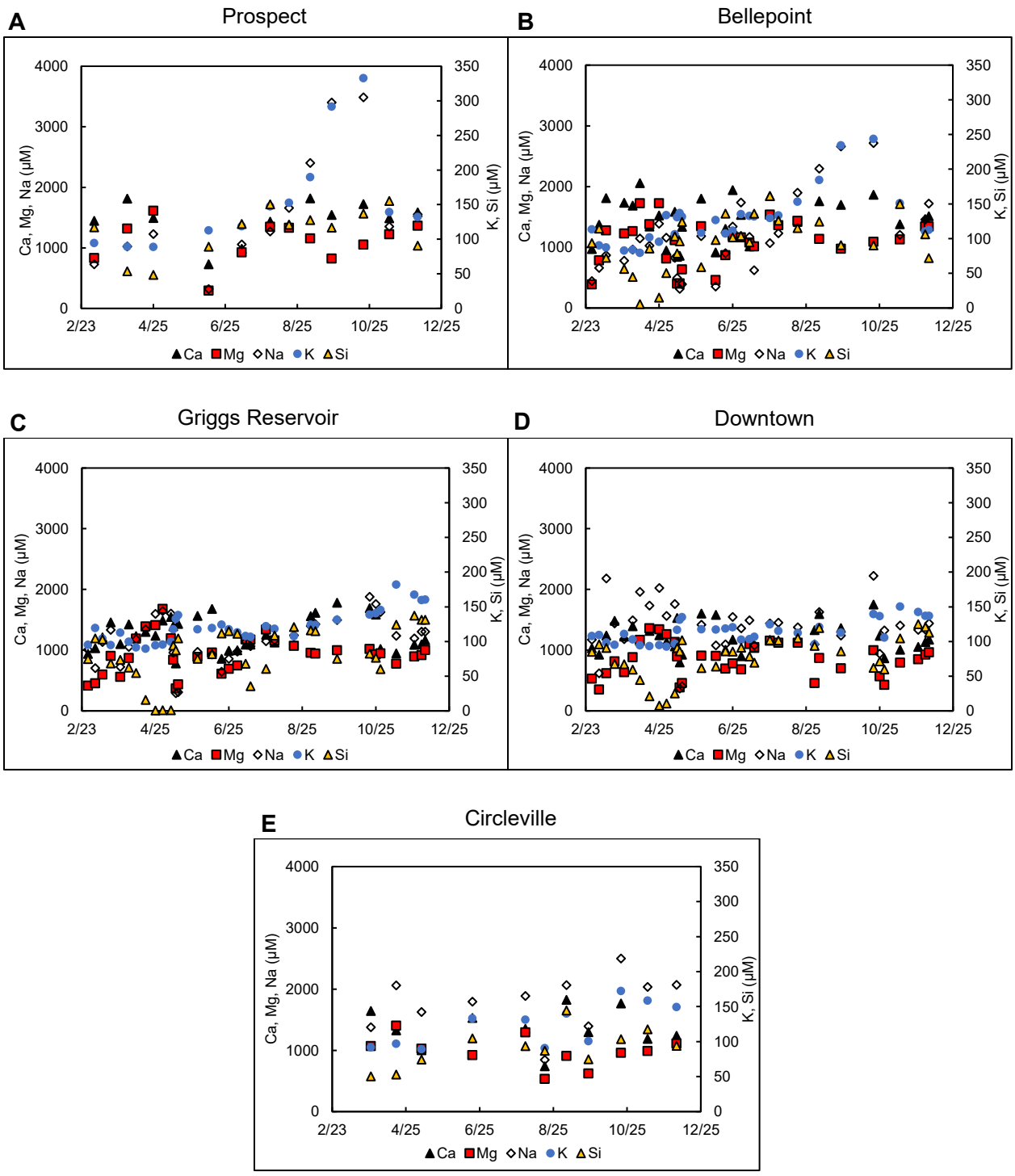

Figure 9. Dissolved cation (Ca, Mg, Na, K, H_4SiO_4) concentrations from February 2021 to December 2021 at each sampling location. All concentrations are in µM.

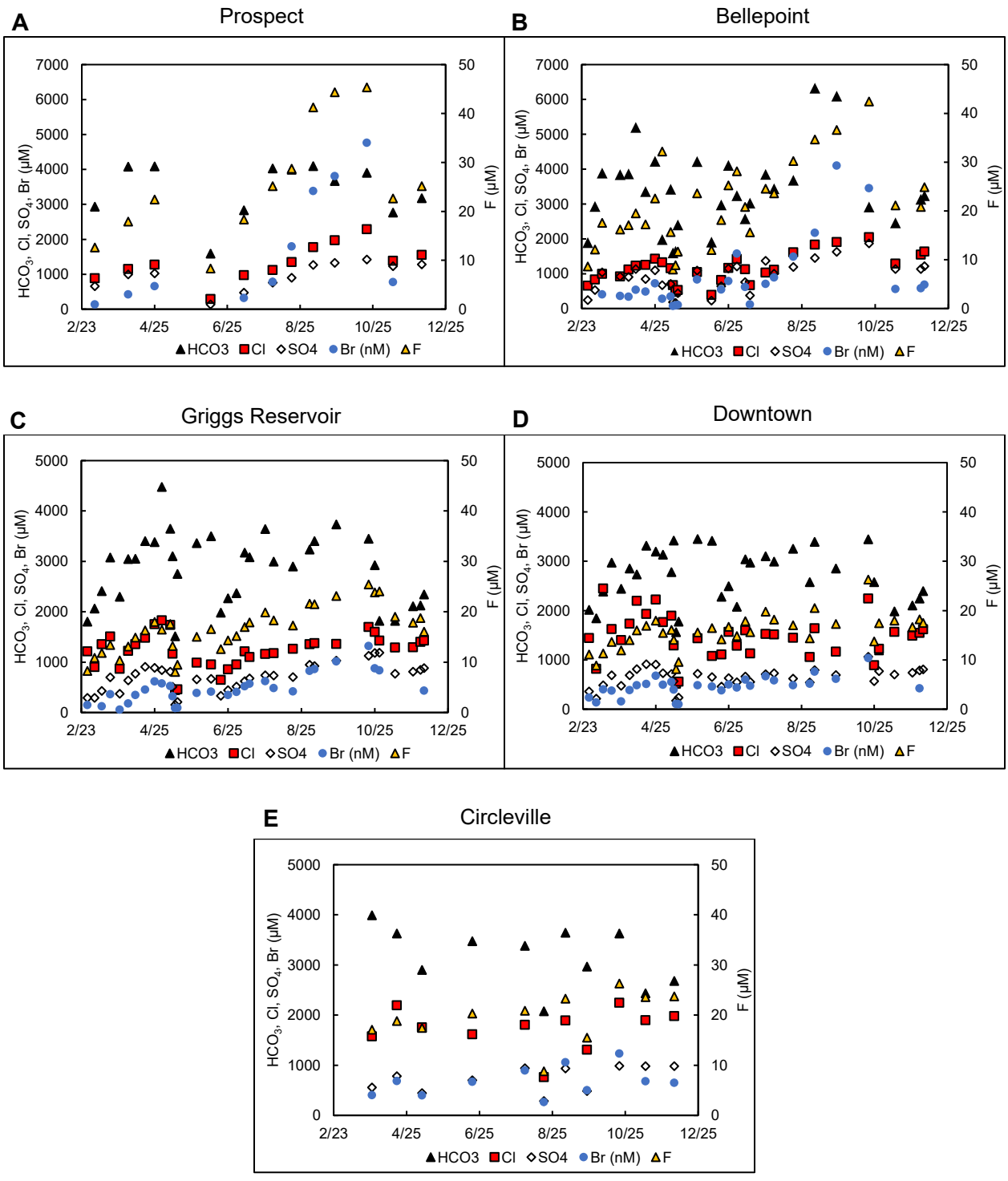

Figure 10. Dissolved anion (HCO_3, Cl, SO_4, Br, F) concentrations from February 2021 to December 2021 at each sampling location. All concentrations are in µM except for Br which is plotted in nM (noted in legend). Samples that had detectable Br that was below the detection limit are still plotted here, though concentrations are not absolutely quantifiable. Br DL= 0.28 µM.

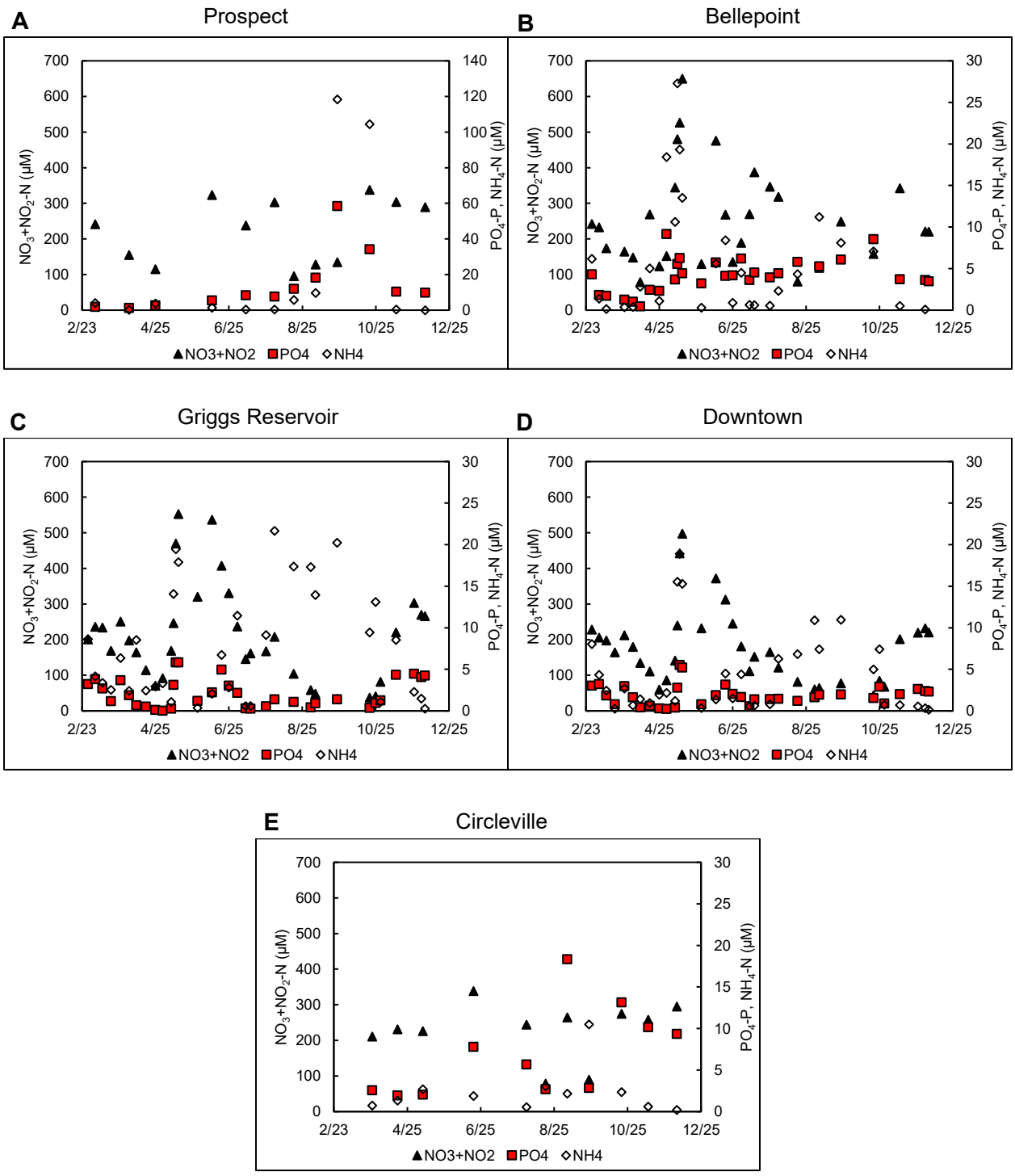

Figure 11. Dissolved nutrient (NO_3+NO_2, PO_4, NH_4) concentrations from February 2021 to December 2021 at each sampling location. All concentrations are in µM. Samples that had detectable PO_4 and NH_4 that were below the detection limit are still plotted here, though concentrations are not absolutely quantifiable. PO_4 DL= 0.13 µM. NH_4 DL= 1.3 µM.

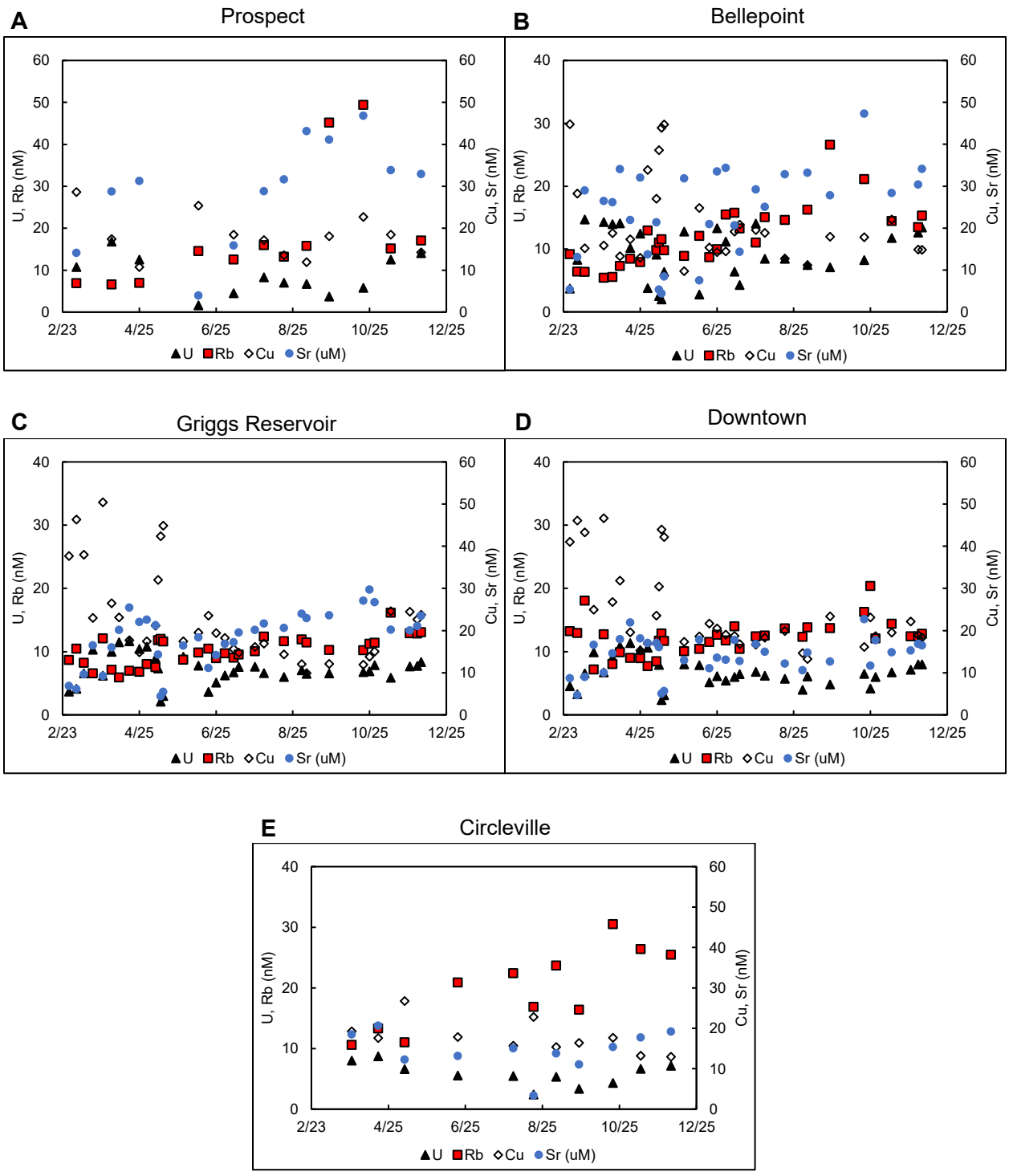

Figure 12. Dissolved trace element (U, Rb, Cu, Sr) concentrations from February 2021 to December 2021 at each sampling location. All concentrations are in nM except for Sr which is plotted in µM (noted in legend).

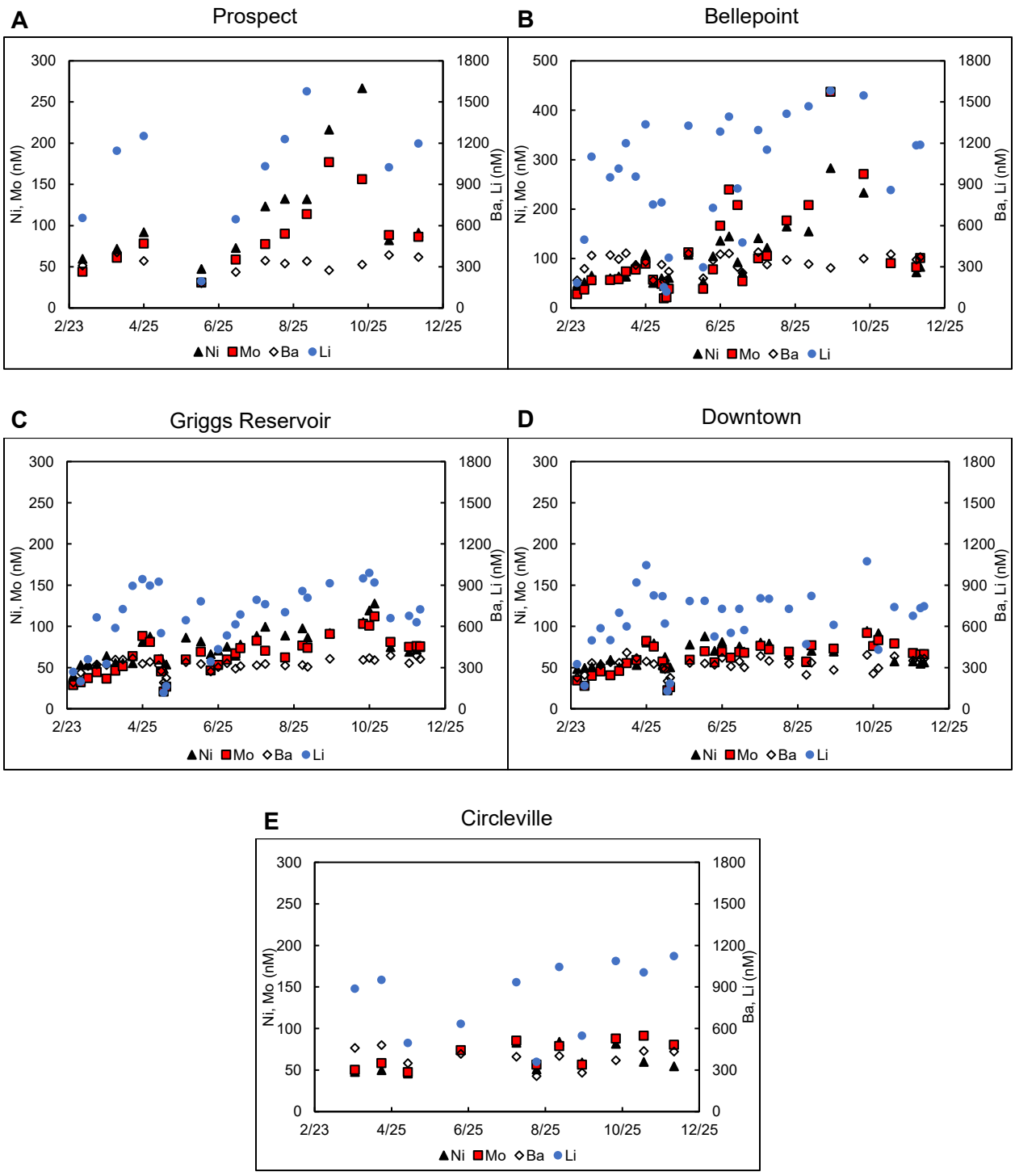

Figure 13. Dissolved trace element (Ni, Mo, Ba, Li) concentrations from February 2021 to December 2021 at each sampling location. All concentrations are in nM.

NH_4 concentrations from August to December, where NH_4 concentrations in Griggs Reservoir were higher than all sample locations (with the exception of two Prospect samples where the NH_4 concentrations were exceptionally high) (Figure 11C). As mentioned previously, Prospect samples from the end of September and October had significantly higher concentrations of NH_4 and PO_4 (Figure 11A) compared to the rest of the dataset, though this was not observed in NO_3+NO_2 concentrations.

Lithium, Ni, and U showed similar seasonal variability, with low concentrations at the start of the study period increasing to mid-April and decreasing again during the May high flow event (Figures 12 and 13). Lithium and Ni concentrations then increased at all locations until November, with the highest concentrations at Bellepoint and Prospect. Uranium concentrations stayed relatively constant for the rest of the study period at all locations except for Prospect and Bellepoint. September and October samples at Bellepoint and Prospect also have exceptionally high concentrations of Ni, Rb, Mo, and Sr, as seen in some of the major ion and nutrients. Similar to NO_3+NO_2, Cu is the only trace element that increased in concentration with increasing flow during the May precipitation event. Rubidium concentrations increased slightly throughout the sampling period at all locations. From June through December, Circleville generally had the highest Rb concentration of all locations as a result of input from eastern tributaries draining shales and sandstones. Molybdenum, Ba, and Sr also decrease with increasing flow in mid-May. Molybdenum and Sr concentrations at Prospect then increased through the fall. Molybdenum, Ba and Sr concentrations at Bellepoint varied significantly through the rest of the study period, while concentrations of these elements remained nearly constant at Griggs Reservoir, downtown, and Circleville through December.

3.5 Stable Water Isotopes

Sample $\delta^{18}O$ and δD values became more enriched (more positive) from the beginning of the study period (February 2021) until mid to late summer, then became more depleted (more negative) toward the end of the study period (December 2021) (Figures 14 and 15). Differences between sample location $\delta^{18}O$ were most pronounced in March and mid-August to December. There was no consistent trend in isotopic composition when comparing sample locations, although Griggs Reservoir and downtown samples often had similar $\delta^{18}O$ values, likely as a result of these sample locations only being 11 km apart. The same is true for Prospect and Bellepoint $\delta^{18}O$ values. Data plot along the central Ohio local meteoric water line (Smith et al., 2021) as shown in Figure 15, except for a notable deviation for seven samples that plot significantly above the LMWL (further discussed in Section 4.7). Samples that plot above the LMWL and GMWL ($\delta^{18}O < -7.75$) were collected between February 28th and May 10th. Samples that plot slightly below the LMWL and along the GMWL ($\delta^{18}O > -7.37$) were collected from May 14th through December 5th.

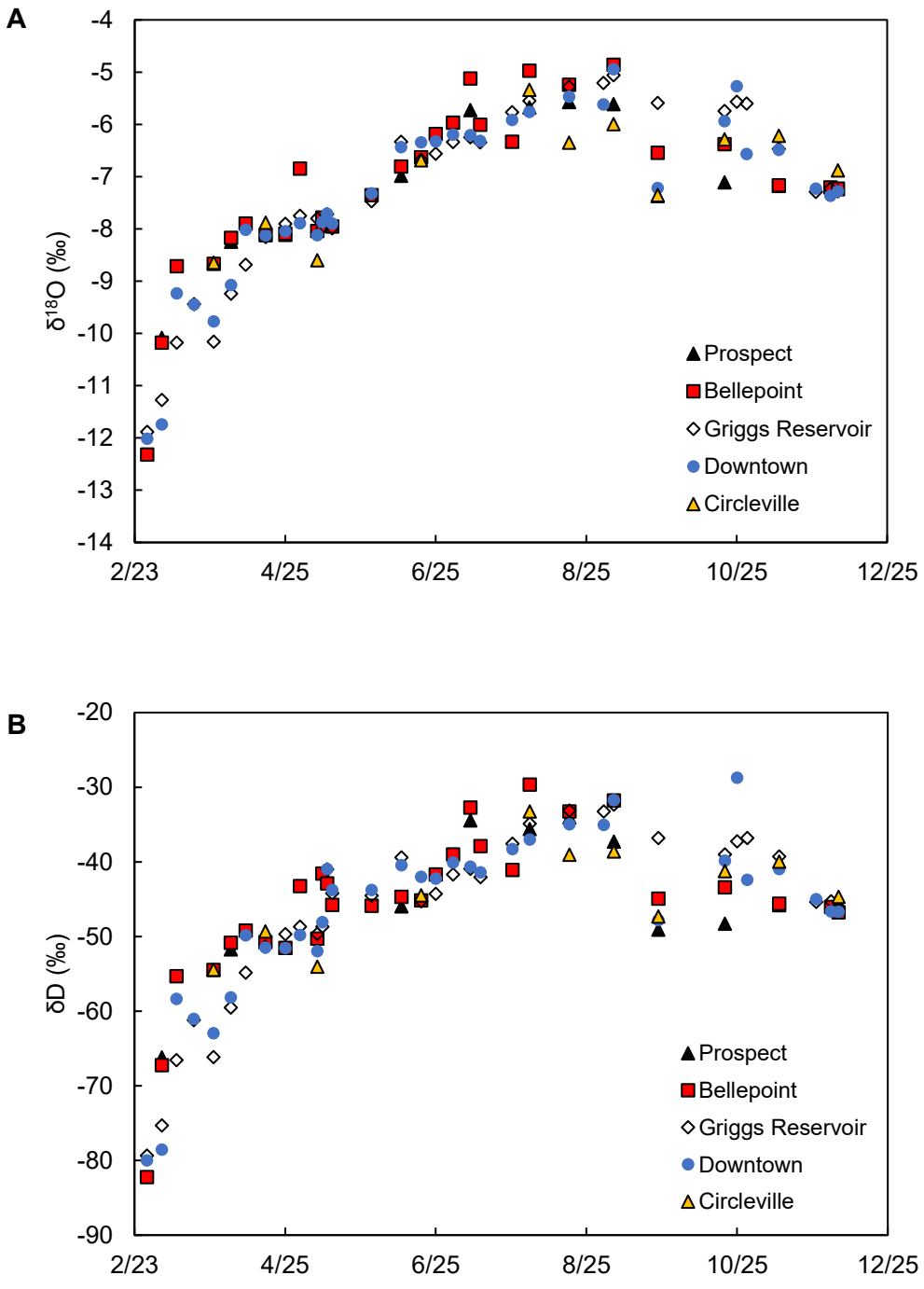

Figure 14. River water δ18O and δD over study period. A. δ18O over study period. B. δD over study period. Error bars are smaller than symbols.

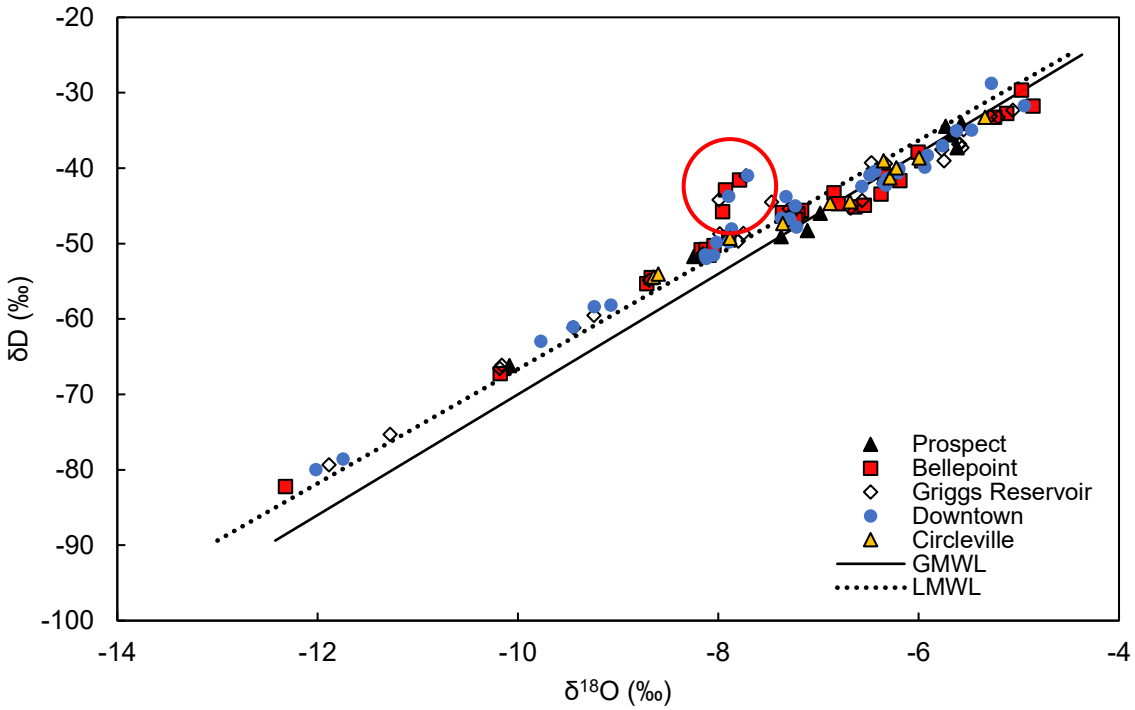

Figure 15. Stable water isotopic values plotted with the local meteoric water line from Smith et al. (2021) and global meteoric water line from Craig (1961). Circled points are those that fall off the LMWL.
Error bars are smaller than data points.

4. DISCUSSION

4.1 Lithology

The concentration of major ions in global river waters are primarily controlled by the watershed's geology and contributions from atmospheric input (Berner & Berner, 1987). Major ion river chemistry of the Scioto River is dominated by rock weathering, as indicated by the Gibbs (1970) plot (Figure 16). The Mississippi River plots in the same region of the Gibbs plot (Gibbs, 1970). Na/(Na+Ca) ratios had a greater range of values compared to $Cl/(Cl+HCO_3)$ (Figures 16A-B). Samples from all locations except Circleville had a range of Na/(Na+Ca) ratios between 0.11-0.56, while Circleville samples are more closely clustered at higher Na/(Na+Ca) ratios (0.33-0.50), reflecting the higher percentage of siliciclastic rocks in the drainage area of Circleville compared to upstream sample locations.

Although the study area is predominately underlain by carbonate bedrock, river water samples have a Ca:Na molar ratio of 1:1. Rakowsky (2000) found similar concentrations in the Scioto River, attributing the elevated Na concentrations to weathering of silicate minerals in the glacial till overlying much of the study area. Sodium from road salt could also contribute to high Na concentrations (Dailey et al., 2014). Samples collected at Circleville plot closest to the silicate end member on the Gaillardet et al. (1999) plot and had higher Na concentrations relative to other locations, potentially as a result of the higher concentration of shale and sandstone in the drainage basin of Circleville compared to upstream locations (Figure 17). Figure 17, plotted after Gaillardet et al. (1999) also indicates a potential evaporitic signal influencing the major ion chemistry of the Scioto River.

Discharge-weighted yields of Ca and Si were calculated to understand the influence of Ca versus Si weathering in the study area. At Bellepoint, Ca yields were 10.2 tons/km^2/yr, while dissolved Si yields were 0.63 tons/km^2/yr. Calcium yields were between 15-22 times the dissolved Si yields at all sample locations, demonstrating that carbonate weathering dominates aluminosilicate weathering in the study

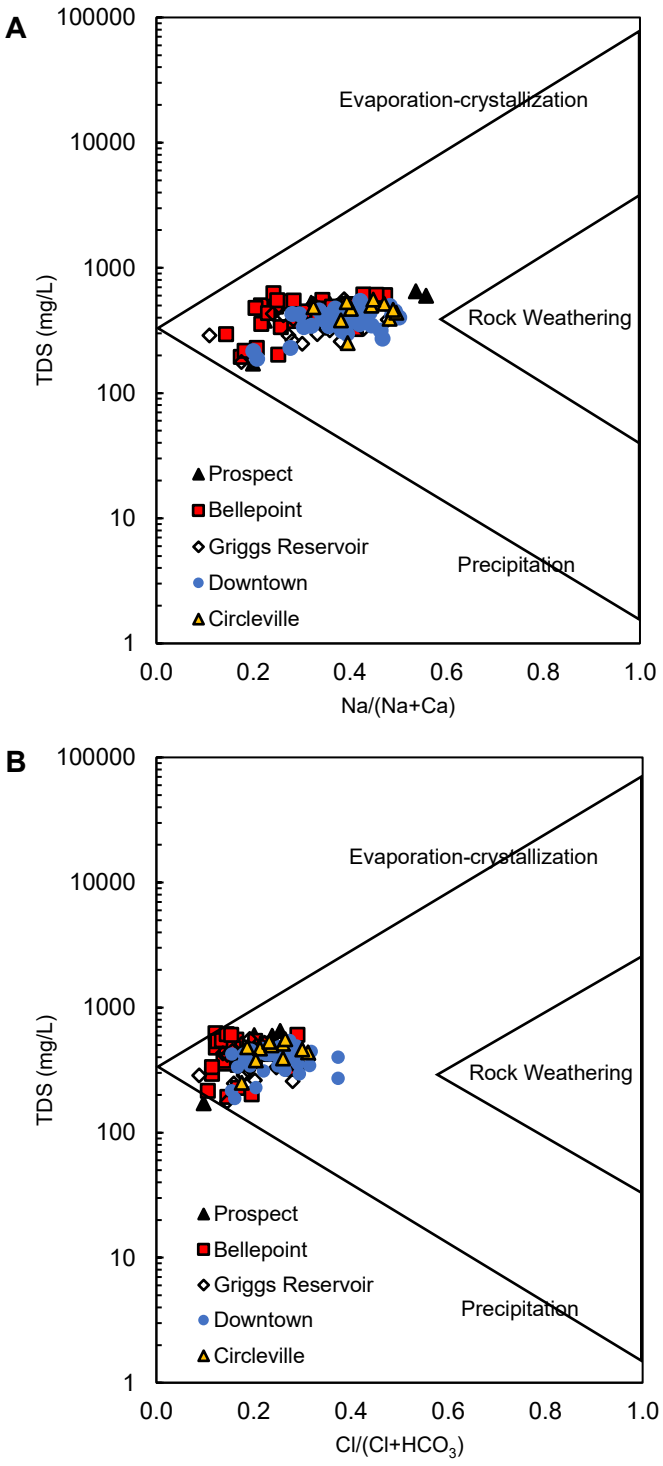

Figure 16. Gibbs plot. TDS and Ca, Na, Cl, HCO_3 data plotted with evaporation/crystallization, precipitation, and rock weathering signatures based on Gibbs (1970). A. TDS and Na/(Na+Ca) data for all samples. B. TDS and $Cl/(Cl+HCO_3)$ for all samples.

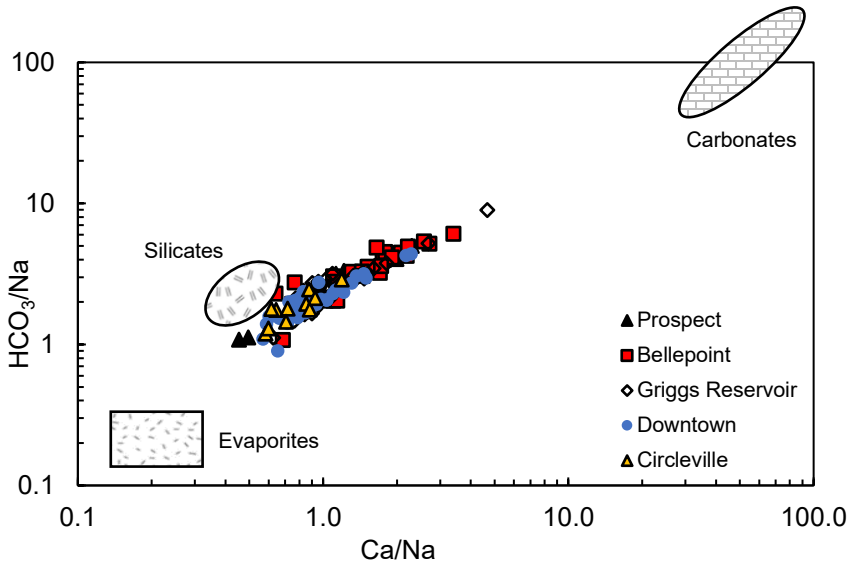

Figure 17. Gaillardet plot. HCO_3/Na and Ca/Na data for all samples. Plotted after Gaillardet et al. (1999).

area, even at Circleville which drains sandstone and shale units on the eastern edge of the watershed, although H_4SiO_4 yields increase at Circleville.

4.2 Concentration-Discharge Relationships

Variations in solute concentrations under changing discharge volumes can be evaluated to better understand sources of solutes, the magnitude of these sources, analyte solubility and reactivity, and transport pathways (Pohle et al., 2021). Generally, concentration-discharge (C – Q) relationships can be summarized into three categories: mobilization, chemostasis, and dilution (examples of these behaviors in Appendix E) (Knapp et al., 2020). These behaviors are a result of many factors related to watershed characteristics including land cover, bedrock lithology, soil parameters, topography, hydroclimatic factors, and more (Godsey et al., 2019; Pohle et al., 2021). Mobilization of a solute indicates increasing concentrations with increasing discharge, and suggests flushing of a solute and/or

increased connectivity of water transport pathways during higher flows (Knapp et al., 2020; Pohle et al., 2021). Decreasing solute concentrations with increasing discharge indicates dilution and suggests a finite source of a constituent or the influx of waters with lower solute concentrations (e.g. solute-rich deep groundwater mixing with more dilute rainfall during precipitation events) (Basu et al., 2011; Knapp et al., 2020). Chemostatic behavior indicates nearly constant concentrations with changes in discharge and is influenced by many factors and processes that help "buffer" concentration. Chemostatic behavior can occur due to input from a large source of an analyte, such as bedrock or stored legacy contaminants, masking concentration variability, thus resulting in apparent constant concentrations with changes in discharge (Thompson et al., 2011). Influxes from shallow groundwater have also been shown to overprint natural C – Q relationships, resulting in apparent chemostatic behavior (Cartwright et al., 2020). This behavior can also result from a balance between hydrologic sources and biological uptake (Bao et al., 2017; Moatar et al., 2017). Chemostasis suggests that rates of solute production and mobilization are proportional to discharge volumes (Godsey et al., 2009, 2019). After analyzing 59 headwater catchments, Godsey et al. (2009) found that many weathering-derived solutes displayed chemostatic or weak dilution behavior on event and interannual time scales. This was in contrast to previous findings that suggested many weathering products were diluted with increasing flow (Hem, 1943). This conclusion was later reinforced by analysis of 2,186 catchments by Godsey et al. (2019).

Many of the elements analyzed in this study displayed chemostatic or weak dilution behavior with discharge, based on log C – log Q relationships (Figure 18). C – Q behaviors follow a power law relationship ($C=aQ^b$; where a and b are constants) (Bao et al., 2017; Pohle et al., 2021). After a log transformation of this relationship (log (C) = log (a) + b*log (Q)), values of b can be used to investigate C – Q behaviors (Knapp et al., 2020). Chemostatic relationships are represented by a log C – log Q slope equal to 0, while a slope of -1 indicates dilution, and a slope of +1 indicates mobilization. Log C – log Q

slopes are plotted with error bars that represent the 95% confidence interval (CI) for the calculated slope. Error bars were larger at Prospect and Circleville compared to Bellepoint, Griggs Reservoir, and downtown in part because fewer samples were collected at these two locations.

Major ions (Ca, Mg, Na, K, Si, HCO_3, Cl, SO_4, F, Br) display chemostatic or weak dilution behavior (slopes= 0- +1) (Figure 18A), though variation is visible between sites (Figures 18B-F). This finding agrees with results of the Godsey et al. (2019) analysis of log C – log Q relationships of 59 headwater catchments. Of the major ions analyzed, Ca, K, Si, and HCO_3 had slopes closest to zero, while Mg, Na, Cl, SO_4, and F show slightly stronger dilution behavior and had slopes between -0.17 and -0.45 at most locations. For the majority of analytes, slopes were closest to zero at Griggs Reservoir and downtown, likely as a result of the reservoirs upstream of these locations, dampening natural relationships between concentration and discharge. Bromide concentrations show a moderate to strong dilution effect at Prospect, Bellepoint, and Circleville (slopes= -0.63- -0.49) though error is large at Prospect and Circleville compared to many of the other analytes (Figures 18B-18F). Slopes of log H_4SiO_4 – log Q also had significant error, likely due to the wide range of concentrations measured in the samples (range= 1-161 μM).

Nitrate, PO_4, and NH_4 have varying relationships with discharge among locations. Nitrate had a chemostatic to slightly positive relationship with discharge at all locations except for Circleville, which indicates dilution (slope= -0.40). Godsey et al. (2019) also observed a chemostatic or mobilization behavior in N species, but chemostatic to slight dilution behavior for dissolved P. Phosphate slopes indicate chemostasis or slight mobilization with discharge at Bellepoint, Griggs Reservoir, and downtown, but moderate to strong dilution at Prospect and Circleville, though the error associated with slopes calculated at Prospect and Circleville is significant. Confidence intervals of log NH_4 – log Q slopes were large, making it difficult to draw meaningful conclusions about relationships with flow. Marinos et

al. (2020) found that increasing tile drainage resulted in nearly chemostatic behavior because tile drainage reduced the amount of groundwater flowing through shallow NO_3 rich soil during high flows. This likely plays a role in this catchment as NO_3+NO_2 exhibits a chemostatic to slight mobilization behavior. Legacy storage of NO_3 in agricultural soils also provides a lasting source of NO_3 to surface waters, reducing concentration variability related to flow volume (Basu et al., 2011). Log PO_4 – log Q and log NH_4 – log Q slopes were recalculated for the whole dataset and for only those samples collected at Prospect excluding samples with high concentrations (collected on 9/23/21 and 10/20/21). Slopes changed less than 0.04 units except for log NH_4 – log Q at Prospect, where the slope increased from -0.20 to -0.10 and CI decreased from ± 0.75 to ± 0.62.

Rubidium and Ba display the closest to chemostatic behavior of the trace/minor elements, with the exception of Rb at Circleville, which shows stronger dilution behavior. This is likely because of higher concentrations of Rb at Circleville due to the increase in Rb-bearing shales in the eastern portion of the drainage area of Circleville. Nickel, U, Mo, Li, and Sr also showed weak to moderate dilution. Similar to the pattern seen in major ions, log C – log Q relationships were closest to chemostatic at Griggs Reservoir and downtown for all trace elements. Copper is the only trace element that had a positive relationship with discharge, indicating mobilization of Cu with increasing discharge. Log C – log Q slopes for Cu ranged from 0.16 at Prospect to 0.25 at Bellepoint, so although the slopes are small, they are positive at all locations. Because of the large error reported for Cu concentrations of samples 106-120 (discussed in section 2.5), slopes and errors were recalculated without these samples. Slopes increased by less than 0.03 units for all locations except for Circleville, where slope decreased by 0.04 units. The difference in calculated error was less than ±0.02 units. Slopes and CI displayed in Figure 18 include all samples.

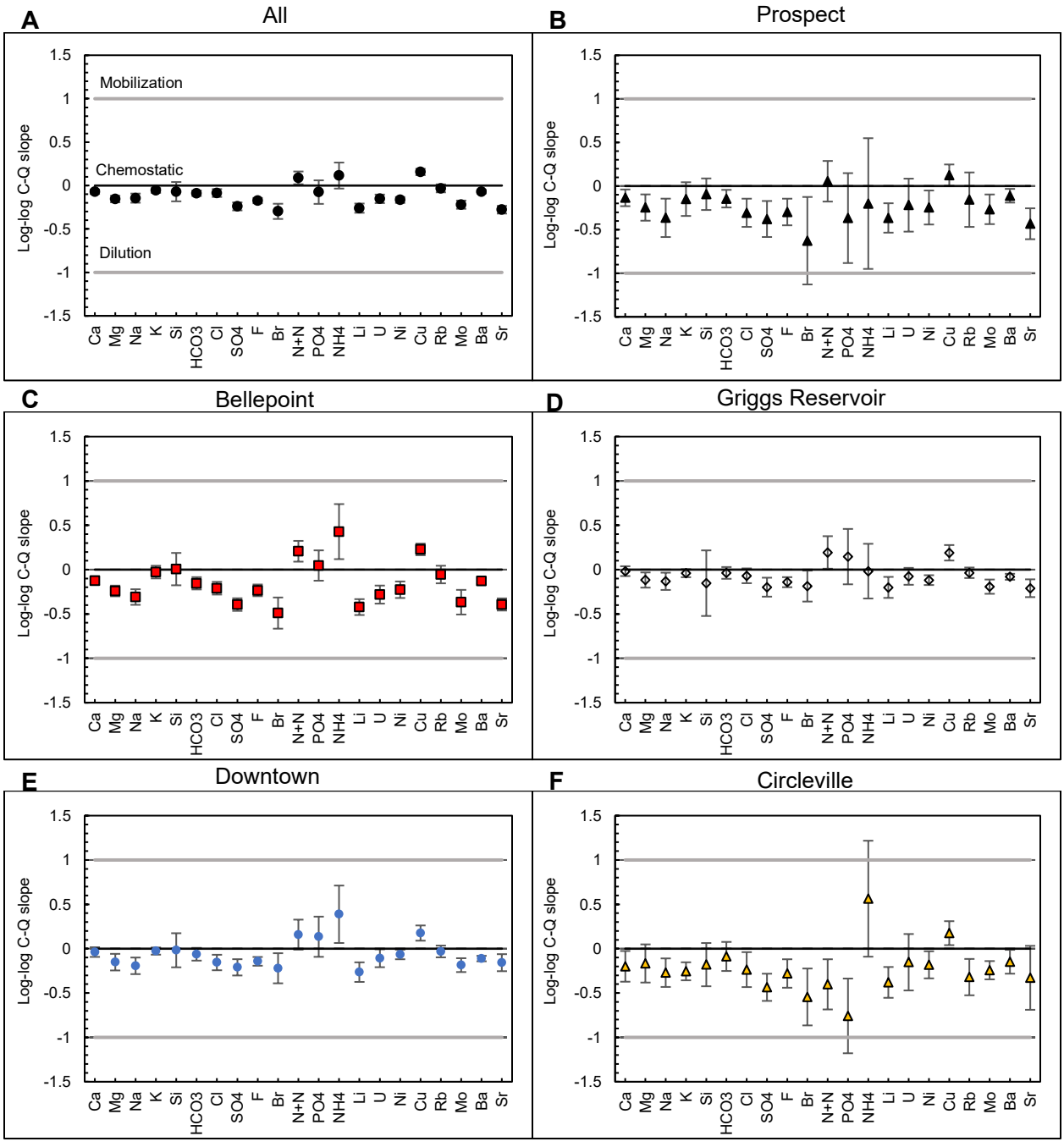

Figure 18. Slope of best fit lines of log C – log Q scatter plots, modeled after Godsey et al. (2019). Simple dilution shown by line y=-1 (labeled in Figure 18A). Chemostatic behavior shown by line y=0. Mobilization behavior shown by line y=+1. A. Samples from all locations. B-F. Samples separated by location. NO_3+NO_2 shortened to 'N+N' in x-axis labels. Error bars represent 95% confidence intervals of calculated log C – log Q slopes.

4.3 Interelement Correlations

Correlation statistics were calculated between analytes for all samples and separately for each location. Spearman's correlation (ρ) is a nonparametric rank-ordered correlation and was chosen because many of the analytes did not have normal distributions and the test is not sensitive to outliers (Helsel et al., 2020). Significance was determined for probability less than 0.05. All correlation coefficients are provided in Appendix D.

Because the Upper Scioto River Basin is dominated by carbonate bedrock, positive correlations with Ca and Mg indicate a geogenic source of solutes. It is assumed that analytes with positive correlations with Ca and Mg are at least partially derived from carbonate mineral weathering or the consequences of this weathering (i.e. neutral to alkaline pH). There are fewer strong and significant correlations at Prospect and Circleville because of fewer samples collected at these locations. Bicarbonate, SO_4, Li, U, and Sr had strong ($\rho > 0.68$) positive correlations with Ca and/or Mg at all locations except for Sr ($\rho = 0.66$), SO_4 at Griggs Reservoir ($\rho = 0.66$) and Circleville ($p > 0.05$), and Li at Circleville ($p > 0.05$) (Table 7). Barium had a strong positive correlation with Ca and/or Mg at Prospect and Bellepoint, and moderate ($0.50 < \rho < 0.68$) correlations with Mg at downtown and Circleville. Sodium, Cl, F, and Br had moderate positive correlations with Ca and/or Mg at Bellepoint, Griggs Reservoir, and downtown. Nickel had a moderate positive relationship with Ca and/or Mg at Prospect, Bellepoint, and Circleville, though the relationship is not statistically significant at Prospect and Circleville. Molybdenum had a moderate positive correlation with Ca and/or Mg at Prospect ($p > 0.05$), Bellepoint, and Griggs Reservoir, and a weak positive correlation at downtown. Copper had a moderate to strong negative correlation with Ca and/or Mg at Prospect, Bellepoint, and Griggs Reservoir, making it the only trace element with a significant negative correlation with Ca or Mg. Correlation coefficients between Ca/Mg and Cu were recalculated after removing the last 15 samples because of high error, but

changes were less than 0.05 units. Values for Ca/Mg – Cu correlations reported in Table 7 include all samples. Rubidium had a weak negative correlation with Mg at downtown but did not display a significant correlation with Ca or Mg at any other sample locations.

Any significant relationships between nutrients and Ca or Mg are negative, indicating that these elements are not predominately geogenic in source and likely show some enrichment with increasing flow, as demonstrated in section 4.2. Nitrate and PO_4 had moderate to strong negative correlations with Ca and/or Mg at Bellepoint and Griggs Reservoir, while NH_4 had a weak to moderate negative correlation with Ca and/or Mg at Bellepoint and downtown, and a strong negative relationship with Mg at Circleville.

Elemental correlations with SO_4 may indicate the influence of shale weathering in the catchment as well, due to the presence of shale bedrock in the eastern Upper Scioto River Basin, interbedded carbonate and shale bedrock, and sulfide and sulfate minerals in glacial tills (Hubbard et al., 1914). Moderate to strong correlations (0.61-0.92) between SO_4 and Ca, Mg, Na, HCO_3, F, Br, and Li are likely related to general bedrock weathering in the catchment which produces proportional amounts of the most soluble elements through mineral dissolution or chemical weathering. Strong correlations between SO_4 and Ca (0.67), Ba (0.70), and Sr (0.90) perhaps suggest the presence of sulfate minerals in carbonate bedrock and glacial till, such as $SrSO_4$ in tills investigated by Curtis & Stueber (1973). Moderate to strong correlations between SO_4 and U (0.64), Ni (0.69), and Mo (0.84), coupled with elevated concentrations of Ni and Mo measured in the fall at Bellepoint suggest an association between these elements and sulfide minerals present in shale bedrock and glacial tills in the watershed.

Because much of the land use in the study area is dominated by agriculture, positive correlations of elements with NO_3+NO_2 may indicate a potential agricultural source, or more generally, a non-geogenic source of constituents, as NO_3+NO_2 concentrations increased slightly with increasing

discharge (discussed in section 4.2). This is likely a result of nutrient rich surface runoff and shallow groundwater from agricultural fields, though tile drainage can impede the relationship of NO_3+NO_2 with discharge (Marinos et al., 2020). Nitrate had moderate to strong negative correlations with Ca, Mg, Na, HCO_3, Cl, SO_4, F, Br, Li, Mo, and Sr at Bellepoint and Griggs Reservoir (Table 8). This supports correlations with Ca and Mg discussed in the previous paragraph, as many of these elements had moderate to strong positive correlations with Ca and/or Mg, indicating a primarily geogenic source. Many of these relationships with NO_3+NO_2 were weak or insignificant at the downtown location, which could be a result of regulated flow from upstream reservoirs, disturbing natural relationships between elements. With the exception of K, Br, PO_4, and Mo, correlations between NO_3+NO_2 and other analytes were weakest or insignificant at downtown when compared to Bellepoint and Griggs Reservoir (excluding Prospect and Circleville because of small sample size). Nitrate also had a moderate to strong positive correlation with PO_4 at Griggs Reservoir, downtown, and Circleville.

Nitrate had a strong positive correlation with Cu at Prospect, Bellepoint, and Griggs Reservoir, a weak positive correlation at downtown (ρ=0.49), and an insignificant relationship in Circleville. These correlation statistics were recalculated after removing the last 15 samples because of significant error, but changes in correlation coefficients were not significant except for at downtown. Correlations between NO_3+NO_2 and Cu went from 0.51 to 0.60 for all samples, 0.70 to 0.81 at Prospect, 0.76 to 0.82 at Griggs Reservoir, 0.49 to 0.60 at downtown, stayed the same at Bellepoint, and were still insignificant at Circleville. These data suggest that an unknown anthropogenic source is contributing Cu to the river. It seems unlikely that Cu is coming from an agricultural source because mean concentrations increase downstream toward Columbus. Instead, the source could be from urban/suburban infrastructure or runoff from impermeable surfaces containing elevated concentrations of trace metals from vehicle wear

	Prospect		Bellepoint		Griggs Reservoir		Downtown		Circleville		All	
	Ca	Mg	Ca	Mg	Ca	Mg	Ca	Mg	Ca	Mg	Ca	Mg
Mg			0.64		0.42						0.52	
Na			0.54	0.52	0.47	0.67	0.39	0.65			0.41	0.45
K												
H_4SiO_4						-0.48						-0.20
HCO_3	0.60		0.82	0.73	0.82	0.72	0.78	0.70	0.88		0.84	0.74
Cl	0.71		0.49	0.50	0.47	0.62	0.37	0.65			0.36	0.42
SO_4	0.79		0.79	0.74	0.49	0.66	0.36	0.70			0.67	0.74
F			0.54	0.46	0.38	0.61		0.61			0.55	0.64
Br			0.52	0.40	0.56	0.72	0.49	0.63	0.69		0.54	0.54
NO_3+ NO_2			-0.61	-0.54	-0.42	-0.61					-0.21	-0.30
PO_4				-0.51	-0.49	-0.81		-0.73				-0.24 (-0.24)
NH_4			-0.41	-0.59				-0.44		-0.73		-0.40 (-0.41)
Li	0.71	0.67	0.78	0.68	0.60	0.81	0.50	0.82			0.72	0.83
U		0.74	0.76	0.78	0.47	0.69	0.41	0.73		0.81	0.58	0.75
Ni			0.56	0.51	0.36	0.49					0.51	0.50
Cu		-0.76	-0.68	-0.73	-0.44	-0.67		-0.47			-0.53	-0.64
Rb								-0.39				
Mo			0.54	0.48		0.63		0.41			0.48	0.60
Ba		0.77	0.81	0.73		0.41		0.61		0.66	0.51	0.60
Sr	0.66		0.81	0.71	0.46	0.73		0.74		0.79	0.64	0.79
Discharge			-0.77					-0.41			-0.42	-0.55

Table 7. Spearman's correlation coefficients between Ca, Mg and all analytes. Blank boxes indicate insignificant relationships ($p > 0.05$). Values in parentheses indicate correlation coefficients between analytes when high PO_4 and NH_4 values at Prospect were removed.

and motor fluids (Sansalone & Buchberger, 1997). Gardner and Carey (2005) observed enriched Cr, Ni, V, Ni, and Zn in runoff from a metropolitan Columbus highway relative to the Olentangy River. Directions of correlations (positive or inverse) between NO_3+NO_2 and many analytes reversed at Circleville, where NO_3+NO_2 had a moderate positive correlation with Cl, Br, Rb, and Mo, and strong positive correlations with Na, K, Si, SO_4, F, PO_4, and Li (Table 8). Nitrate had a weak to moderate positive correlation with discharge at Bellepoint and for the whole dataset, but this reversed at Circleville (ρ= -0.75), indicating dilution of NO_3+NO_2 at Circleville. This may be explained by the convergence of three tributaries just north of this sampling point, causing the strong dilution of NO_3+NO_2, and might lead to the positive correlations of NO_3+NO_2 with many geogenic elements at Circleville. The drainage area of Big Walnut Creek, which joins the Scioto River 31 kilometers above Circleville, is 18% of the drainage area of the Circleville site and contributed an average of 27% of the Scioto River's daily flow, calculated using USGS gage measurements during the study period at this location. In contrast to Circleville, the land use of Big Walnut Creek is nearly equal amounts of agricultural and developed land cover (30% and 37%, respectively), as it drains the eastern half of the Columbus metropolitan area. Forests cover almost 20% of the drainage area. For reference, the drainage basin of Circleville (the same as entire Upper Scioto River Basin) is comprised of 56% agricultural land, 21% developed, and 12% forested. The difference in percentage of agricultural land and forested area may help contribute to the change in the NO_3+NO_2 – Q relationship seen at Circleville. Less agricultural activity and more forest cover could lead to lower concentrations of NO_3+NO_2 in Big Walnut Creek, which then dilutes NO_3+NO_2 concentrations in the Scioto River.

Additionally, Big Walnut Creek drains two lacustrine-type reservoirs (Alum Creek Lake and Hoover Reservoir), and the majority of agricultural land cover in this drainage basin is upstream of these reservoirs. Biological uptake of nutrients promoted by longer residence times of water and

denitrification in deep reservoir waters could decrease NO_3+NO_2 concentrations, so the influx of nutrients from agricultural land could be buffered by this. This would lead to lower concentrations of NO_3+NO_2 downstream of the reservoirs. Allen (2011) found mean NO_3+NO_2 concentrations in Griggs and O'Shaughnessy Reservoirs to be more than double that of Alum Creek Lake and Hoover Reservoir. In contrast, Big Darby Creek contributes an average of 14% of the Scioto River's daily flow at Circleville and drains 17% of Circleville's drainage area in the western part of the basin. Big Darby Creek has even greater agricultural cover (69%) and less urban area (10%) than the drainage area of the Scioto River at Circleville and is similar to the drainage area of Bellepoint, which has a moderate positive correlation between NO_3+NO_2 and discharge. The third tributary that joins the Scioto River just north of Circleville is Walnut Creek, which made up 7% of the Scioto River's average daily flow and drains only 9% of Circleville's drainage basin, has land use very similar to that of the entire Circleville drainage basin and Upper Scioto River Basin (53% agricultural, 18% urban, 13% forested).

	Prospect	Bellepoint	Griggs Reservoir	Downtown	Circleville	All
Ca		-0.61	-0.42			-0.21
Mg		-0.54	-0.61			-0.30
Na		-0.60	-0.81	-0.46	0.76	-0.44
K				0.40	0.77	0.32
H_4SiO_4		0.47	0.40		0.69	0.42
HCO_3	-0.59	-0.64	-0.50	-0.38		-0.31
Cl		-0.60	-0.70	-0.38	0.63	-0.40
SO_4		-0.59	-0.72	-0.48	0.75	-0.36
F		-0.56	-0.64	-0.46	0.83	-0.29
Br		-0.49	-0.79	-0.58	0.62	-0.40
PO_4			0.78	0.63	0.68	0.59 (0.61)
NH_4						
Li	-0.72	-0.67	-0.75	-0.39	0.70	-0.35
U		-0.49				-0.20
Ni		-0.37	-0.51			-0.21
Cu	0.71	0.78	0.76	0.49		0.51
Rb					0.67	
Mo		-0.47	-0.61	-0.58	0.66	-0.33
Ba		-0.51				
Sr		-0.70	-0.73	-0.37		-0.31
Discharge		0.51			-0.75	

Table 8. Spearman's correlation coefficients between NO_3+NO_2 and all analytes. Blank boxes indicate insignificant relationships ($p > 0.05$). Values in parentheses indicate correlation coefficients between analytes when high PO_4 and NH_4 values at Prospect were removed.

4.4 Influence of Reservoirs

The presence of dams has been shown to increase diatom uptake of Si behind dams as water sits for extended periods of time (Humborg, 1997). Rakowsky (2000) measured low dissolved Si concentrations (25 and 37 μM) behind the Delaware Dam on the Olentangy River and attributed this to uptake by diatoms. Dissolved Si concentrations in several samples had values that deviated from the overall relationship with discharge. Values that departed from the general chemostatic behavior of H_4SiO_4 were only observed in those sampling locations closest to the reservoirs. Evidence of H_4SiO_4 uptake was shown by the exceptionally low concentrations of dissolved Si measured at Bellepoint, Griggs Reservoir, and downtown in the spring (Figure 19). These low concentrations were also likely affected by dilution during a high flow event. Dissolved Si concentrations below 1 μM are close to or less than dissolved Si concentrations measured in 6 of 24 field blanks (Appendix C), so sample concentrations

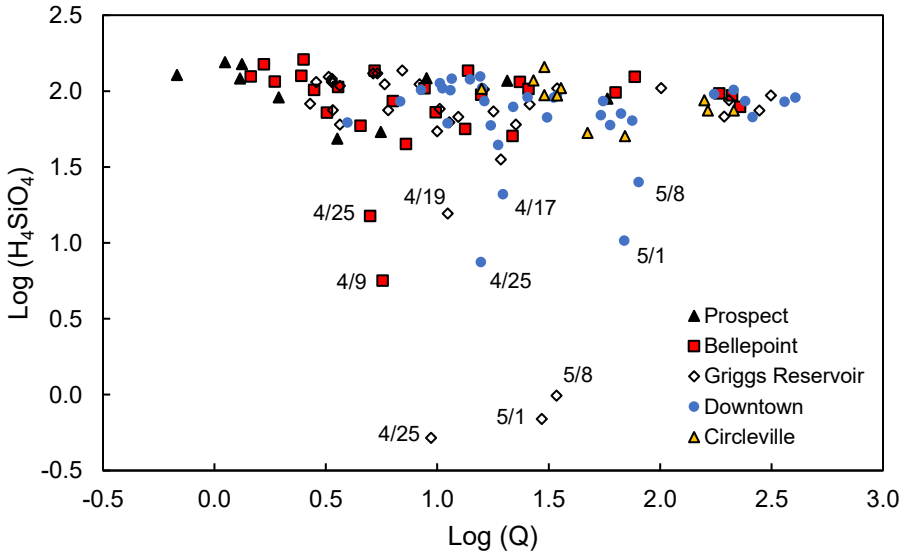

Figure 19. H_4SiO_4 versus discharge. Log dissolved Si (μM) and log discharge (m^3/s) at all locations.

cannot be stated with certainty, but it can be said that several exceptionally low concentrations of dissolved Si were measured during the study at locations in or just downstream of dams. Water collected at Bellepoint, Griggs Reservoir, and downtown has experienced extended residence times within reservoirs as these sample locations are within or only a few kilometers downstream of a dam.

Concentrations of dissolved Si over the sampling period showed influences of both discharge variations and biological activity. The lowest H_4SiO_4 concentrations were recorded in spring (Figure 20), when diatom blooms most often occur because of cooler temperatures (Sun J. et al., 2001; Waite et al., 1992). This spring low in dissolved Si concentrations coincided with a large precipitation event at the beginning of May as noted previously, but concentrations at Prospect, Bellepoint, Griggs Reservoir and downtown began decreasing in early March. These lower H_4SiO_4 concentrations were likely first driven

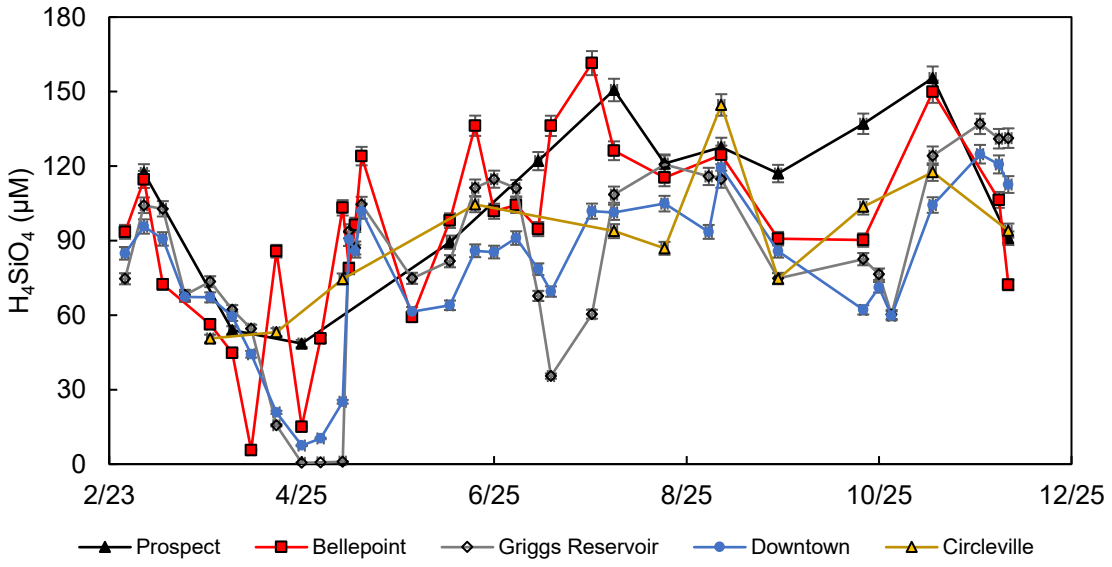

Figure 20. Dissolved Si concentrations over study period at each location. Error bars represent average precision of H_4SiO_4 analysis.

by the uptake by diatoms and compounded by dilution effects from the precipitation event, resulting in near zero values for dissolved Si concentrations measured in Griggs Reservoir at this time. Samples from Prospect and Circleville did not reach such low concentrations like those at Bellepoint, Griggs Reservoir, and downtown, which could reflect the extended holding time in reservoirs, allowing for the uptake of H_4SiO_4. However, Prospect and Circleville were not sampled during the May precipitation event where dissolved Si concentrations were nearly zero, but H_4SiO_4 at Prospect were typically higher than at Griggs Reservoir and downtown at all flow volumes. After May, concentrations increased into September, when concentrations decreased again until reaching lows at all locations in September or October. This is potentially indicative of a fall diatom bloom of a smaller magnitude. Sun et al. (2001) measured peaks in diatom cell abundance in the Bohai Sea, China and found a primary peak of diatom abundance in April and a secondary peak in September, supporting the trend in H_4SiO_4 observed in this study. Dissolved Si concentrations in the Scioto River then increased at all locations until another decrease at the end of the study period in early December. Allen (2011) analyzed algal concentrations in O'Shaughnessy Reservoir from 2003-2008 and found that the highest monthly mean diatom abundances were recorded in May and June, followed by December and March, similar to what is indicated by dissolved Si concentrations measured in this study. There is another notable low in dissolved Si concentrations in mid-July at Bellepoint, Griggs Reservoir, and downtown that also coincided with a high flow event (Figure 20).

Mean NH_4 concentrations were highest at Griggs Reservoir, with the greatest difference in NH_4 concentrations between Griggs and other locations from August to December, with the exception of the anomalous NH_4 concentrations measured at Prospect (Figure 21). We attribute this to the discharge of deep-water richer in NH_4 from O'Shaughnessy Reservoir into Griggs Reservoir. According to the City of Columbus who manages reservoir operations, there are three gates on O'Shaughnessy Dam near the

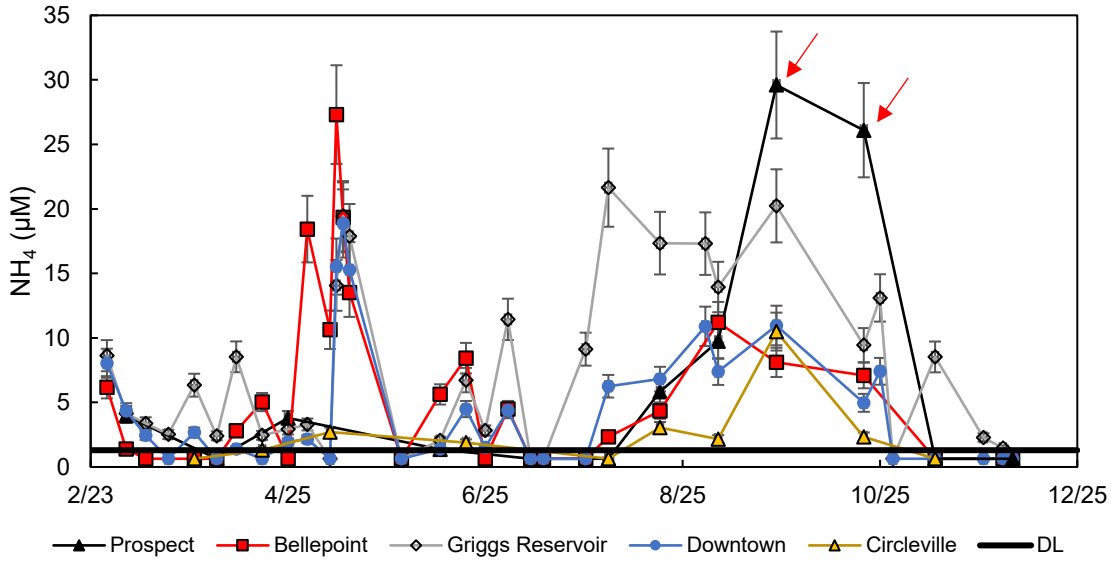

Figure 21. Dissolved NH_4 concentrations over study period at each location. Solid black line indicates NH_4 detection limit (1.3 µM). Error bars represent average precision of NH_4 analyses (14%), although most precision measurements were below 6%. Concentrations of data points indicated by red arrows were divided by 4 to fit on graph.

top, middle and bottom of the dam, that are opened to release water from O'Shaughnessy Reservoir into Griggs Reservoir. Releases from O'Shaughnessy into Griggs Reservoir were likely greater during this period (August to December) to sustain the level of Griggs Reservoir during the drier part of the year, leading to higher concentrations of NH_4 in Griggs Reservoir. Fourteen samples had NH_4 concentrations below 0.36 µM, the average concentration measured in field blanks.

4.5 Influence of Agriculture

Seasonal trends in NO_3+NO_2 concentrations reflect agricultural and biological influences. Nitrate concentrations at Bellepoint, Griggs Reservoir, downtown decreased from the start of the sampling period through late April, until concentrations peaked during the heavy precipitation event in early May

2021. Nitrate concentrations also were greatest at these locations during this storm event, then decreased until November. Nitrate concentrations during this storm event were greatest at Bellepoint (Prospect and Circleville were not sampled during this event) likely as a result of surface runoff and shallow subsurface discharge of nutrient rich waters from recent fertilizer application. The decrease in NO_3+NO_2 concentrations leading up to this event were likely driven by biological uptake as air temperatures began to increase with the onset of spring, and concentrations decreased again after this event, again likely resulting from biological activity in the river. Concentrations then increased again at these three locations in November, probably due to a decrease in biological activity as temperatures dropped and sunlight decreases into the late fall and winter. Prospect shows similar trends with the highest NO_3+NO_2 concentrations in early summer and winter, and lowest concentrations in early spring and late summer/fall. Concentrations at Circleville were less variable than at other locations (perhaps due to lower sampling frequency) and averaged ~250 μM for most of the study period (except for two samples collected in late August and September where concentrations were ~75 μM). Nitrate concentrations measured in the Scioto River never exceeded the EPA Drinking Water Limit of 10 mg/L NO_3-N (714 μM), but the highest NO_3+NO_2 concentration measured at Bellepoint was measured at 9.1 mg/L NO_3-N (650 μM) during high flow in May.

Large-scale fertilizer application has led to increased N concentrations and thus high N:P ratios in rivers in agricultural areas, evident in the Scioto River system (Berner & Berner, 2012). N:P ratios were greater than the Redfield ratio of 16:1 in all but six samples and showed similar seasonal trends as NO_3+NO_2 concentrations. The highest N:P ratios were observed in spring and the lowest in fall, the same pattern observed in an agricultural watershed in Vermont by Kincaid et al. (2020). Mean N:P ratios were greatest at Griggs Reservoir and downtown, and lowest at Prospect and Circleville. Griggs Reservoir and downtown had the lowest dissolved PO_4 concentrations, which may be attributed to biological uptake

and/or adsorption onto particles, enhanced by extended residence times in the reservoirs. Two samples from Griggs Reservoir had PO_4 below the detection limit (0.13 μM). Nitrate yields were greatest at Bellepoint, downtown, and Prospect, but were not found to correlate with percent agricultural land use in the drainage area of each sample point (Figure 22). This relationship may be masked by the input of NO_3+NO_2 from urban sources in and around Columbus, or from the input of the Olentangy River, which drains both developed and agricultural land. Phosphate yields were greatest at Prospect, followed by Circleville and Bellepoint, again likely due to runoff from agricultural fields.

	Average N:P	Range N:P	Discharge-weighted mean NO_3+NO_2 (μM)	Discharge-weighted mean PO_4 (μM)	Discharge-weighted NO_3+NO_2-N yield (ton/km^2/yr)	Discharge-weighted PO_4-P yield (ton/km^2/yr)
Prospect	43 (50)	4.3-131	271	8.2 (5.0)	1.19	0.079 (0.049)
Bellepoint	77	15-181	398	5.0	1.35	0.038
Griggs Reservoir	235	39-1506	270	3.1	0.926	0.024
Downtown	132	32-402	240	2.7	1.19	0.029
Circleville	51	15-119	182	4.1	0.862	0.043

Table 9. Discharge-weighted mean dissolved NO_3+NO_2 and PO_4 concentrations and yields and N:P molar ratios. Values in parentheses indicate the calculated value without anomalous PO_4 concentrations.

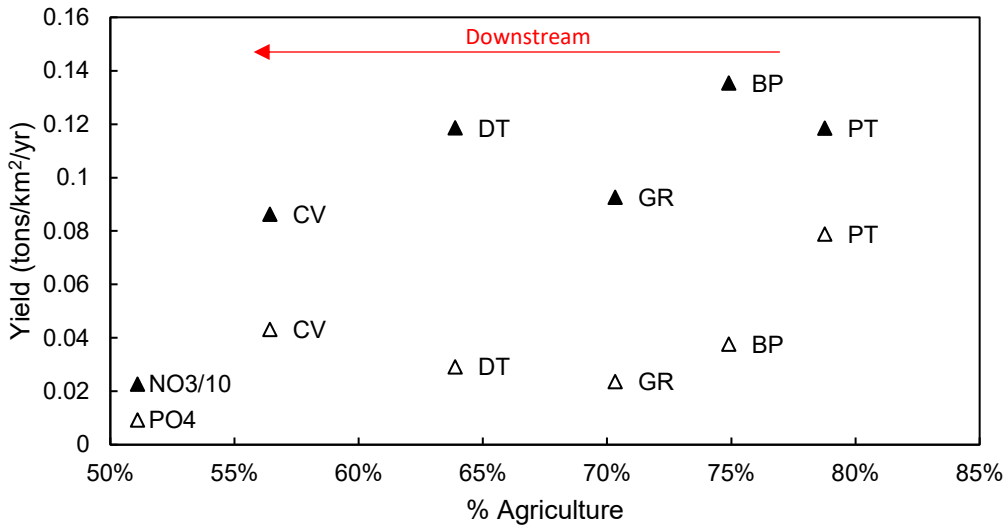

Figure 22. Discharge-weighted yields of dissolved NO_3+NO_2 and PO_4 by percent agricultural land use. NO_3+NO_2 yields were divided by 10 to plot in the same range as PO_4 yields. Yields reported in metric tons/km^2/yr. Closed triangles represent NO_3+NO_2 yields (divided by 10) and open triangles represent dissolved PO_4 yields. Data labels indicate sample location, where PT= Prospect, BP= Bellepoint, GR= Griggs Reservoir, DT= downtown, and CV= Circleville.

4.6 Influence of Urban Areas

NO_3+NO_2 yields versus developed land cover reveal a dilution of NO_3+NO_2 as the river flows from Bellepoint to Griggs Reservoir, demonstrating the decreasing influence of agricultural runoff on nutrient input as developed areas increase downstream (Figure 23). However, NO_3+NO_2 yields increased at downtown, which could indicate a source of NO_3+NO_2 from urban areas, as discussed previously. An urban input of NO_3+NO_2 between downtown and Circleville is complicated by the added agricultural land use between downtown and Circleville, though Big Walnut Creek, which joins the river upstream of Circleville, is 37% developed and drains the eastern half of metropolitan Columbus.

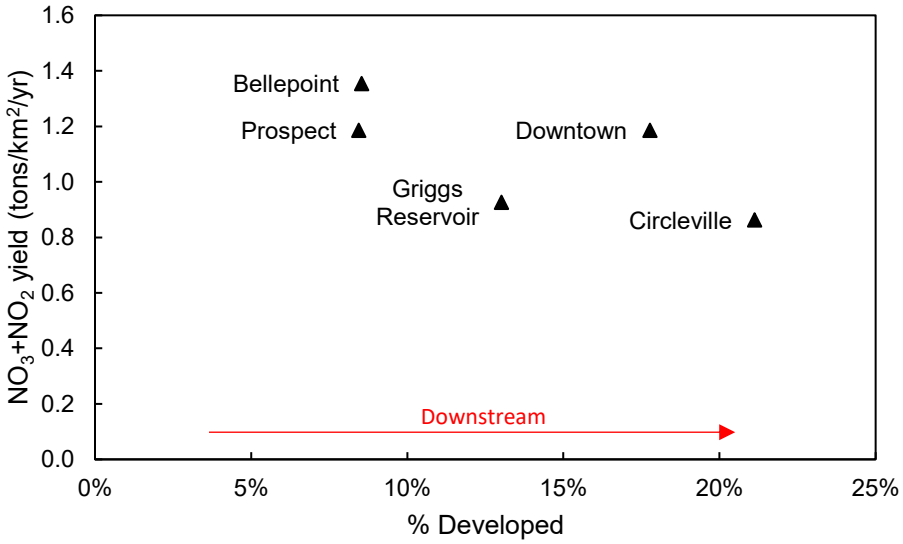

Figure 23. Discharge-weighted yields of dissolved NO_3+NO_2 by percent of developed land in drainage area. Yields reported in metric tons/km^2/yr.

Additionally, the effects of urbanization in Columbus are evidenced by a significant increase in Cu yields at the downtown location, while yields are similar at all other sample locations (Figure 24). The Cu yield at downtown is 20-40% greater than that measured at all other locations, indicating an urban input of Cu from the city of Columbus. Anthropogenic sources of Cu to the environment include fossil fuel combustion products, wastewater or industrial discharges, vehicle and tire wear, and fertilizer (Kaushal et al., 2020; Otero et al., 2005; Sansalone & Buchberger, 1997). Because Cu yields decreased at Griggs Reservoir and increased again at the downtown site, we conclude that fertilizer is not the primary source of elevated Cu yields in downtown. Stucker and Lyons (2017) measured Cu in the Olentangy River 5 kilometers north of the confluence with the Scioto River in July 2010 and April 2011, and recorded concentrations of 29 and 60 nM, similar to concentrations measured in the Scioto River. They also found a correlation between Cu concentrations in first order urban streams and green space in urban areas. They suggested that the source of Cu could originate from $CuSO_4$ additions used to control algal blooms

in ponds and artificial water features in urban green spaces. Because Cu yields are highest at downtown, a pattern not seen in any other trace elements, we attribute this to a source of Cu from urban areas such as runoff from impermeable surfaces. One potential source of Cu in urban runoff is brake pad wear as Cu is used in brake pads for its frictional and thermal conductivity properties, and as a result has been regulated by the EPA because of its toxic effects on aquatic life at high levels (EPA, 2015). Elevated levels of Cu have also been found in wastewater treatment plant effluent, with contributions from industrial discharges and leaching from pipes (Oskarsson & Norrgren, 1998). Small wastewater treatment plants may contribute to major and trace element concentrations at locations upstream of downtown Columbus, but the influence of larger wastewater treatment plants such as those that treat water from metropolitan Columbus (located downtown of Columbus) was not investigated in this study.

Additional anthropogenic sources of Cu include runoff of manure applied to agricultural fields, which may influence Cu concentrations observed in this study and the mobilization trend of Cu observed

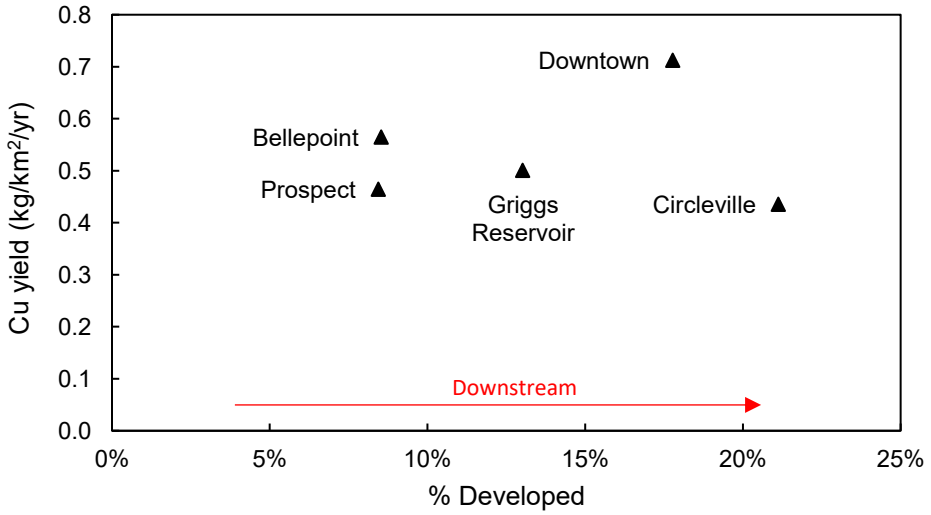

Figure 24. Yields of dissolved Cu by percent of developed land in drainage area. Yields reported in kg/km^2/yr.

at agricultural locations upstream of metropolitan Columbus. Copper is added to livestock feed as a micronutrient and to fungicides for use on agricultural fields, and excess Cu can build up in soils when livestock manure is applied as fertilizer to agricultural fields (Brock et al., 2006; Ogiyama et al., 2005). Bellepoint had the second greatest Cu yield and the highest discharge-weighted mean Cu concentration, indicating a potential source of Cu from unknown agricultural sources.

Elements considered to be geogenic in source (based on previously discussed analyses) show a regular pattern of yields decreasing from Prospect to Griggs Reservoir then increasing in downtown and reaching a maximum at Circleville, though the differences between locations vary significantly (Table 10). One complicating factor is the smaller number of samples collected at Prospect and Circleville. Flow volume on 6/11/2021 at Prospect accounted for more than half of the total flow volume sampled, heavily skewing the discharge-weighted yields. Higher flow volume on this day diluted concentrations of geogenic analytes, resulting in lower yields. If this sample is removed, yields at Prospect for Ca, Mg, Na, HCO_3, Cl, SO_4, F, Br, Li, U, Ni, Mo, Ba and Sr increase and are close to or greater than yields at Circleville. However, removing this point leads to lower NO_3+NO_2 and Cu yields, suggesting that these are mobilized during high flows, while the other analytes decreased with higher flow at Prospect.

Yields of Li, Mo, Rb, Ba, and Sr decreased from Prospect to Griggs Reservoir and increased at the downtown site and again at Circleville. Yields of U and Ni decreased slightly from Prospect to Bellepoint then increased to downtown and decreased slightly in Circleville. However, the 6/11/2021 sample from Prospect heavily weights the yields of these elements. Removing this sample increases the U yield at Prospect from 0.40 kg/km^2/yr to 0.71 kg/km^2/yr, higher than any other location. Yields of Ni increase from 1.3 kg/km^2/yr to 1.8 kg/km^2/yr, while Cu yields decrease from 0.46 kg/km^2/yr to 0.42 kg/km^2/yr. Based on the interpretation of log C – log Q relationships, the source of U and Ni are primarily geogenic and are not input in any large quantity from the urban environment. Additionally, the increase in trace

elements in downtown may be partially attributed to the joining of the Olentangy River, which partially drains Devonian black shales that are enriched in U, Ni, Cu, Rb, and Mo relative to the average upper continental crust (Wedepohl, 1995; Leventhal, 1979). Lithogenic contributions of these trace and minor elements should vary with Ca and/or Si yields and will be further evaluated in the future.

		Prospect		Bellepoint		Griggs Reservoir		Downtown		Circleville	
		Mean	Yield	Mean	Yield	Mean	Yield	Mean	Yield	Mean	Yield
μM tons/km^2/yr	Ca	1070	13.3	1050	10.2	1200	11.8	1180	16.6	1180	16.1
	Mg	635	4.81	571	3.36	705	4.18	701	5.98	882	7.24
	Na	786	5.65	573	3.19	937	5.28	1080	8.75	1520	11.8
	K	121	1.48	126	1.20	113	1.08	113	1.56	104	1.38
	Si	98	0.86	92	0.63	79	0.55	80	0.79	81	0.77
	HCO_3	2400	45.7	2150	31.9	2560	38.2	2500	53.7	2950	61.1
	Cl	709	7.86	709	6.10	1100	9.53	1230	15.4	1510	18.2
	SO_4	465	14.0	345	8.03	467	11.0	489	16.6	550	17.9
	F	14	0.085	12	0.054	12	0.056	13	0.086	17	0.11
	Br	0.47	0.012	0.27	0.0052	0.28	0.0055	0.30	0.0085	0.48	0.013
	NO_3+NO_2 (as N)	271	1.19	398	1.35	270	0.926	240	1.19	182	0.862
	PO_4 (as P)	8.2 (5.0)	0.079 (0.049)	5.0	0.038	3.1	0.024	2.7	0.029	4.1	0.043
	NH_4 (as N)	9.1 (2.0)	0.040 (0.009)	14	0.048	10	0.035	8.3	0.041	3.8	0.018
	Sr	13	0.35	9.3	0.20	12	0.26	12	0.36	12	0.36
nM tons/km^2/yr	Li	450	0.97	350	0.58	450	0.77	470	1.2	630	1.5
	U	5.4	0.40	4.4	0.26	6.1	0.35	6.1	0.51	5.2	0.42
	Ni	69	1.3	59	0.85	57	0.83	59	1.3	55	1.1
	Cu	24	0.46	37	0.56	32	0.50	32	0.71	20	0.44
	Rb	14	0.38	11	0.22	10	0.21	12	0.35	16	0.46
	Mo	51	1.5	44	1.0	42	0.99	46	1.6	59	1.9
	Ba	250	11	230	7.7	260	8.7	270	13	350	16

Table 10. Discharge-weighted means and annual yield of analytes at each location. Means reported as μM or nM (indicated by leftmost column). Yields of major ions, nutrients, and Sr reported as metric tons/km^2/yr. Yields of trace elements reported as kg/km^2/yr. Values in parentheses represent mean/yield calculated after removing anomalous PO_4 and NH_4 concentrations at Prospect.

4.7 Stable Water Isotopes

Stable water isotopes were further evaluated to discern differences between samples collected from the reservoirs and other locations, particularly the downtown site, to elucidate effects of the reservoirs on isotopic composition. The difference in $\delta^{18}O$ and δD between Bellepoint and Griggs is

greater than the difference between Griggs and downtown. Differences in $\delta^{18}O$ and δD between locations were greatest in the spring. This could be because of the greater distance between Bellepoint and Griggs Reservoir versus Griggs Reservoir and downtown, allowing for more evaporation to take place in the two reservoirs or that water releases from the reservoir are not always from similar depths. Generally, high flow events in the system correlated with isotopic compositions that were very similar among sample locations, as large volumes of water flowed quickly through the system. However, the sample collected at Griggs Reservoir on 9/23/2021 showed a clear deviation from this pattern (Figure 25). Investigating the hydrographs at each location and precipitation events over the study period (Figures 6 and 7), a precipitation event and resulting high flow event occurred 1-2 days before the samples were collected. However, the hydrograph for Griggs Reservoir shows a very minimal increase in discharge compared to other locations. Isotopic values for Prospect, downtown, and Circleville are similar for samples collected on this day ($\delta^{18}O$ =-7.36, δD =-47.35) (Figure 14). Bellepoint had slightly heavier values than this ($\delta^{18}O$ =-6.54, δD =-44.91), but Griggs Reservoir was far removed from the other samples at this time, with $\delta^{18}O$ =-5.59 and δD =-36.8. Preceding this precipitation event, discharge at Bellepoint and Griggs Reservoir had remained at baseflow conditions since early August. Based on USGS reservoir elevations, it appears that during this time, O'Shaughnessy Reservoir was releasing significant amounts of water to sustain the level of Griggs (Figure 26), and O'Shaughnessy elevations dropped 1.2 meters from August to late September, while the elevation of Griggs only dropped ~0.1 meter. This decrease in O'Shaughnessy elevation continued until the precipitation event around 9/22/21, where levels increased close to 1.1 meters. Releases of isotopically enriched deep water from O'Shaughnessy Reservoir likely led to a heavier signature downstream in Griggs Reservoir.

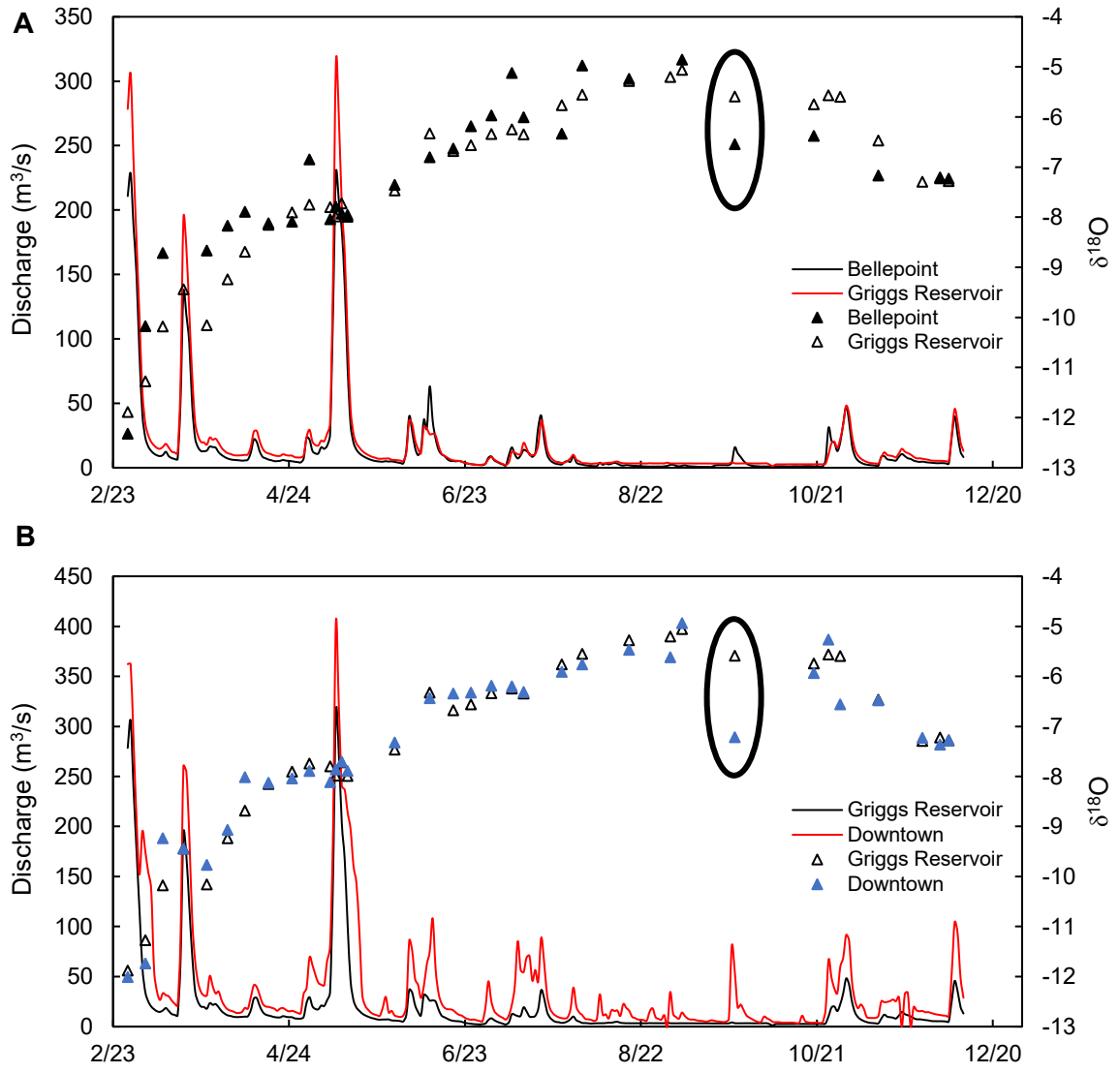

Figure 25. Discharge and $\delta^{18}O$ for Bellepoint, Griggs Reservoir, and downtown samples. A. Bellepoint and Griggs Reservoir. B. Griggs Reservoir and downtown. Circled samples are discussed further in discussion regarding the relatively large separation between locations relative to samples collected during the same time period. Error bars are smaller than symbols.

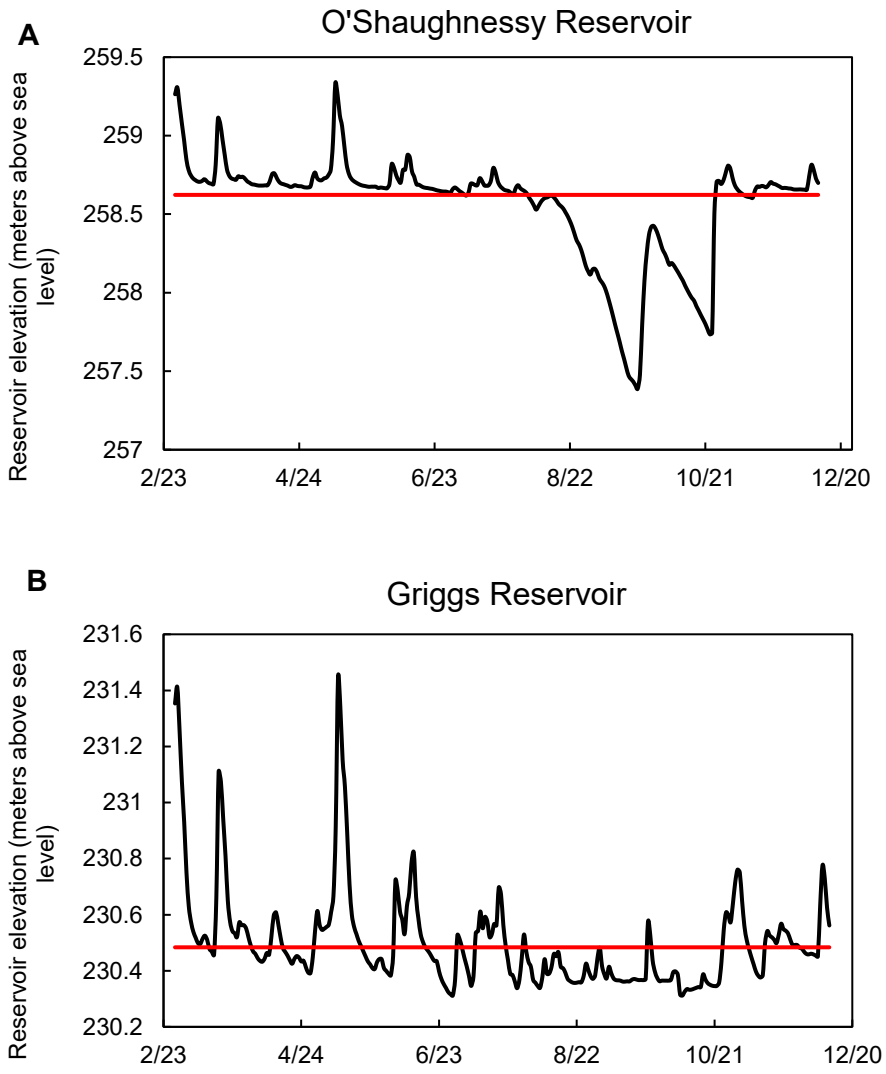

Figure 26. Reservoir elevations for O'Shaughnessy and Griggs reservoirs. Reservoir elevations in meters above sea level. A. O'Shaughnessy Reservoir. B. Griggs Reservoir. Red lines represent spillway heights at the dam.

There is a noticeable deviation between a number of river samples and the local meteoric water line at isotopic values between $\delta^{18}O$ =-7.47- 8.0 and δD =-40.97- -45.7 (Figure 15). This group of samples was collected between 5/10/21-5/14/21 at Bellepoint, Griggs Reservoir, and downtown (Prospect and Circleville were not samples these days). A major precipitation event occurred during this time, resulting in the greatest discharges during the study period. In central Ohio, most summer storm tracks are derived from Gulf of Mexico moisture sources (Leslie et al., 2014; Walsh et al., 1982). However, this

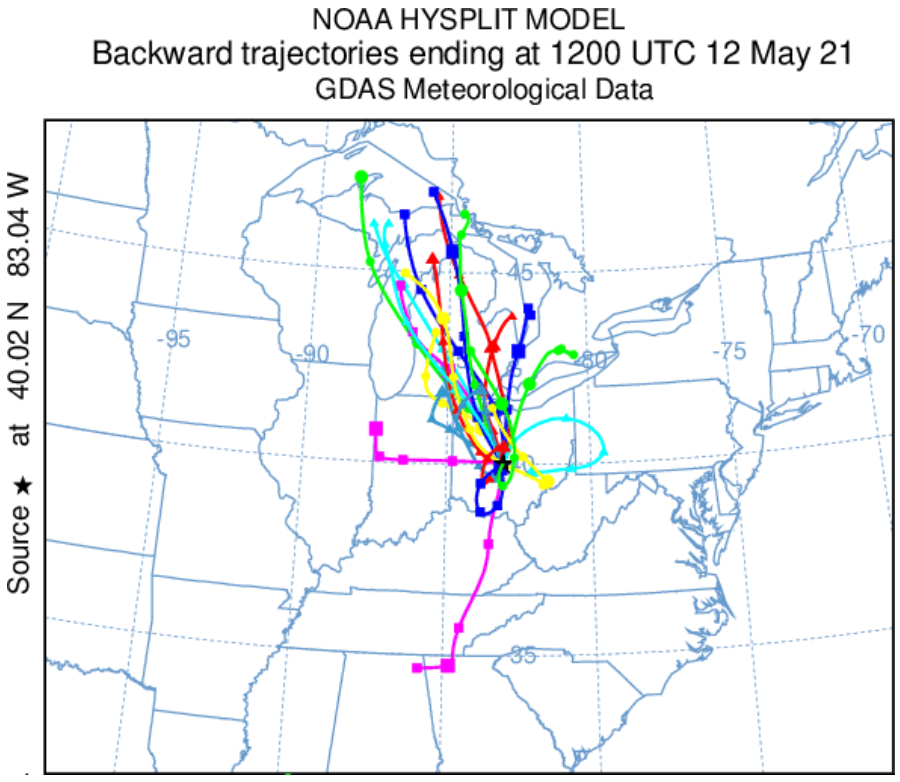

Figure 27. NOAA HYSPLIT model for the precipitation event in early May from https://www.ready.noaa.gov/HYSPLIT_traj.php. Trajectories show storm tracks from the Great Lakes region into central Ohio.

storm in May originated in the Great Lakes region, according to a NOAA HYSPLIT model (Figure 27). A different moisture source likely caused the anomalous $\delta^{18}O$ and δD values measured in the river at this time. While these data plot above the LMWL, they are similar to historic precipitation data used to calculate the LMWL that are characteristic of central Ohio precipitation (Smith et al., 2021).

4.8 Comparison with Existing Data

Data from selected studies of the geochemistry of the Scioto River were compiled to evaluate changes over time. Calcium, Na, and Mg concentrations were measured along the length of the river in May 1973, November 1992, and July 2000- July 2001. Data collected in 1973 were analyzed with the 1992 samples, so concentrations are expressed as molar ratios relative to Mg to minimize the effects of evaporation during storage (Hicks, 1994). Data from July 2000-2001 and 2021 (this study) are averages of all samples collected from the respective locations during the study period, excluding high flow data. Rabb (2005) collected his samples in July 2000-July 2001 and compared these data with the 1973 and 1992 data of Hicks (1994). The comparison of all these data could prove insightful in revealing any changes in major ion chemistry in the last ~50 years.

Ca/Mg ratios are relatively constant downstream in the 1992, 2000-2001, and 2021 datasets, but show considerable variability in the 1973 study period (Figure 23A). Ca/Mg ratios decreased over time from the 1992 dataset to 2021. In contrast, Na/Mg ratios increase downstream in all datasets and increased from 1973 to 2021. Particularly after 140 kilometers downstream, the difference in Na/Mg ratios between datasets is the greatest. This location corresponds with the location of metropolitan Columbus; Griggs Reservoir (in a suburb of Columbus) is roughly 140 kilometers downstream, and downtown Columbus is about 150 kilometers downstream. This increase in Na/Mg starting in metro Columbus is likely a result of the increased use of road deicing salt in and around the city. The

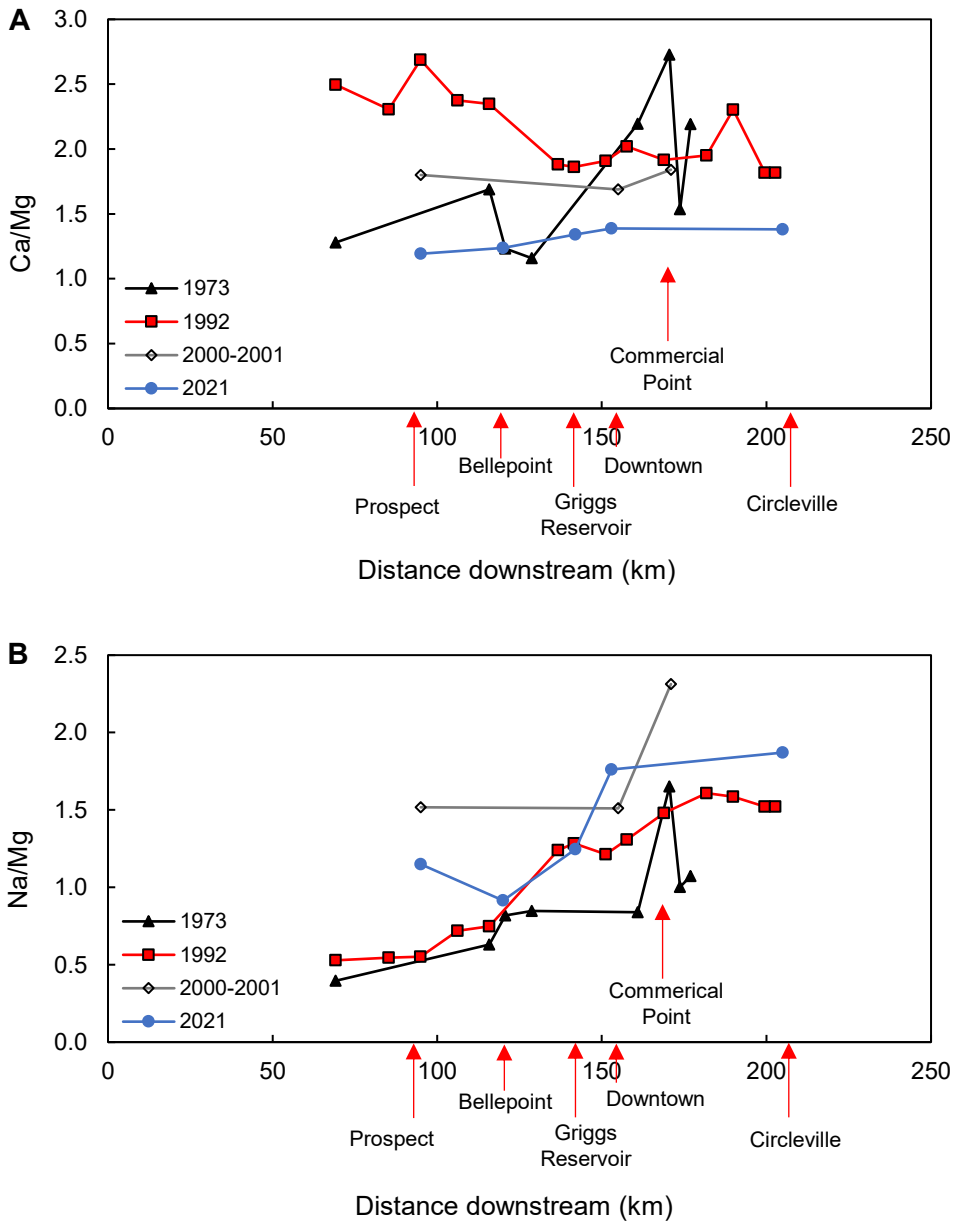

Figure 28. Ca and Na concentrations compared to existing studies. Major cation concentrations ratioed to Mg as a function of distance downstream. Data from 2000-2001 and 2021 (this study) excludes high flow data. 1973 and 1992 data from Hicks (1994). 2000-2001 data from Rabb (2005). 1973 data collected in May, 1992 data collected in November, 2000-2001 data collected monthly from July-October 2000 and bimonthly from February-July 2001. 2021 data is average of analytes at each location excluding samples where discharge was greater than the 50th percentile of the 30-year average for that day (explained in detail in Appendix B).

wastewater treatment plants that receive the city's wastewater are roughly 170 kilometers downstream at Commercial Point, and peaks in Ca/Mg and Na/Mg occur at or near this point in 1973 and Na/Mg in July 2000-2001. Treated wastewater has been shown to have high Na concentrations, so discharges from the wastewater treatment plant could be contributing excess Na (Kaushal et al., 2020). These data exhibit an urban influence on Na concentrations relative to Ca in both time and space, reflecting an increase in Na/Mg ratios as the river flows through metropolitan Columbus, with the greatest increase in Na/Mg over time observed in the urbanized portion of the river. These data suggest that the wastewater discharge also had elevated Ca concentrations relative to Mg as well.

Sodium and Cl concentrations are high relative to the Mississippi River and "unpolluted" world rivers (Meybeck, 1979). Dailey (2014) observed increases in Na and Cl in both the Olentangy River and Darby Creek as they approached downtown Columbus. Gardner and Carey (2004) measured Na and Cl concentrations in a stormwater outfall that partially drained State Route 315, a major highway in central Ohio, and flowed into the Olentangy River. They found that average Na and Cl concentrations in road runoff were 19 and 15 times greater than concentrations in the river during a precipitation event that occurred soon after the application of road deicing salt. Historical analysis of Na and Cl concentrations and fluxes measured in the Hocking River at Athens, Ohio, demonstrated increasing Na and Cl concentrations and higher Cl fluxes beginning in the 1960s, with the highest concentrations measured from October to December and the highest fluxes in January to April (Dailey et al., 2014). The same trend in concentrations was observed at the Little Miami River in Ohio, where Na and Cl concentrations increased from the mid 1960s-90s, attributed to the onset of the large-scale application of road salt.

In this study, mean Na and Cl concentrations and fluxes were highest at downtown and Circleville, which have the greatest developed area in their watersheds compared to upstream sampling locations. As noted above, Circleville also receives discharge from the Columbus wastewater treatment

facilities. Na and Cl fluxes were greatest from February to May due to several major precipitation events that occurred in this period. This period also represents the months that deicing salts would have been recently applied. Cl:Br ratios are useful in identifying the source of these ions to the environment because of the concentrations of Cl and Br in precipitation versus salt. Bromide is more soluble than Cl, so as water evaporates, Cl will preferentially be evaporated out, leaving behind a brine with higher Br concentrations (Davis et al., 1998). Davis et al. (1998) found that waters affected by halite dissolution generally have Cl:Br ratios between 1000-10000. Mass ratios of Cl/Br ranged from 233 to 5064. It should be noted that Br concentrations below the detection limit were set equal to half the detection limit. This affected the following number of samples at each location: Prospect: 3 out of 10; Bellepoint: 8 out of 27; Griggs Reservoir: 11 out of 34; downtown: 10 out of 34; Circleville: 1 out of 11. The mean Cl:Br mass ratios were greater than 1000 at all locations, indicative of halite contamination (Table 11). Griggs

	Mean Cl (mg/L)	Mean Cl:Br mass ratio	Median Cl:Br
Prospect	51	1062	711
Bellepoint	43	1127	1022
Griggs Reservoir	44	1782	1396
Downtown	52	2051	1551
Circleville	61	1345	1238
All	48	1572	1252

Table 11. Cl concentrations and Cl:Br ratios at each location.

Reservoir and downtown had the greatest mean and median Cl:Br mass ratios (mean= 1782 and 2051, median= 1396 and 1551, respectively). Circleville had the third highest mean and median Cl:Br ratio, and the highest Na and Cl mean fluxes. Griggs Reservoir and downtown are likely the most affected by runoff of road deicing salt, as these two locations are in closest proximity to an urban area. Circleville is assumed to be influenced by runoff of deicing salt as well, as Big Walnut Creek drains the eastern half of metropolitan Columbus, but the influx of eastern tributaries draining more clastic lithologies complicates this interpretation, especially for Na. Circleville is also downstream of the city's wastewater treatment plants, so sewage effluent further influences the sources of Na and Cl and Cl:Br ratios measured at Circleville. Further, Cl:Br ratios greater than 1000 were measured at Griggs Reservoir, downtown, and Circleville into the late summer and peaked again in November, while ratios generally did not exceed 1000 at Prospect and Bellepoint after late spring to early summer until November.

Trace elements in the Scioto River were analyzed by Rabb (2005) to characterize seasonal patterns and anthropogenic effects. He measured lower concentrations of Li, Ni, Mo, and Rb in the spring and summer and higher concentrations in the fall and winter at Prospect from 2000-2001. A similar seasonal trend was observed in samples collected in this study. The exception was during/after the major precipitation event in May that diluted concentrations of all trace elements except for Cu. Rabb (2005) found Ba concentrations increased from spring to fall as well, but concentrations remained nearly constant over time in this work. Uranium concentrations varied considerably in 2000-2001, which was also seen in this study. However, Rabb (2005) found that seasonal changes were not evident in samples collected downstream at Commercial Point (between Columbus and Circleville) and attributed this to reservoir effects and anthropogenic inputs from downtown. In contrast, Shiller (1997) observed higher concentrations of Mo and U in the lower Mississippi River in the spring, and a similar trend in Cu, Ni, Rb, and Ba, but with less seasonal variability. He hypothesized that redox processes (removal via

mineral precipitation as the insoluble reduced form under reducing conditions) likely controlled seasonal variability of Mo and U, and that biological uptake was not a significant control as concentrations were higher during the spring/summer when biological activity is highest. Biological uptake could have some influence on Mo concentrations measured in the Scioto River, as concentrations were lowest at Prospect, Bellepoint, Griggs Reservoir, and downtown in the spring and early summer, and highest in the fall, although differentiating the impact of biological activity from hydrologic conditions is difficult here.

Mean Ni, Mo, and Rb concentrations measured in this study and by Rabb were 2-3 times the mean concentrations measured in the lower Mississippi River. Copper in the Mississippi River had higher values than those measured in the Scioto River. Rubidium was observed at similar mean concentrations, and Ba had lower concentrations in the Scioto River than in the Mississippi River. These differences are probably related to both differences in watershed lithologies and anthropogenic activities occurring within the watersheds.

Mean concentrations of all analytes decreased at Prospect from 2000 to 2021 and increased at downtown, except for Ni that increased at both locations and Mo that remained similar at downtown. Rabb (2005) also measured trace concentrations at Commercial Point, downstream of the city's wastewater treatment plants. Mean Li, Rb, and Mo concentrations were greater at this location than any locations in this study, and he attributed this to the input of Columbus wastewater. Correlations between Cl and Li, Rb, and Mo at Commercial Point were strong in the 2000-2001 dataset, supporting the influence of treated wastewater as wastewater discharges have been shown to have high Cl concentrations (Kaushal et al., 2020). Lithium, Rb, and Mo increased in 2021 samples from downtown to Circleville, but differentiating the influence of sewage versus the influx of river water draining shales and sandstones is not currently possible to discern. Rabb (2005) concluded that geology and basement

lithologies dominate the trace element signature of the Scioto River upstream of the reservoirs, but anthropogenic influences dictate or mask natural patterns downstream of reservoirs and downtown Columbus. This conclusion is supported by the findings of this study as well. Natural hydrologic relationships and interelement correlations were strongest upstream and dampened downstream due to the reservoirs and influences from downtown.

5. CONCLUSION

5.1 Summary of Findings

As previous studies over the past few decades have shown, anthropogenic influences have significantly affected the geochemistry of the Scioto River, through land use changes (agricultural and urban) and hydrologic modification of the natural river system. Analysis of C – Q relationships, correlations between elements, and relating land use to geochemical trends revealed both an urban and anthropogenic influence on the river. However, many of the analytes in this study were determined to be primarily controlled by lithology of the drainage basin (Ca, Mg, Na, K, Si, HCO_3, Cl, F, SO_4, Br, Li, U, Ni, Rb, Mo, Ba, Sr), though there are undoubtedly anthropogenic impacts on the concentrations of these analytes as well. Geogenic influence was determined based on chemostatic or weak dilution behavior of these analytes, and moderate to positive correlations with Ca and/or Mg. Many other potential sources of contamination are possible, but were not analyzed in this study, such as U and other trace metals leaching from PO_4 fertilizer, dissolution of urban infrastructure, and more.

However, Cu was the only trace element that showed mobilization behavior with positive log C – log Q slopes. Concentrations were greatest at downtown, indicating an urban source, likely runoff from impermeable surfaces in metropolitan Columbus. Discharge-weighted yields of Cu were 20-30% greater at the downtown site compared to other locations, a pattern not observed in other trace elements.

Additionally, NO_3+NO_2 also showed a slight mobilization behavior based on log slopes, and trends in NO_3+NO_2 concentrations and discharge during the May sampling event showed a clear inverse relationship. Further, NO_3+NO_2 had negative correlations with those elements considered to be geogenic in source, and positive correlations with Cu. N:P ratios were far above the Redfield ratio for all but six samples collected in this study, demonstrating NO_3+NO_2 saturation that stems from fertilizer

runoff and the difference in geochemical behavior between the more soluble NO_3 and more particle reactive PO_4. Nitrate yields were greatest upstream at Prospect and Bellepoint due to fertilizer runoff, then decreased at Griggs Reservoir and increased again at the downtown site. This suggests an urban input of NO_3+NO_2 to the Scioto River at downtown Columbus, although this signal may be partially attributed to inflow from the Olentangy River, which drains urban and agricultural land.

Lastly, the influence of O'Shaughnessy and Griggs reservoirs on the river system was evaluated to understand impacts of modification of natural flow paths on river chemistry. Log C – Q slopes were generally closest to 0 (chemostatic) at Griggs Reservoir and downtown, and correlations between elements were typically weakest at these two locations as well. This is attributed to the increase in holding times of water in the reservoirs, resulting in longer times for physiochemical and/or biogeochemical processes to occur and modify the chemistry of river water. These factors lead to weakened natural relationships between analytes. Several reservoir water samples had dissolved Si concentrations near the detection limit, suggesting the biological removal of this constituent. The damming of rivers has been shown to decrease H_4SiO_4 downstream of reservoirs as a result of increased uptake of H_4SiO_4 by diatoms.

This study was designed to evaluate urban and agricultural effects on the geochemistry of the Scioto River. Because upstream agriculture in the watershed dominates the land use, it was thought that signals from agricultural practices such as fertilizer application may overprint any urban signal in the river's geochemistry. However, the analysis of a wide suite of dissolved chemical species and regular weekly sampling (for much of the study period) during both baseflow and event flow, urban and agricultural influences were differentiated. Additionally, this dataset has allowed for a better understanding of how the biogeochemistry of the Scioto River in the Upper Scioto River Basin in central Ohio varies during changing hydrological regimes.

5.2 Future Work

Future work on the Upper Scioto River Basin should focus on further understanding the influence of tributaries and impermeable surface runoff on the geochemistry of the Scioto River. The Olentangy River complicates the urban signature measured at Columbus because it drains a distinctly different lithology than upstream of the confluence. Similarly, the tributaries of Big Walnut Creek drain a significant portion of eastern Columbus, so higher frequency sampling of these tributaries along with mainstem Scioto River sampling would be beneficial in revealing an urban signature on the river. Sampling urban runoff flowing into the Scioto River, as Gardner and Carey (2004) did for the Olentangy River would aid in better determining urban contaminants. Future studies that aim to discern differences in contamination sources should strongly consider frequency of sampling and tributary inputs based on desired outcomes when designing a study. Monitoring of water quality at a range of flow conditions should be continued as it is necessary to evaluate the sources and controls of analytes in a watershed.

REFERENCES

Adeloye, A. J., Nawaz, N. R., & Montaseri, M. (1999). Climate change water resources planning impacts incorporating reservoir surface net evaporation fluxes: A case study. *International Journal of Water Resources Development*, *15*(4), 561–581. https://doi.org/10.1080/07900629948763

Admiraal, W., Breugem, P., Jacobs, D. M. L. H. A., & De Ruyter Van Steveninck, E. D. (1990). Fixation of dissolved silicate and sedimentation of biogenic silicate in the lower river Rhine during diatom blooms. *Biogeochemistry*, *9*, 175–185.

Allen, G. (2011). *An Analysis of the Fate and Transport of Nutrients in the Upper and Lower Scioto Watersheds of Ohio [Ph.D. Dissertation]*. The Ohio State University.

Bannerman, R. T., Owens, D. W., Dodds, R. B., & Hornewer, N. J. (1993). Sources of pollutants in Wisconsin stormwater. *Water Science and Technology*, *28*(3–5), 241–259. https://doi.org/10.2166/wst.1993.0426

Bao, C., Li, L., Shi, Y., & Duffy, C. (2017). Understanding watershed hydrogeochemistry: 2. synchronized hydrological and geochemical processes drive stream chemostatic behavior. *Water Resources Research*, *53*(3), 2328–2345. https://doi.org/10.1002/2016WR018934

Basu, N. B., Thompson, S. E., & Rao, P. S. C. (2011). Hydrologic and biogeochemical functioning of intensively managed catchments: A synthesis of top-down analyses. *Water Resources Research*, *47*(10), 1–12. https://doi.org/10.1029/2011WR010800

Bernard-Michel, C., & de Fouquet, C. (2005). Estimating indicators of river quality by geostatistics. *Geostatistics for Environmental Applications*, *1*, 443–454. https://doi.org/10.1007/3-540-26535-x_37

Berner, E. K., & Berner, R. A. (1987). *The global water cycle: geochemistry and environment* (1st ed.). Prentice-Hall.

Berner, E. K., & Berner, R. A. (2012). *Global environment: water, air, and geochemical cycles* (2nd ed.). Princeton and Oxford: Princeton University Press.

Blann, K. L., Anderson, J. L., Sands, G. R., & Vondracek, B. (2009). Effects of agricultural drainage on aquatic ecosystems: A review. *Critical Reviews in Environmental Science and Technology*, *39*(11), 909–1001. https://doi.org/10.1080/10643380801977966

Brock, E. H., Ketterings, Q. M., & McBride, M. (2006). Copper and zinc accumulation in poultry and dairy manure-amended fields. *Soil Science*, *171*(5), 388–399. https://doi.org/10.1097/01.ss.0000209360.62945.95

Burns, N. M., Rockwell, D. C., Bertram, P. E., Dolan, D. M., & Ciborowski, J. J. H. (2005). Trends in temperature, secchi depth, and dissolved oxygen depletion rates in the central basin of Lake Erie, 1983-2002. *Journal of Great Lakes Research*, *31*(SUPPL. 2), 35–49. https://doi.org/10.1016/S0380-1330(05)70303-8

Byrnes, D. K., Van Meter, K. J., & Basu, N. B. (2020). Long-Term Shifts in U.S. Nitrogen Sources and Sinks Revealed by the New TREND-Nitrogen Data Set (1930–2017). *Global Biogeochemical Cycles*, *34*(9), 1–16. https://doi.org/10.1029/2020GB006626

Carpenter, S. R., Caraco, N. F., Correll, D. L., Howarth, R. W., Sharpley, A. N., & Smith, V. H. (1998). Nonpoint pollution of surface waters with phosphorus and nitrogen. *Ecological Applications*, *8*(3), 559–568.

Cartwright, I., Morgenstern, U., & Hofmann, H. (2020). Concentration versus streamflow trends of major ions and tritium in headwater streams as indicators of changing water stores. *Hydrological Processes*, *34*(2), 485–505. https://doi.org/10.1002/hyp.13600

CFAES. (n.d.). CFAES weather system. Retrieved from https://weather.cfaes.osu.edu//

Chalise, D. R., Sankarasubramanian, A., & Ruhi, A. (2021). Dams and Climate Interact to Alter River Flow Regimes Across the United States. *Earth's Future*, *9*(4). https://doi.org/10.1029/2020EF001816

City of Columbus. (n.d.). Public Utilities: Water Sources. Retrieved March 30, 2021, from https://www.columbus.gov/utilities/water-protection/Water-Sources/

Connor, N. P., Sarraino, S., Frantz, D. E., Bushaw-Newton, K., & MacAvoy, S. E. (2014). Geochemical characteristics of an urban river: Influences of an anthropogenic landscape. *Applied Geochemistry*, *47*, 209–216. https://doi.org/10.1016/j.apgeochem.2014.06.012

Craig, H. (1961). Isotopic variations in meteoric waters. *Science*, *133*(3465), 1702–1703.

Curtis, J. B., & Stueber, A. M. (1973). 87Sr/86Sr ratios and total strontium concentrations in surface waters of the Scioto River drainage basin, Ohio. *Ohio Journal of Science*, *73*(3), 166–175.

Dailey, K. R., Welch, K. A., & Lyons, W. B. (2014). Evaluating the influence of road salt on water quality of Ohio rivers over time. *Applied Geochemistry*, *47*, 25–35. https://doi.org/10.1016/j.apgeochem.2014.05.006

David, M. B., Gentry, L. E., Kovacic, D. A., & Smith, K. M. (1997). Nitrogen Balance in and Export from an Agricultural Watershed. *Journal of Environmental Quality*, *26*(4), 1038–1048. https://doi.org/10.2134/jeq1997.00472425002600040015x

Davidson, E. A., David, M. B., Galloway, J. N., Goodale, C. L., Haeuber, R., Harrison, J. A., et al. (2012). *Excess nitrogen in the U.S. environment: trends, risks, and solutions*. *Issues in Ecology*.

Davis, S., Whittemore, D., & Fabryka-Martin, J. (1998). Uses of chloride bromide ratios in studies of potable water.pdf. *Groundwater*, *36*(2), 338–350.

Dieter, C. A., Maupin, M. A., Caldwell, R. R., Harris, M. A., Ivahnenko, T. I., Lovelace, J. K., et al. (2018). *Estimated Use of Water in the United States in 2015*. https://doi.org/10.3133/cir1441

EPA. (2015). *Memorandum understanding on copper mitigation in watersheds and waterways*.

Van Esbroeck, C. J., Macrae, M. L., Brunke, R. I., & McKague, K. (2016). Annual and seasonal phosphorus export in surface runoff and tile drainage from agricultural fields with cold temperate climates. *Journal of Great Lakes Research*, *42*(6), 1271–1280. https://doi.org/10.1016/j.jglr.2015.12.014

Ferrazzi, M., Woods, R. A., & Botter, G. (2021). Climatic signatures in regulated flow regimes across the Central and Eastern United States. *Journal of Hydrology: Regional Studies*, *35*(March), 100809. https://doi.org/10.1016/j.ejrh.2021.100809

Fitzpatrick, M. L., Long, D. T., & Pijanowski, B. C. (2007). Exploring the effects of urban and agricultural land use on surface water chemistry, across a regional watershed, using multivariate statistics. *Applied Geochemistry*, *22*(8 SPEC. ISS.), 1825–1840. https://doi.org/10.1016/j.apgeochem.2007.03.047

Gaillardet, J., Dupre, B., Louvat, P., & Allegre, C. J. (1999). Global silicate weathering and CO2 consumption rates deduced from the chemistry of large rivers. *Chemical Geology*, *159*(8), 3–30.

Gaillardet, J., Viers, J., & Dupre, B. (2003). Trace elements in river waters. In J. I. Drever (Ed.), *Treatise on Geochemistry Vol. 5* (1st ed., pp. 225–272). Pergamon, Oxford: Elsevier.

Gardner, C. B., & Carey, A. E. (2004). Trace metal and major ion inputs into the Olentangy River from an urban storm sewer. *Environmental Science and Technology*, *38*(20), 5319–5326. https://doi.org/10.1021/es0497835

Gibbs, R. J. (1970). Mechanisms controlling world water chemistry. *Science*, *170*(3962), 1088–1090.

Godsey, S. E., Kirchner, J. W., & Clow, D. W. (2009). Concentration-discharge relationships reflect chemostatic characteristics of US catchments. *Hydrological Processes*, *23*(13), 1844–1864. https://doi.org/10.1002/hyp.7315

Godsey, S. E., Hartmann, J., & Kirchner, J. W. (2019). Catchment chemostasis revisited: Water quality responds differently to variations in weather and climate. *Hydrological Processes*, *33*(24), 3056–3069. https://doi.org/10.1002/hyp.13554

Graf, W. L. (1999). Dam nation: A geographic census of american dams and their large-scale hydrologic impacts. *Water Resources Research*, *35*(4), 1305–1311. https://doi.org/10.1029/1999WR900016

Halliday, S. J., Skeffington, R. A., Bowes, M. J., Gozzard, E., Newman, J. R., Loewenthal, M., et al. (2014). The water quality of the River Enborne, UK: Observations from high-frequency monitoring in a rural, lowland river system. *Water (Switzerland)*, *6*(1), 150–180. https://doi.org/10.3390/w6010150

Helsel, D. R., Hirsch, R. M., Ryberg, K. R., Archfield, S. A., & Gilroy, E. J. (2020). Statistical methods in water resources. In *USGS Techniques and Methods 4-A3* (p. 458). U.S. Geological Survey, U.S. Department of the Interior. https://doi.org/https://doi.org/10.3133/tm4a3

Hem, J. D. (1943). Fluctuations in concentration of dissolved solids of some southwestern streams. *Transactions*, *29*(1), 80–84.

Hicks, J. E. (1994). *Mixing and anthropogenic influences on the chemical composition of water along the course of the Scioto River, Ohio*. Ohio State University.

Hintz, W. D., Fay, L., & Relyea, R. A. (2022). Road salts, human safety, and the rising salinity of our fresh waters. *Frontiers in Ecology and the Environment*, *20*(1), 22–30. https://doi.org/10.1002/fee.2433

Hubbard, G. D., Stauffer, C. R., Bownoeker, J. A., Prosser, C. S., & Cumings, E. R. (1914). *Description of the Columbus quadrangle*.

Huber, M., Welker, A., & Helmreich, B. (2016). Critical review of heavy metal pollution of traffic area runoff: Occurrence, influencing factors, and partitioning. *Science of the Total Environment*, *541*, 895–919. https://doi.org/10.1016/j.scitotenv.2015.09.033

Humborg, C. (1997). Effect of Danube river dam on Black sea biogeochemistry. *Nature*, *386*(March), 385–388.

Ittekkot, V., Humborg, C., & Schäfer, P. (2000). Hydrological alterations and marine biogeochemistry: A silicate issue? *BioScience*, *50*(9), 776–782. https://doi.org/10.1641/0006-3568(2000)050[0776:HAAMBA]2.0.CO;2

Johnson, H. M., & Stets, E. G. (2020). Nitrate in Streams During Winter Low-Flow Conditions as an Indicator of Legacy Nitrate. *Water Resources Research*, *56*(11). https://doi.org/10.1029/2019WR026996

Jossette, G., Leporcq, B., Sanchez, N., & Philippon. (1999). Biogeochemical mass-balances (C, N, P, Si) in three large reservoirs of the Seine Basin (France). *Biogeochemistry*, *47*(2), 119–146. https://doi.org/10.1023/A:1006101318417

Karbassi, A. R., Torabi, F., Ghazban, F., & Ardestani, M. (2011). Association of trace metals with various sedimentary phases in dam reservoirs. *International Journal of Environmental Science & Technology*, *8*(4), 841–852. https://doi.org/10.1007/BF03326267

Kaushal, S. S., Groffman, P. M., Likens, G. E., Belt, K. T., Stack, W. P., Kelly, V. R., et al. (2005). Increased salinization of fresh water in the Northeastern United States. *Proceedings of the National Academy of Sciences of the United States of America*, *102*(38), 13517–13520. https://doi.org/10.1073/pnas.0506414102

Kaushal, S. S., Wood, K. L., Galella, J. G., Gion, A. M., Haq, S., Goodling, P. J., et al. (2020). Making 'chemical cocktails' – Evolution of urban geochemical processes across the periodic table of elements. *Applied Geochemistry*, *119*(August 2019), 104632. https://doi.org/10.1016/j.apgeochem.2020.104632

Kincaid, D. W., Seybold, E. C., Adair, E. C., Bowden, W. B., Perdrial, J. N., Vaughan, M. C. H., & Schroth, A. W. (2020). Land Use and Season Influence Event-Scale Nitrate and Soluble Reactive Phosphorus Exports and Export Stoichiometry from Headwater Catchments. *Water Resources Research*, *56*(10), 1–20. https://doi.org/10.1029/2020WR027361

Knapp, J. L. A., Von Freyberg, J., Studer, B., Kiewiet, L., & Kirchner, J. W. (2020). Concentration-discharge relationships vary among hydrological events, reflecting differences in event characteristics. *Hydrology and Earth System Sciences*, *24*(5), 2561–2576. https://doi.org/10.5194/hess-24-2561-2020

Leslie, D., Welch, K., & Lyons, W. B. (2014). Domestic Water Supply Dynamics Using Stable Isotopes δ18O, δD, and d-Excess. *Journal of Water Resource and Protection*, *6*, 1517–1532.

Leventhal, J. S. (1979). Chemical analysis and geochemical associations in Devonian black shale core samples from Martin County, Kentucky; Carroll and Washington Counties, Ohio; Wise County, Virginia; and Overton County, Tennessee, 59.

Loftis, J. C., & Ward, R. C. (1980). Water quality monitoring-Some practical sampling frequency considerations. *Environmental Management*, *4*(6), 521–526. https://doi.org/10.1007/BF01876889

Lyons, W. B., Carey, A. E., Gardner, C. B., Welch, S. A., Smith, D. F., Szynkiewicz, A., et al. (2021). The geochemistry of Irish rivers. *Journal of Hydrology: Regional Studies*, *37*(February), 100881. https://doi.org/10.1016/j.ejrh.2021.100881

Macrae, M. L., English, M. C., Schiff, S. L., & Stone, M. (2007). Intra-annual variability in the contribution of tile drains to basin discharge and phosphorus export in a first-order agricultural catchment. *Agricultural Water Management*, *92*(3), 171–182. https://doi.org/10.1016/j.agwat.2007.05.015

Marinos, R. E., Van Meter, K. J., & Basu, N. B. (2020). Is the River a Chemostat?: Scale Versus Land Use Controls on Nitrate Concentration-Discharge Dynamics in the Upper Mississippi River Basin. *Geophysical Research Letters*, *47*(16), 1–11. https://doi.org/10.1029/2020GL087051

Meybeck, M. (1979). Concentrations des eaux fluviales en elements majeurs et apports en solution aux oceans. *Revue de Geologie Dynamique et Geographie Physique*, *21*(3), 215–246.

Meybeck, M. (1998). Man and river interface: Multiple impacts on water and particulates chemistry illustrated in the Seine river basin. *Hydrobiologia*, *373–374*, 1–20. https://doi.org/10.1007/978-94-011-5266-2_1

Meyer, J. L., Paul, M. J., & Taulbee, W. K. (2005). Stream ecosystem function in urbanizing landscapes. *Journal of the North American Benthological Society*, *24*(3), 602–612. https://doi.org/10.1899/04-021.1

Michalak, A. M., Anderson, E. J., Beletsky, D., Boland, S., Bosch, N. S., Bridgeman, T. B., et al. (2013). Record-setting algal bloom in Lake Erie caused by agricultural and meteorological trends consistent with expected future conditions. *Proceedings of the National Academy of Sciences of the United States of America*, *110*(16), 6448–6452. https://doi.org/10.1073/pnas.1216006110

Miller, C. A., Peucker-Ehrenbrink, B., Walker, B. D., & Marcantonio, F. (2011). Re-assessing the surface cycling of molybdenum and rhenium. *Geochimica et Cosmochimica Acta*, *75*(22), 7146–7179. https://doi.org/10.1016/j.gca.2011.09.005

Moatar, F., Abbott, B. W., Minaudo, C., Curie, F., & Pinay, G. (2017). Elemental properties, hydrology, and biology interact to shape concentration-discharge curves for carbon, nutrients, sediment, and major ions. *Water Resources Research*, *53*(2), 1270–1287. https://doi.org/10.1002/2016WR019635

MRLC. (2019). *NLCD 2019 Land Cover*. Retrieved from https://www.mrlc.gov/data?f%5B0%5D=category%3ALand Cover&f%5B1%5D=category%3Aland cover&f%5B2%5D=region%3Aconus&f%5B3%5D=year%3A2019

NOAA. (2021). Climate Data Online. Retrieved April 4, 2022, from https://www.ncdc.noaa.gov/cdo-web/

Ogiyama, S., Sakamoto, K., Suzuki, H., Ushio, S., Anzai, T., & Inubushi, K. (2005). Accumulation of zinc and copper in an arable field after animal manure application. *Soil Science and Plant Nutrition*, *51*(6), 801–808. https://doi.org/10.1111/j.1747-0765.2005.tb00114.x

Ohio Division of Geological Survey. (2006). Bedrock geologic map of Ohio. Retrieved from https://ohiodnr.gov/wps/wcm/connect/gov/af200770-8656-455b-b41b-ee19ef48ef45/BG-1_8.5x11.pdf?MOD=AJPERES&CVID=ne.WWkh

Ohio EPA. (1997). *Biological and Water Quality Study of The Upper Scioto River Basin*. Retrieved from http://www.epa.ohio.gov/Portals/35/documents/LMR_Upper_Basin_2011_TSD.pdf

Ohio EPA. (1999). *Biological and Water Quality Study of the Middle Scioto River and Alum Creek*.

Oskarsson, A., & Norrgren, L. (1998). Copper pipes as a source of copper exposure in man and environment. *Environmental Reviews*, *6*(3–4), 139–150. https://doi.org/10.1139/a98-009

Otero, N., Vitòria, L., Soler, A., & Canals, A. (2005). Fertiliser characterisation: Major, trace and rare earth elements. *Applied Geochemistry*, *20*(8), 1473–1488. https://doi.org/10.1016/j.apgeochem.2005.04.002

Palmer, M. R., & Edmond, J. M. (1993). Uranium in river water. *Geochimica et Cosmochimica Acta*, *57*(20), 4947–4955. https://doi.org/10.1016/0016-7037(93)90131-F

Pease, L. A., King, K. W., Williams, M. R., LaBarge, G. A., Duncan, E. W., & Fausey, N. R. (2018). Phosphorus export from artificially drained fields across the Eastern Corn Belt. *Journal of Great Lakes Research*, *44*(1), 43–53. https://doi.org/10.1016/j.jglr.2017.11.009

Poff, N. L. R., Olden, J. D., Merritt, D. M., & Pepin, D. M. (2007). Homogenization of regional river dynamics by dams and global biodiversity implications. *Proceedings of the National Academy of Sciences of the United States of America*, *104*(14), 5732–5737. https://doi.org/10.1073/pnas.0609812104

Pohle, I., Baggaley, N., Palarea-Albaladejo, J., Stutter, M., & Glendell, M. (2021). A Framework for Assessing Concentration-Discharge Catchment Behavior From Low-Frequency Water Quality Data. *Water Resources Research*, *57*(9). https://doi.org/10.1029/2021WR029692

Rabb, S. (2005). *The Investigation of High Performance Techniques and Application to Complex Matrices Using Inductively Coupled Plasma Spectrometry and the Impact of Urbanization on the Scioto River System [Ph.D. Dissertation]*. The Ohio State University.

Rakowsky, P. I. (2000). *The effect of bedrock geology on the chemistry of natural waters in central Ohio [Undergraduate Thesis]*. The Ohio State University.

Royer, T. V., David, M. B., & Gentry, L. E. (2006). Timing of riverine export of nitrate and phosphorus from agricultural watersheds in Illinois: Implications for reducing nutrient loading to the Mississippi River. *Environmental Science and Technology*, *40*(13), 4126–4131. https://doi.org/10.1021/es052573n

Sansalone, J. J., & Buchberger, S. G. (1997). Partitioning and first flush of metals in urban roadway storm water. *Journal of Environmental Engineering*, *123*(2), 134–143. https://doi.org/10.1061/(ASCE)0733-9372(1997)123:2(134)

Sañudo-Wilhelmy, S. A., & Gill, G. A. (1999). Impact of the Clean Water Act on the levels of toxic metals in urban estuaries: The Hudson River estuary revisited. *Environmental Science and Technology*, *33*(20), 3477–3481. https://doi.org/10.1021/es981130z

Schiefer, M. C. (2002). *Basin descriptions and flow characteristics of Ohio streams*. Retrieved from https://water.ohiodnr.gov/portals/soilwater/pdf/stream/Bulletin47.pdf

Schmidt, J. J., & Goldthwait, R. P. (1958). *The groundwater resources of Franklin County, Ohio*.

Shiller, A. M. (1997). Dissolved trace elements in the Mississippi River: Seasonal, interannual, and decadal variability. *Geochimica et Cosmochimica Acta*, *61*(20), 4321–4330. https://doi.org/10.1016/S0016-7037(97)00245-7

Smith, D. F., Saelens, E., Leslie, D. L., & Carey, A. E. (2021). Local meteoric water lines describe extratropical precipitation. *Hydrological Processes*, *35*(2), 1–15. https://doi.org/10.1002/hyp.14059

Stets, E. G., Kelly, V. J., & Crawford, C. G. (2015). Regional and Temporal Differences in Nitrate Trends Discerned from Long-Term Water Quality Monitoring Data. *Journal of the American Water Resources Association*, *51*(5), 1394–1407. https://doi.org/10.1111/1752-1688.12321

Steuer, J. J., Selbig, W., Hornewer, N., & Prey, J. (1997). *Sources of contamination in an urban basin in Marquette, Michigan and an analysis of concentrations, loads, and data quality*. *U.S. Geological Survey*. Retrieved from http://hdl.handle.net/2027/mdp.39015053337971

Sun J., J., Liu D., D., & Qian S., S. (2001). Preliminary study on seasonal succession and development pathway of phytoplankton community in the Bohai Sea. *Acta Oceanologica Sinica*.

Swinford, E. M., & Slucher, E. R. (1995). *Regional bedrock geology of the Bellefontaine, Ohio, 30x60 minute quadrangle*.

Thompson, S. E., Basu, N. B., Lascurain, J., Aubeneau, A., & Rao, P. S. C. (2011). Relative dominance of hydrologic versus biogeochemical factors on solute export across impact gradients. *Water Resources Research*, *47*(7), 1–20. https://doi.org/10.1029/2010WR009605

U.S. EPA. (2011). *Reactive nitrogen in the United States: an analysis of inputs, flows, consequences, and management options*.

U.S. EPA. (2017). *National Water Quality Inventory: Report to Congress*. Retrieved from http://www.ncbi.nlm.nih.gov/pubmed/2347274

United Nations. (2018). *World Urbanization Prospects 2018*. *Department of Economic and Social Affairs United Nations*. Retrieved from https://population.un.org/wup/

United States Census Bureau. (1920). *U.S. Census state summary report: Ohio*.

United States Census Bureau. (2019). Delaware County. Retrieved March 30, 2021, from https://www.census.gov/quickfacts/geo/chart/delawarecountyohio/PST120219

United States Census Bureau. (2021). Quick facts: Columbus, Ohio. Retrieved from https://www.census.gov/quickfacts/fact/table/columbuscityohio/PST045221

US EPA Office of Water. (2016). *Definition and procedure for the determination of the method detection limit, revision 2*. Retrieved from https://www.epa.gov/sites/default/files/2016-12/documents/mdl-procedure_rev2_12-13-2016.pdf

Valayamkunnath, P., Barlage, M., Chen, F., Gochis, D. J., & Franz, K. J. (2020). Mapping of 30-meter resolution tile-drained croplands using a geospatial modeling approach. *Scientific Data*, *7*(1), 1–10. https://doi.org/10.1038/s41597-020-00596-x

Vilmin, L., Flipo, N., Escoffier, N., & Groleau, A. (2018). Estimation of the water quality of a large urbanized river as defined by the European WFD: what is the optimal sampling frequency? *Environmental Science and Pollution Research*, *25*(24), 23485–23501. https://doi.org/10.1007/s11356-016-7109-z

Vorosmarty, C. J., Meybeck, M., Fekete, B., & Sharma, K. (1997). The potential impact of neo-Castorization on sediment transport by the global network of rivers. *Human Impact on Erosion and Sedimentation. Proc. International Symposium, Rabat, Morocco, 1997*, (245), 261–273.

Waite, A., Bienfang, P. K., & Harrison, P. J. (1992). Spring bloom sedimentation in a subarctic ecosystem - II. Succession and sedimentation. *Marine Biology*, *114*(1), 131–138. https://doi.org/10.1007/BF00350862

Walsh, C. J., Roy, A. H., Feminella, J. W., Cottingham, P. D., Groffman, P. M., & Morgan, R. P. (2005). The urban stream syndrome: Current knowledge and the search for a cure. *Journal of the North American Benthological Society*, *24*(3), 706–723. https://doi.org/10.1899/04-028.1

Walsh, J., Richman, M., & Allen, D. (1982). Spatial coherence of monthly precipitation in the United States. *Monthly Weather Review*, *110*, 272–286.

Wedepohl, K. H. (1995). The composition of the continental crust. *Geochimica et Cosmochimica Acta*, *59*(7), 1217–1232. https://doi.org/10.1016/0016-7037(95)00038-2

Welch, K. A., Lyons, W. B., Whisner, C., Gardner, C. B., Gooseff, M. N., McKnight, D. M., & Priscu, J. C. (2010). Spatial variations in the geochemistry of glacial meltwater streams in the Taylor Valley, Antarctica. *Antarctic Science*, *22*(6), 662–672. https://doi.org/10.1017/S0954102010000702

APPENDIX A: SAMPLE METADATA

Sample Number	Sample ID	Location	Collection Date
1	DT1	Downtown	2/28/2021
2	GR2	Griggs	2/28/2021
3	BP3	Bellepoint	2/28/2021
4	DT4	Downtown	3/6/2021
5	GR5	Griggs	3/6/2021
6	BP6	Bellepoint	3/6/2021
7	PT7	Prospect	3/6/2021
8	DT8	Downtown	3/12/2021
9	GR9	Griggs	3/12/2021
10	BP10	Bellepoint	3/12/2021
11	DT11	Downtown	3/19/2021
12	GR12	Griggs	3/19/2021
13	CV13	Circleville	3/27/2021
14	DT14	Downtown	3/27/2021
15	GR15	Griggs	3/27/2021
16	BP16	Bellepoint	3/27/2021
17	DT17	Downtown	4/3/2021
18	GR18	Griggs	4/3/2021
19	BP19	Bellepoint	4/3/2021
20	PT20	Prospect	4/3/2021
21	DT21	Downtown	4/9/2021
22	GR22	Griggs	4/9/2021
23	BP23	Bellepoint	4/9/2021
24	CV24	Circleville	4/17/2021
25	DT25	Downtown	4/17/2021
26	GR26	Griggs	4/17/2021
27	BP27	Bellepoint	4/17/2021
28	DT28	Downtown	4/25/2021
29	GR29	Griggs	4/25/2021
30	BP30	Bellepoint	4/25/2021
31	PT31	Prospect	4/25/2021
32	DT32	Downtown	5/1/2021
33	GR33	Griggs	5/1/2021
34	BP34	Bellepoint	5/1/2021
35	CV35	Circleville	5/8/2021
36	DT36	Downtown	5/8/2021
37	GR37	Griggs	5/8/2021
38	BP38	Bellepoint	5/8/2021
39	DT39	Downtown	5/10/2021
40	GR40	Griggs	5/10/2021
41	BP41	Bellepoint	5/10/2021
42	DT42	Downtown	5/12/2021
43	GR43	Griggs	5/12/2021
44	BP44	Bellepoint	5/12/2021
45	DT45	Downtown	5/14/2021
46	GR46	Griggs	5/14/2021
47	BP47	Bellepoint	5/14/2021
48	DT48	Downtown	5/30/2021
49	GR49	Griggs	5/30/2021
50	BP50	Bellepoint	5/30/2021
51	DT51	Downtown	6/11/2021
52	GR52	Griggs	6/11/2021
53	BP53	Bellepoint	6/11/2021
54	PT54	Prospect	6/11/2021
55	CV55	Circleville	6/19/2021
56	DT56	Downtown	6/19/2021
57	GR57	Griggs	6/19/2021
58	BP58	Bellepoint	6/19/2021
59	DT59	Downtown	6/25/2021
60	GR60	Griggs	6/25/2021
61	BP61	Bellepoint	6/25/2021
62	DT62	Downtown	7/2/2021
63	GR63	Griggs	7/2/2021
64	BP64	Bellepoint	7/2/2021
65	DT65	Downtown	7/9/2021
66	GR66	Griggs	7/9/2021
67	BP67	Bellepoint	7/9/2021
68	PT68	Prospect	7/9/2021
69	DT69	Downtown	7/13/2021
70	GR70	Griggs	7/13/2021
71	BP71	Bellepoint	7/13/2021
72	DT72	Downtown	7/26/2021
73	GR73	Griggs	7/26/2021
74	BP74	Bellepoint	7/26/2021
75	CV75	Circleville	8/2/2021
76	DT76	Downtown	8/2/2021

Table A.1. List of all samples, locations, and dates.

Sample Number	Sample ID	Location	Collection Date
77	GR77	Griggs	8/2/2021
78	BP78	Bellepoint	8/2/2021
79	PT79	Prospect	8/2/2021
80	CV80	Circleville	8/18/2021
81	DT81	Downtown	8/18/2021
82	GR82	Griggs	8/18/2021
83	BP83	Bellepoint	8/18/2021
84	PT84	Prospect	8/18/2021
85	DT85	Downtown	9/1/2021
86	GR86	Griggs	9/1/2021
87	CV87	Circleville	9/5/2021
88	DT88	Downtown	9/5/2021
89	GR89	Griggs	9/5/2021
90	BP90	Bellepoint	9/5/2021
91	PT91	Prospect	9/5/2021
92	CV92	Circleville	9/23/2021
93	DT93	Downtown	9/23/2021
94	GR94	Griggs	9/23/2021
95	BP95	Bellepoint	9/23/2021
96	PT96	Prospect	9/23/2021
97	CV97	Circleville	10/20/2021
98	DT98	Downtown	10/20/2021
99	GR99	Griggs	10/20/2021
100	BP100	Bellepoint	10/20/2021
101	PT101	Prospect	10/20/2021
102	DT102	Downtown	10/25/2021
103	GR103	Griggs	10/25/2021
104	DT104	Downtown	10/29/2021
105	GR105	Griggs	10/29/2021
106	CV106	Circleville	11/11/2021
107	DT107	Downtown	11/11/2021
108	GR108	Griggs	11/11/2021
109	BP109	Bellepoint	11/11/2021
110	PT110	Prospect	11/11/2021
111	DT111	Downtown	11/26/2021
112	GR112	Griggs	11/26/2021
113	DT113	Downtown	12/2/2021
114	GR114	Griggs	12/2/2021
115	BP115	Bellepoint	12/2/2021
116	CV116	Circleville	12/5/2021
117	DT117	Downtown	12/5/2021
118	GR118	Griggs	12/5/2021
119	BP119	Bellepoint	12/5/2021
120	PT120	Prospect	12/5/2021

Table A.1 cont. List of all samples, locations, and dates.

Location	Total Number of Samples
Prospect	12
Bellepoint	29
Griggs Reservoir	34
Downtown	34
Circleville	11
Total:	**120**

Table A.2. Number of samples per sample location.

Location	Latitude	Longitude
Prospect	40.4499	-83.1909
Bellepoint	40.2383	-83.1461
Griggs Reservoir	40.0336	-83.0960
Downtown	39.9599	-83.0180
Circleville	39.5896	-82.9716

Table A.3. Location of sample points.

Blank Number	Blank ID	Location	Collection Date
1	Field blank 1	Downtown	2/28/2021
2	Field blank 2	Griggs Reservoir	3/12/2021
3	Field blank 3	Circleville	3/27/2021
4	Field blank 4	Bellepoint	4/9/2021
5	Field blank 5	Prospect	4/25/2021
6	Field blank 6	Bellepoint	5/12/2021
7	Field blank 7	Circleville	6/19/2021
8	Field blank 8	Bellepoint	6/25/2021
9	Field blank 9	Griggs Reservoir	7/2/2021
10	Field blank 10	Prospect	7/9/2021
11	Field blank 11	Downtown	7/13/2021
12	Field blank 12	Bellepoint	7/26/2021
13	Field blank 13	Circleville	8/2/2021
14	Field blank 14	Prospect	8/18/2021
15	Field blank 15	Griggs Reservoir	9/1/2021
16	Field blank 16	Downtown	9/5/2021
17	Field blank 17	Bellepoint	9/23/2021
18	Field blank 18	Circleville	10/20/2021
19	Field blank 19	Griggs Reservoir	10/25/2021
20	Field blank 20	Downtown	10/29/2021
21	Field blank 21	Griggs Reservoir	11/11/2021
22	Field blank 22	Downtown	11/26/2021
23	Field blank 23	Bellepoint	12/2/2021
24	Field blank 24	Prospect	12/5/2021

Table A.4. Field blank collection date and location opened.

APPENDIX B: METHODS AND ANALYTICAL CERTAINTY

	Run 1: samples 1-26; 34-47				Run 2: samples 27-33; 49-92			
	Standard used	Certified concentration (μg/L)	% difference	Check standard RSD (%)	Standard used	Certified concentration (μg/L)	% difference	Check standard RSD (%)
U	TMDA 64.2	142	9	4	TMDA 64.2	142	8	7
Ni	NIST 1643e	62.41	2	9	TMDA 64.2	260	9	8
Cu	NIST 1643e	22.76	1	9	NIST 1643f	21.66	5	5
Rb	NIST 1643e	14.14	9	3	NIST 1643f	12.64	7	7
Mo	NIST 1643e	121.4	17	4	NIST 1643f	115.3	12	5
Ba	NIST 1643e	544.2	1	4	NIST 1643f	518.2	4	5
Sr	TMDA 64.2	635	4	3	TMDA 62.2	635	2	7
	Run 3: samples 93-105				**Run 4: samples 106-120**			
	Standard used	Certified concentration (μg/L)	% difference	Check standard RSD (%)	Standard used	Certified concentration (μg/L)	% difference	Check standard RSD (%)
U	TMDA 64.2	142	15	2	TMDA 64.2	142	13	13
Ni	TMDA 64.2	260	14	9	TMDA 64.2	260	3	6
Cu	NIST 1643f	21.66	9	5	TMDA 64.2	270	30	7
Rb	TMDA 64.2	30.8	3	6	NIST 1643f	12.64	12	9
Mo	NIST 1643f	115.3	8	8	NIST 1643f	115.3	2	6
Ba	NIST 1643f	518.2	6	5	NIST 1643f	518.2	2	8
Sr	TMDA 64.2	635	2	6	NIST 1643f	314	0	10

Table B.1 Precision and accuracy of trace element analysis per run. Precision denoted by 'Check standard RSD'. Accuracy denoted by '% difference' from external standard certified values. External standards were diluted to within calibration range for accuracy calculations. Certified concentrations listed here are undilute concentrations published by Environment Canada and National Institute of Standards and Technology.

B.1 Stable Water Isotope Analysis

Samples were pipetted into 2 mL glass vials and 2 μL were injected by the instrument for analysis. For each sample, seven injections were made, and the last four were averaged to determine isotopic composition. The first three injections were discarded to avoid influence of previous sample measurements (Smith et al., 2021). $\delta^{18}O$ and $\delta^{2}H$ values for internal standards are listed in Table A.3 below.

Standard	$\delta^{18}O$	$\delta^{2}H$
Florida	-2.09‰	-9.69‰
Ohio	-8.99‰	-61.80‰
Colorado	-16.53‰	-126.3‰
Nevada	-14.20‰	-104.80‰

Table B.2. Internal standard isotopic composition used for instrument calibration and data correction

B.2 USGS Discharge Data

Discharge data were collected from USGS flow gages at the closest locations to each sampling site. Because there is not a USGS gage between the Prospect gage and Bellepoint and Mill Creek joins the Scioto River just north of the Bellepoint sample location, Bellepoint discharge values were calculated by summing discharge values from the USGS gage near Prospect (USGS 03219500) and the Mill Creek gage (USGS 03220000).

USGS Gage Number	USGS Gage Name	Sample Location
03219500	Scioto River near Prospect OH	Prospect
03220000	Mill Creek near Bellepoint OH	Bellepoint (sum of Prospect and Mill Creek gages)
03221000	Scioto River below O'Shaughnessy Dam near Dublin OH	Griggs Reservoir
03227500	Scioto River at Columbus OH	Downtown
03230700	Scioto River at Circleville OH	Circleville

Table B.3. USGS gages used for Scioto River discharge values during sample period and determination of percentile flow.

To determine flow percentiles, daily discharge data from the last 31 years (1990-2021) were used to calculate 25th, 50th, and 75th flow percentiles for the gage associated with each sample location (USGS NWIS provides these statistics for daily, monthly, and yearly data; user specifies what time period to calculate data from and what percentile to calculate). Due to a lack of discharge data from 1979-2010 at the Circleville gage, discharge statistics were calculated using data from only the last 11 years (2010-2021). These data were then used to determine the percentile (25th and below, 25-50th percentile, 50-75th percentile, and above 75th percentile) of discharge values observed during the study period.

APPENDIX C: MAJOR ION, NUTRIENT, TRACE ELEMENT, AND STABLE WATER ISOTOPIC RESULTS

	μM												nM							
	Ca	Mg	Na	K	Si	Cl	SO_4	F	Br	NO_3+NO_2	PO_4	NH_4	Li	U	Ni	Cu	Rb	Mo	Ba	Sr
Field blank 1	BDL	BDL	BDL	BDL	BDL	BDL	BDL	1.7	BDL	0.19	BDL	2.5	BDL							
Field blank 2	BDL	BDL	BDL	BDL	BDL	BDL	BDL	BDL	BDL	0.30	BDL	BDL	BDL							
Field blank 3	4.1	BDL	BDL	BDL	BDL	BDL	BDL	BDL	BDL	BDL	BDL	BDL	BDL							
Field blank 4	BDL	BDL	BDL	BDL	BDL	BDL	BDL	BDL	BDL	BDL	BDL	BDL	BDL							
Field blank 5	BDL	BDL	BDL	BDL	BDL	BDL	BDL	BDL	BDL	BDL	BDL	BDL	BDL							
Field blank 6	3.0	BDL	BDL	BDL	BDL	BDL	BDL	BDL	BDL	BDL	BDL	BDL	BDL							
Field blank 7	BDL	0.74	BDL	BDL	BDL	BDL	BDL	BDL	BDL	0.48	BDL	BDL	BDL	BDL	BDL	BDL	BDL	BDL	BDL	BDL
Field blank 8	BDL	BDL	BDL	BDL	BDL	BDL	BDL	BDL	BDL	0.47	BDL	BDL	BDL	BDL	BDL	BDL	BDL	BDL	BDL	BDL
Field blank 9	BDL	BDL	BDL	BDL	BDL	BDL	BDL	BDL	BDL	BDL	BDL	BDL	BDL	BDL	BDL	BDL	BDL	BDL	BDL	BDL
Field blank 10	4.5	1.3	BDL	BDL	0.28	BDL	BDL	BDL	BDL	0.31	BDL	BDL	BDL	BDL	BDL	BDL	BDL	BDL	BDL	BDL
Field blank 11	BDL	1.0	BDL	0.51	0.50	BDL	BDL	BDL	BDL	0.36	BDL	BDL	BDL	BDL	BDL	BDL	BDL	BDL	BDL	BDL
Field blank 12	BDL	0.67	BDL	BDL	0.66	BDL	BDL	BDL	BDL	BDL	BDL	BDL	BDL	BDL	BDL	BDL	BDL	BDL	BDL	BDL
Field blank 13	BDL	BDL	BDL	BDL	0.67	BDL	BDL	BDL	BDL	BDL	BDL	BDL	BDL	BDL	BDL	BDL	BDL	BDL	BDL	BDL
Field blank 14	BDL	BDL	BDL	0.59	0.72	BDL	BDL	BDL	BDL	BDL	BDL	BDL	BDL	BDL	BDL	BDL	BDL	BDL	BDL	BDL
Field blank 15	5.2	BDL	BDL	0.47	0.65	BDL	BDL	BDL	BDL	BDL	BDL	BDL	BDL	BDL	BDL	BDL	BDL	BDL	BDL	BDL
Field blank 16	6.2	BDL	BDL	0.94	0.54	BDL	BDL	BDL	BDL	BDL	BDL	BDL	BDL	BDL	BDL	BDL	BDL	BDL	BDL	BDL
Field blank 17	3.9	BDL	BDL	BDL	BDL	BDL	BDL	BDL	BDL	0.19	BDL	BDL	BDL	BDL	2.7	BDL	BDL	BDL	BDL	BDL
Field blank 18	3.1	BDL	BDL	BDL	BDL	BDL	BDL	BDL	BDL	BDL	BDL	BDL	BDL	BDL	BDL	BDL	BDL	BDL	BDL	BDL
Field blank 19	BDL	BDL	BDL	BDL	BDL	BDL	BDL	BDL	BDL	BDL	BDL	BDL	BDL	BDL	BDL	BDL	BDL	BDL	BDL	BDL
Field blank 20	5.9	BDL	BDL	BDL	BDL	BDL	BDL	BDL	BDL	BDL	BDL	BDL	BDL	BDL	BDL	BDL	BDL	BDL	BDL	BDL
Field blank 21	6.4	1.3	BDL	BDL	BDL	BDL	BDL	BDL	BDL	BDL	BDL	BDL	BDL	BDL	BDL	BDL	BDL	BDL	BDL	BDL
Field blank 22	4.1	BDL	BDL	BDL	BDL	BDL	BDL	BDL	BDL	BDL	BDL	BDL	BDL	BDL	BDL	BDL	BDL	BDL	BDL	BDL
Field blank 23	4.8	BDL	BDL	BDL	BDL	BDL	BDL	BDL	BDL	BDL	BDL	BDL	BDL	BDL	BDL	BDL	BDL	BDL	BDL	BDL
Field blank 24	5.2	BDL	BDL	BDL	BDL	BDL	BDL	BDL	BDL	BDL	BDL	BDL	BDL							

Table C.1. Concentrations of analytes in field blanks. Trace element concentrations for field blanks 1-6 and 24 are not included because of incorrect trace sampling collection methods.

			μM												
Sample ID	Location	Collection Date	Ca	Mg	Na	K	Si	HCO_3	Cl	SO_4	F	Br	NO_3+NO_2 (as N)	PO_4 (as P)	NH_4 (as N)
DT1	Downtown	2/28/2021	1030	531	1170	108	85	2011	1441	359	11	0.14*	228	3.0	8.0
GR2	Griggs Reservoir	2/28/2021	936	412	1006	95	75	1803	1209	292	8	0.14*	200	3.2	8.6
BP3	Bellepoint	2/28/2021	972	391	444	113	94	1891	655	247	9	0.14*	242	4.3	6.2
DT4	Downtown	3/6/2021	926	352	620	109	96	1839	814	213	9	0.14*	205	3.2	4.3
GR5	Griggs Reservoir	3/6/2021	1030	450	702	119	104	2063	903	290	11	0.14*	236	3.8	4.2
BP6	Bellepoint	3/6/2021	1372	784	663	90	115	2936	837	529	12	0.14*	233	1.8	1.4
PT7	Prospect	3/6/2021	1449	834	729	95	117	2933	891	662	13	0.14*	241	1.9	4.0
DT8	Downtown	3/12/2021	1241	620	2180	98	91	2383	2447	486	11	0.40	198	1.9	2.4
GR9	Griggs Reservoir	3/12/2021	1208	599	1133	104	103	2407	1354	428	12	0.14*	233	2.7	3.4
BP10	Bellepoint	3/12/2021	1811	1280	871	87	72	3892	994	1039	18	0.41	174	1.7	0.64*
DT11	Downtown	3/19/2021	1484	815	1438	95	67	2973	1624	685	14	0.37	164	0.8	0.64*
GR12	Griggs Reservoir	3/19/2021	1455	903	1333	95	68	3077	1505	696	13	0.36	169	1.1	2.5
CV13	Circleville	3/27/2021	1643	1069	1380	92	51	3990	1575	559	17	0.40	211	2.6	0.64*
DT14	Downtown	3/27/2021	1222	635	1180	111	67	2440	1400	476	12	0.14*	212	3.0	2.7
GR15	Griggs Reservoir	3/27/2021	1101	559	723	113	73	2296	866	371	10	0.14*	250	3.7	6.3
BP16	Bellepoint	3/27/2021	1733	1228	781	83	56	3849	925	923	16	0.36	165	1.3	0.64*
DT17	Downtown	4/3/2021	1393	882	1489	103	59	2850	1734	688	14	0.39	179	1.6	0.64*
GR18	Griggs Reservoir	4/3/2021	1424	869	1052	100	62	3044	1221	637	13	0.14*	198	1.9	2.4
BP19	Bellepoint	4/3/2021	1687	1266	965	84	45	3864	1120	911	17	0.34	148	1.0	0.64*
PT20	Prospect	4/3/2021	1815	1320	1027	89	54	4083	1153	996	18	0.42	155	1.3	0.64*
DT21	Downtown	4/9/2021	1151	1166	1957	94	44	2729	2196	813	16	0.48	134	0.4	1.4
GR22	Griggs Reservoir	4/9/2021	1231	1187	1180	91	55	3052	1354	768	15	0.35	164	0.6	8.5
BP23	Bellepoint	4/9/2021	2059	1725	1149	80	6	5199	1236	1140	20	0.54	79	0.5	2.8
CV24	Circleville	4/17/2021	1327	1405	2062	97	53	3628	2198	781	19	0.69	231	2.0	1.3
DT25	Downtown	4/17/2021	1315	1358	1735	93	21	3314	1929	910	17	0.51	111	0.6	0.64*
GR26	Griggs Reservoir	4/17/2021	1298	1388	1343	90	16	3400	1483	904	16	0.45	114	0.5	2.4
BP27	Bellepoint	4/17/2021	1344	1382	1027	102	86	3358	1255	849	17	0.49	269	2.5	5.0
DT28	Downtown	4/25/2021	1244	1341	2024	95	7	3193	2221	907	18	0.67	59	0.3	1.9
GR29	Griggs Reservoir	4/25/2021	1234	1412	1597	94	1	3384	1752	888	18	0.61	70	0.063*	2.9
BP30	Bellepoint	4/25/2021	1525	1726	1389	95	15	4229	1429	1101	23	0.72	123	2.3	0.64*
PT31	Prospect	4/25/2021	1495	1615	1228	89	49	4088	1280	1028	22	0.66	115	2.8	3.8

Table C.2. Concentrations of major cations, anions, and nutrients. All concentrations in μM. * indicates that concentration was below detection limit and set equal to half the detection limit.

DT32	Downtown	5/1/2021	1133	1263	1562	92	10	3132	1766	730	15	0.50	86	0.2	2.2
GR33	Griggs Reservoir	5/1/2021	1488	1679	1646	95	1	4474	1826	841	16	0.58	92	0.063*	3.3
BP34	Bellepoint	5/1/2021	946	815	1159	134	51	1984	1327	675	32	0.14*	153	9.2	18.4
CV35	Circleville	5/8/2021	1002	1030	1629	89	75	2903	1758	447	17	0.40	226	2.0	2.7
DT36	Downtown	5/8/2021	1059	1134	1758	96	25	2777	1892	715	16	0.55	141	0.4	0.64*
GR37	Griggs Reservoir	5/8/2021	1544	1192	1602	99	1	3646	1739	809	18	0.53	169	0.3	0.64*
BP38	Bellepoint	5/8/2021	1586	1118	830	106	103	3430	1156	706	16	0.35	344	3.7	10.6
DT39	Downtown	5/10/2021	1530	895	1119	116	91	3419	1289	569	14	0.40	239	2.8	15.5
GR40	Griggs Reservoir	5/10/2021	1391	840	958	117	94	3102	1167	511	13	0.32	246	3.1	14.1
BP41	Bellepoint	5/10/2021	847	402	498	131	79	1600	670	188	8	0.14*	480	5.6	27.3
DT42	Downtown	5/12/2021	797	384	366	131	86	1558	514	173	8	0.14*	442	5.5	18.9
GR43	Griggs Reservoir	5/12/2021	782	369	291	133	87	1510	442	151	8	0.14*	470	5.8	19.4
BP44	Bellepoint	5/12/2021	863	406	318	137	96	1647	484	167	9	0.14*	527	6.3	19.3
DT45	Downtown	5/14/2021	924	455	404	135	102	1773	557	234	10	0.14*	497	5.2	15.3
GR46	Griggs Reservoir	5/14/2021	1431	435	307	138	104	2748	457	208	9	0.14*	553	5.8	17.9
BP47	Bellepoint	5/14/2021	1338	637	394	132	124	2401	535	444	12	0.14*	650	4.4	13.5
DT48	Downtown	5/30/2021	1602	908	1420	117	61	3449	1436	720	16	0.49	231	0.8	0.64*
GR49	Griggs Reservoir	5/30/2021	1564	887	973	117	75	3363	990	659	15	0.39	320	1.2	0.64*
BP50	Bellepoint	5/30/2021	1802	1347	1185	109	59	4224	1046	1095	24	0.83	130	3.2	0.64*
DT51	Downtown	6/11/2021	1582	903	1079	117	64	3415	1078	651	16	0.46	372	1.9	1.4
GR52	Griggs Reservoir	6/11/2021	1680	957	928	119	82	3498	952	667	17	0.41	537	2.2	2.1
BP53	Bellepoint	6/11/2021	917	462	356	127	98	1913	390	230	12	0.14*	476	5.8	5.6
PT54	Prospect	6/11/2021	732	294	319	113	89	1590	296	138	8	0.14*	324	5.5	1.4
CV55	Circleville	6/19/2021	1531	922	1795	133	105	3476	1618	699	20	0.67	339	7.8	1.9
DT56	Downtown	6/19/2021	1007	694	1095	119	86	2279	1110	458	14	0.38	312	3.1	4.5
GR57	Griggs Reservoir	6/19/2021	855	608	643	124	111	1981	646	329	13	0.14*	407	5.0	6.7
BP58	Bellepoint	6/19/2021	1303	869	906	107	136	2978	823	644	18	0.55	268	4.1	8.4
DT59	Downtown	6/25/2021	1171	779	1547	120	85	2492	1567	631	17	0.50	245	2.0	1.5
GR60	Griggs Reservoir	6/25/2021	988	690	858	117	115	2266	853	440	14	0.35	330	3.0	2.8
BP61	Bellepoint	6/25/2021	1943	1186	1343	111	102	4110	1164	1151	25	0.79	136	4.2	0.64*
DT62	Downtown	7/2/2021	900	684	1357	103	91	2076	1283	543	15	0.44	181	1.7	4.4
GR63	Griggs Reservoir	7/2/2021	999	747	975	113	111	2370	950	512	15	0.41	236	2.2	11.4
BP64	Bellepoint	7/2/2021	1534	1162	1739	136	104	3240	1421	1208	28	1.6	190	6.2	4.5
DT65	Downtown	7/9/2021	1136	1100	1492	103	78	3037	1597	660	18	0.60	111	0.5	0.64*

Table C.2 cont. Concentrations of major cations, anions, and nutrients. All concentrations in µM. * indicates that concentration was below detection limit and set equal to half the detection limit.

GR66	Griggs Reservoir	7/9/2021	1089	1177	1139	108	68	3173	1213	623	17	0.52	145	0.3	0.64*
BP67	Bellepoint	7/9/2021	1017	1080	1172	133	95	2583	1130	758	21	0.62	269	3.6	0.64*
PT68	Prospect	7/9/2021	986	927	1058	119	122	2834	976	477	18	0.32	238	8.4	0.64*
DT69	Downtown	7/13/2021	1034	1050	1078	107	69	2971	1128	550	16	0.47	152	1.4	0.64*
GR70	Griggs Reservoir	7/13/2021	1091	1172	1066	107	35	3081	1099	679	18	0.57	161	0.3	0.64*
BP71	Bellepoint	7/13/2021	1031	1016	624	132	136	3028	674	380	16	0.14*	387	4.5	0.64*
DT72	Downtown	7/26/2021	1166	1156	1441	125	102	3100	1526	709	20	0.66	165	1.4	0.64*
GR73	Griggs Reservoir	7/26/2021	1254	1336	1148	122	60	3641	1160	741	20	0.62	167	0.6	9.1
BP74	Bellepoint	7/26/2021	1847	1541	1072	130	161	3850	1033	1373	25	0.71	347	3.9	0.64*
CV75	Circleville	8/2/2021	1354	1292	1888	131	94	3382	1807	940	21	0.90	244	5.7	0.64*
DT76	Downtown	8/2/2021	1137	1119	1452	115	101	2993	1514	726	18	0.58	121	1.4	6.3
GR77	Griggs Reservoir	8/2/2021	1124	1160	1163	118	108	2993	1178	735	18	0.48	208	1.4	21.6
BP78	Bellepoint	8/2/2021	1399	1363	1234	133	126	3440	1118	1007	24	0.89	319	4.4	2.3
PT79	Prospect	8/2/2021	1434	1350	1272	147	151	4032	1119	766	25	0.79	303	7.6	0.64*
CV80	Circleville	8/18/2021	743	535	849	91	87	2078	761	289	9	0.14*	79	2.7	3.1
DT81	Downtown	8/18/2021	1143	1120	1377	112	105	3251	1447	617	17	0.49	82	1.2	6.8
GR82	Griggs Reservoir	8/18/2021	1091	1068	1243	107	121	2898	1261	702	17	0.42	104	1.1	17.3
BP83	Bellepoint	8/18/2021	1421	1435	1902	153	115	3683	1615	1193	30	1.5	80	5.8	4.3
PT84	Prospect	8/18/2021	1382	1333	1662	153	121	3990	1353	902	29	1.8	96	12	5.8
DT85	Downtown	9/1/2021	1331	457	1097	96	94	2573	1056	539	14	0.51	60	1.6	10.9
GR86	Griggs Reservoir	9/1/2021	1558	953	1397	124	116	3234	1355	948	22	0.82	58	0.4	17.3
CV87	Circleville	9/5/2021	1825	909	2066	140	145	3644	1893	936	23	1.1	265	18	2.2
DT88	Downtown	9/5/2021	1593	869	1628	121	119	3391	1641	788	20	0.76	64	1.9	7.4
GR89	Griggs Reservoir	9/5/2021	1614	943	1429	124	115	3401	1377	920	22	0.86	48	0.9	13.9
BP90	Bellepoint	9/5/2021	1761	1138	2297	185	125	6325	1837	1451	35	2.2	119	5.3	11.2
PT91	Prospect	9/5/2021	1817	1159	2405	190	128	4096	1777	1272	41	3.4	128	18	9.7
CV92	Circleville	9/23/2021	1297	623	1395	101	75	2966	1310	484	16	0.50	89	2.8	10.5
DT93	Downtown	9/23/2021	1363	700	1240	113	86	2850	1165	693	17	0.61	77	2.0	11.0
GR94	Griggs Reservoir	9/23/2021	1782	996	1496	131	75	3733	1359	1029	23	1.0	33	1.4	20.2
BP95	Bellepoint	9/23/2021	1701	978	2662	234	91	6097	1908	1628	37	4.1	249	6.1	8.11
PT96	Prospect	9/23/2021	1546	826	3403	292	117	3674	1977	1327	44	3.8	135	58	118.4
CV97	Circleville	10/20/2021	1767	961	2503	172	104	3626	2248	990	26	1.2	275	13	2.3
DT98	Downtown	10/20/2021	1751	996	2225	139	62	3444	2243	1062	26	1.0	44	1.5	5.0
GR99	Griggs Reservoir	10/20/2021	1690	1017	1878	139	83	3447	1693	1126	25	1.3	37	0.4	9.4

Table C.2 cont. Concentrations of major cations, anions, and nutrients. All concentrations in µM. * indicates that concentration was below detection limit and set equal to half the detection limit.

BP100	Bellepoint	10/20/2021	1866	1090	2719	244	90	2918	2052	1873	42	3.5	158	8.5	7.1
PT101	Prospect	10/20/2021	1726	1057	3487	333	137	3905	2291	1426	45	4.8	338	34	104
DT102	Downtown	10/25/2021	1233	565	943	136	71	2575	887	565	14	0.14*	84	2.9	7.4
GR103	Griggs Reservoir	10/25/2021	1584	927	1760	140	76	2921	1598	1182	24	0.87	41	0.9	13.1
DT104	Downtown	10/29/2021	866	428	1326	106	60	1192	1222	769	17	0.14*	68	0.9	0.64*
GR105	Griggs Reservoir	10/29/2021	1019	945	1627	145	60	1819	1423	1188	24	0.84	81	1.2	0.64*
CV106	Circleville	11/11/2021	1187	992	2037	159	118	2435	1898	981	24	0.68	258	10.2	0.64*
DT107	Downtown	11/11/2021	1006	795	1407	150	104	1980	1568	704	18	0.14*	201	2.0	0.64*
GR108	Griggs Reservoir	11/11/2021	946	777	1237	182	124	1820	1288	769	19	0.14*	220	4.3	8.5
BP109	Bellepoint	11/11/2021	1379	1129	1207	151	150	2464	1288	1139	21	0.56	342	3.7	0.64*
PT110	Prospect	11/11/2021	1489	1225	1353	139	155	2765	1385	1233	23	0.78	304	10.5	0.64*
DT111	Downtown	11/26/2021	1054	850	1332	142	125	2101	1486	738	17	0.14*	219	2.6	0.64*
GR112	Griggs Reservoir	11/26/2021	1087	896	1193	167	137	2107	1295	810	18	0.14*	303	4.5	2.3
DT113	Downtown	12/2/2021	1133	926	1339	137	121	2242	1547	787	18	0.42	232	2.4	0.64*
GR114	Griggs Reservoir	12/2/2021	1095	918	1302	160	131	2125	1400	846	19	0.14*	269	4.1	1.5
BP115	Bellepoint	12/2/2021	1466	1344	1458	110	106	3140	1549	1139	21	0.58	221	3.6	0.64*
CV116	Circleville	12/5/2021	1240	1114	2071	149	94	2683	1979	985	24	0.65	295	9.4	0.64*
DT117	Downtown	12/5/2021	1170	964	1439	137	113	2395	1617	805	17	0.14*	220	2.3	0.64*
GR118	Griggs Reservoir	12/5/2021	1165	1001	1303	160	131	2343	1424	881	16	0.43	266	4.2	0.64*
BP119	Bellepoint	12/5/2021	1512	1342	1720	113	72	3239	1639	1221	25	0.69	220	3.5	0.64*
PT120	Prospect	12/5/2021	1589	1365	1553	132	91	3182	1554	1284	25	0.14*	289	9.8	0.64*

Table C.2 cont. Concentrations of major cations, anions, and nutrients. All concentrations in µM. * indicates that concentration was below detection limit and set equal to half the detection limit.

		nM								‰		m^3/s
Sample ID	Collection Date	Li	U	Ni	Cu	Rb	Mo	Ba	Sr	$\delta^{18}O$	δD	Discharge
DT1	2/28/2021	323	4.5	48	41	13	34	226	8721	-12.02	-79.98	362
GR2	2/28/2021	268	3.7	40	38	8.7	28	190	6864	-11.88	-79.36	278
BP3	2/28/2021	183	3.7	48	45	9.2	28	202	5421	-12.32	-82.22	211
DT4	3/6/2021	167	3.3	50	46	13	28	244	4655	-11.74	-78.55	175
GR5	3/6/2021	198	4.1	53	46	10	32	261	6139	-11.28	-75.30	35
BP6	3/6/2021	497	8.3	52	28	6.4	37	286	13134	-10.17	-67.23	24
PT7	3/6/2021	657	11	60	29	6.9	44	309	14104	-10.08	-66.20	21
DT8	3/12/2021	497	6.6	51	43	18	40	332	8974	-9.24	-58.36	33
GR9	3/12/2021	359	6.6	53	38	8.2	37	311	9590	-10.18	-66.58	16
BP10	3/12/2021	1102	15	65	15	6.4	56	384	28965	-8.71	-55.32	10
DT11	3/19/2021	585	9.9	54	25	7.2	45	317	16638	-9.45	-61.03	260
GR12	3/19/2021	665	10.3	53	23	6.6	44	321	16525	-9.44	-61.19	194
CV13	3/27/2021	888	8.0	48	19	11	50	460	18474	-8.65	-54.44	70
DT14	3/27/2021	498	6.7	59	47	13	40	338	10029	-9.77	-62.94	31
GR15	3/27/2021	325	6.2	64	50	12	36	319	9241	-10.16	-66.15	18
BP16	3/27/2021	952	14	60	16	5.5	57	387	26479	-8.67	-54.50	13
DT17	4/3/2021	699	9.0	50	27	8.0	46	335	14598	-9.07	-58.14	17
GR18	4/3/2021	588	10	56	26	7.2	46	358	16023	-9.24	-59.53	11
BP19	4/3/2021	1015	14	64	19	5.5	58	357	26179	-8.17	-50.83	7
PT20	4/3/2021	1145	17	72	17	6.6	61	405	28744	-8.24	-51.72	6
DT21	4/9/2021	598	11	57	32	10	55	408	17950	-8.02	-49.83	19
GR22	4/9/2021	724	11	56	23	5.9	51	358	20146	-8.69	-54.86	10
BP23	4/9/2021	1200	14	64	13	7.3	74	399	34054	-7.90	-49.22	6
CV24	4/17/2021	950	8.7	50	18	13	58	482	20645	-7.88	-49.31	47
DT25	4/17/2021	919	11	53	20	9.0	59	368	21917	-8.13	-51.48	20
GR26	4/17/2021	894	12	55	18	7.0	64	368	25433	-8.15	-51.37	11
BP27	4/17/2021	957	10	88	17	8.5	78	313	21959	-8.12	-50.76	6
DT28	4/25/2021	1044	10	80	15	9.0	82	344	18151	-8.05	-51.55	16
GR29	4/25/2021	943	10	81	15	6.8	88	328	22013	-7.91	-49.70	9
BP30	4/25/2021	1337	12	109	13	7.9	90	336	32040	-8.09	-51.54	5
PT31	4/25/2021	1252	13	92	11	7.0	78	343	31308	-8.11	-51.48	4
DT32	5/1/2021	825	11	79	17	7.7	75	325	17040	-7.89	-49.79	69
GR33	5/1/2021	895	11	87	17	8.0	81	340	22615	-7.75	-48.67	29
BP34	5/1/2021	753	3.8	51	34	13	57	203	13756	-6.85	-43.25	22
CV35	5/8/2021	495	6.6	46	27	11	48	350	12246	-8.60	-54.05	214
DT36	5/8/2021	818	8.4	53	24	8.5	57	293	17030	-8.12	-51.95	80
GR37	5/8/2021	924	9.0	60	21	7.6	60	315	21222	-7.80	-49.66	34
BP38	5/8/2021	769	9.1	60	27	10	49	316	21394	-8.04	-50.29	26
DT39	5/10/2021	619	7.9	63	30	12	49	288	16044	-7.87	-48.08	405
GR40	5/10/2021	549	7.3	61	32	12	45	274	14302	-7.99	-48.68	314
BP41	5/10/2021	151	2.5	44	39	11	19	193	5347	-7.79	-41.59	229
DT42	5/12/2021	128	2.4	53	44	13	22	201	5051	-7.71	-40.98	241
GR43	5/12/2021	117	2.1	48	42	12	21	190	4420	-7.72	-41.01	204
BP44	5/12/2021	119	2.0	50	44	12	22	203	4410	-7.93	-42.88	184
DT45	5/14/2021	183	3.1	50	42	12	26	226	5676	-7.89	-43.75	214
GR46	5/14/2021	164	3.0	54	45	12	26	224	5475	-7.99	-44.21	101
BP47	5/14/2021	366	6.4	61	45	10	39	266	8466	-7.96	-45.77	77
DT48	5/30/2021	783	8.0	78	17	10	59	334	12952	-7.32	-43.77	11
GR49	5/30/2021	644	9.2	86	17	8.7	60	339	16420	-7.47	-44.51	6

Table C.3. Concentrations of trace elements, stable water isotopes, and discharge. Concentrations of trace elements in nM, $\delta^{18}O$ and δD in ‰, and associated discharge value (m^3/s) of samples.

BP50	5/30/2021	1327	13	108	10	8.9	113	397	31842	-7.36	-45.89	5
DT51	6/11/2021	786	7.9	88	19	10	69	330	17817	-6.44	-40.44	75
GR52	6/11/2021	780	7.8	82	20	10	69	325	18362	-6.33	-39.42	26
BP53	6/11/2021	296	2.8	53	25	12	39	218	7561	-6.80	-44.70	63
PT54	6/11/2021	195	1.7	48	25	15	31	181	3975	-6.98	-45.97	58
CV55	6/19/2021	633	5.6	74	18	21	74	418	13149	-6.69	-44.48	36
DT56	6/19/2021	524	5.1	70	22	12	56	319	11046	-6.35	-42.01	16
GR57	6/19/2021	343	3.6	66	24	10	46	271	11130	-6.68	-45.29	6
BP58	6/19/2021	729	9.0	105	15	8.7	78	348	20962	-6.63	-45.15	5
DT59	6/25/2021	727	6.1	81	21	13	69	370	13561	-6.33	-42.23	7
GR60	6/25/2021	432	5.1	71	19	9.0	53	302	14211	-6.56	-44.28	3
BP61	6/25/2021	1285	13	136	14	10	167	391	33549	-6.18	-41.67	3
DT62	7/2/2021	552	5.4	63	19	12	62	308	13105	-6.19	-40.08	25
GR63	7/2/2021	532	6.2	75	18	10	60	332	16854	-6.34	-41.70	8
BP64	7/2/2021	1394	11	145	14	15	240	398	34373	-5.97	-39.02	9
DT65	7/9/2021	726	6.0	76	19	14	69	344	17760	-6.21	-40.65	22
GR66	7/9/2021	614	6.8	64	16	9.0	67	292	17199	-6.25	-40.93	12
BP67	7/9/2021	870	6.4	93	19	16	208	298	20645	-5.12	-32.74	16
PT68	7/9/2021	646	4.5	73	19	13	59	262	15892	-5.73	-34.46	9
DT69	7/13/2021	571	6.4	69	17	10	68	301	12766	-6.31	-41.41	54
GR70	7/13/2021	684	7.6	78	15	10	73	310	19567	-6.34	-42.05	19
BP71	7/13/2021	478	4.3	71	21	13	54	257	14360	-6.00	-37.89	14
DT72	7/26/2021	803	6.8	80	17	12	76	383	16783	-5.91	-38.29	8
GR73	7/26/2021	791	7.6	88	16	10	83	315	20180	-5.77	-37.56	4
BP74	7/26/2021	1296	14	141	20	11	101	407	29224	-6.33	-41.07	3
CV75	8/2/2021	934	5.5	83	16	22	86	397	15021	-5.34	-33.26	35
DT76	8/2/2021	800	6.2	79	18	13	72	347	14998	-5.76	-37.01	11
GR77	8/2/2021	760	6.6	99	17	12	70	326	21678	-5.55	-34.89	4
BP78	8/2/2021	1154	8.5	122	19	15	105	317	25084	-4.97	-29.66	2
PT79	8/2/2021	1032	8.3	123	17	16	78	345	28857	-5.68	-35.60	1
CV80	8/18/2021	359	2.4	51	23	17	57	258	3366	-6.35	-39.04	158
DT81	8/18/2021	727	5.7	65	20	14	69	326	12196	-5.47	-34.96	16
GR82	8/18/2021	701	6.0	89	14	12	62	315	20665	-5.28	-33.13	3
BP83	8/18/2021	1415	8.5	165	13	15	177	352	32838	-5.24	-33.25	2
PT84	8/18/2021	1231	7.0	133	14	13	90	325	31642	-5.57	-34.05	1
DT85	9/1/2021	469	4.0	56	15	12	57	246	10572	-5.62	-35.04	35
GR86	9/1/2021	857	7.1	97	12	12	76	318	23996	-5.20	-33.27	3
CV87	9/5/2021	1045	5.3	84	15	24	79	402	13749	-5.99	-38.62	30
DT88	9/5/2021	820	6.1	70	13	14	77	335	14807	-4.94	-31.73	14
GR89	9/5/2021	806	6.5	86	10	11	74	305	22944	-5.06	-32.34	3
BP90	9/5/2021	1468	7.5	155	11	16	208	321	33229	-4.86	-31.79	1
PT91	9/5/2021	1577	6.7	132	12	16	114	342	43165	-5.61	-37.28	1
CV92	9/23/2021	548	3.3	59	16	16	56	280	11064	-7.36	-47.35	164
DT93	9/23/2021	609	4.8	69	23	14	73	282	12677	-7.22	-47.79	55
GR94	9/23/2021	912	6.6	92	12	10	90	363	23604	-5.59	-36.81	3
BP95	9/23/2021	1582	7.1	283	18	27	438	292	27800	-6.54	-44.91	16
PT96	9/23/2021		3.7	217	18	45	177	276	41127	-7.37	-49.09	6
CV97	10/20/2021	1088	4.3	82	18	30	88	371	15382	-6.28	-41.27	16
DT98	10/20/2021	1072	6.5	94	16	16	92	391	22699	-5.94	-39.86	4
GR99	10/20/2021	948	6.8	105	12	10	103	355	27109	-5.74	-39.01	3
BP100	10/20/2021	1547	8.2	233	18	21	271	360	47345	-6.38	-43.42	1
PT101	10/20/2021		5.8	267	23	49	156	317	46844	-7.11	-48.29	1

Table C.3 cont. Concentrations of trace elements, stable water isotopes, and discharge. Concentrations of trace elements in nM, $\delta^{18}O$ and δD in ‰, and associated discharge value (m^3/s) of samples.

DT102	10/25/2021		4.2	77	23	20	76	256	11687	-5.27	-28.74	67
GR103	10/25/2021	987	6.9	119	14	11	101	369	29695	-5.57	-37.26	10
DT104	10/29/2021	429	6.0	91	19	12	83	295	17728	-6.57	-42.42	60
GR105	10/29/2021	918	7.9	128	15	11	112	354	26729	-5.60	-36.81	23
CV106	11/11/2021	1005	6.7	60	13	26	91	438	17729	-6.22	-39.97	27
DT107	11/11/2021	739	6.7	57	20	14	79	383	14878	-6.49	-40.95	11
GR108	11/11/2021	658	5.9	74	25	16	81	387	20221	-6.47	-39.27	3
BP109	11/11/2021	859	12	95	22	14	91	392	28365	-7.17	-45.61	2
PT110	11/11/2021	1024	13	82	18	15	89	386	33846	-7.18	-45.79	1
DT111	11/26/2021	676	7.1	57	22	12	67	349	15269	-7.23	-45.02	16
GR112	11/26/2021	675	7.6	69	24	13	75	331	20051	-7.29	-45.38	7
DT113	12/2/2021	732	8.0	55	19	12	66	363	16888	-7.37	-46.65	12
GR114	12/2/2021	628	7.7	72	23	13	76	385	21045	-7.23	-45.30	5
BP115	12/2/2021	1185	13	72	15	13	83	352	30409	-7.20	-46.03	4
CV116	12/5/2021	1123	7.1	55	13	25	80	434	19158	-6.88	-44.67	30
DT117	12/5/2021	745	8.0	56	18	13	66	365	16478	-7.28	-46.71	10
GR118	12/5/2021	723	8.4	75	24	13	76	362	23494	-7.28	-46.19	5
BP119	12/5/2021	1189	13	83	15	15	101	372	34120	-7.23	-46.77	3
PT120	12/5/2021	1197	14	91	14	17	86	371	32966	-7.24	-45.48	2

Table C.3 cont. Concentrations of trace elements, stable water isotopes, and discharge. Concentrations of trace elements in nM, $\delta^{18}O$ and δD in ‰, and associated discharge value (m^3/s) of samples.

APPENDIX D: CORRELATION STATISTICS

	Ca	Mg	Na	K	Si	HCO_3	Cl	SO_4	F	Br	NO_3+NO_2 (as N)	PO_4 (as P)	NH_4 (as N)	Li	U	Ni	Cu	Rb	Mo	Ba	Sr
Ca																					
Mg	0.52																				
Na	0.41	0.45																			
K	0.02	-0.16	0.23																		
Si	-0.04	-0.20	-0.05	0.64																	
HCO3	0.84	0.74	0.41	-0.13	-0.17																
Cl	0.36	0.42	0.95	0.12	-0.14	0.35															
SO4	0.67	0.74	0.66	0.21	0.02	0.61	0.57														
F	0.55	0.64	0.68	0.44	0.19	0.58	0.54	0.86													
Br	0.54	0.54	0.77	0.41	0.17	0.59	0.59	0.82	0.89												
NO_3+NO_2 (as N)	-0.21	-0.30	-0.44	0.32	0.42	-0.31	-0.40	-0.36	-0.29	-0.40											
PO_4 (as P)	-0.04	-0.24	-0.06	0.64	0.61	-0.15	-0.14	-0.03	0.18	0.09	0.59										
NH_4 (as N)	-0.12	-0.40	-0.14	0.18	0.13	-0.14	-0.17	-0.29	-0.16	-0.08	-0.07	0.14									
Li	0.72	0.83	0.63	0.14	-0.07	0.76	0.53	0.92	0.87	0.81	-0.35	-0.01	-0.32								
U	0.58	0.75	0.24	-0.34	-0.28	0.56	0.28	0.64	0.35	0.23	-0.20	-0.35	-0.52	0.66							
Ni	0.51	0.50	0.42	0.40	0.23	0.55	0.23	0.69	0.76	0.77	-0.21	0.08	-0.01	0.68	0.30						
Cu	-0.53	-0.64	-0.53	-0.07	0.05	-0.62	-0.38	-0.72	-0.74	-0.75	0.51	0.16	0.21	-0.77	-0.40	-0.65					
Rb	-0.05	-0.14	0.39	0.70	0.52	-0.13	0.29	0.13	0.39	0.41	0.15	0.62	0.08	0.11	-0.44	0.24	-0.07				
Mo	0.48	0.60	0.65	0.44	0.17	0.51	0.49	0.84	0.90	0.92	-0.33	0.10	-0.16	0.82	0.35	0.86	-0.74	0.38			
Ba	0.51	0.60	0.55	0.05	-0.04	0.43	0.53	0.70	0.57	0.47	-0.16	-0.09	-0.51	0.66	0.62	0.33	-0.50	0.07	0.51		
Sr	0.64	0.79	0.50	0.14	0.01	0.67	0.40	0.90	0.80	0.70	-0.31	-0.05	-0.22	0.88	0.70	0.72	-0.70	0.00	0.78	0.58	
Discharge	-0.42	-0.55	-0.31	-0.31	-0.33	-0.43	-0.18	-0.68	-0.69	-0.58	0.17	-0.07	0.13	-0.63	-0.42	-0.72	0.58	-0.11	-0.67	-0.46	-0.75

Table D.1. Spearman's correlation coefficients for entire dataset. Shaded gray boxes indicate statistically insignificant relationships ($p>0.05$).

	Ca	Mg	Na	K	Si	HCO_3	Cl	SO_4	F	Br	NO_3+NO_2 (as N)	PO_4 (as P)	NH_4 (as N)	Li	U	Ni	Cu	Rb	Mo	Ba	Sr
Ca																					
Mg	0.24																				
Na	0.51	0.14																			
K	0.22	-0.18	0.88																		
Si	-0.05	-0.08	0.46	0.67																	
HCO3	0.60	0.56	0.34	0.09	-0.12																
Cl	0.71	0.17	0.94	0.73	0.30	0.35															
SO4	0.79	0.21	0.85	0.58	0.17	0.34	0.97														
F	0.51	0.17	0.99	0.89	0.46	0.43	0.91	0.81													
Br	0.42	-0.05	0.98	0.90	0.36	0.24	0.90	0.81	1.00												
NO_3+NO_2 (as N)	-0.15	-0.31	-0.13	0.11	0.36	-0.59	-0.10	-0.02	-0.13	-0.01											
PO_4 (as P)	0.24	-0.18	0.91	0.94	0.54	0.02	0.81	0.66	0.87	0.87	-0.01										
NH_4 (as N)	0.14	-0.44	0.54	0.60	0.16	0.21	0.44	0.35	0.55	0.72	-0.24	0.60									
Li	0.71	0.67	0.75	0.30	-0.10	0.87	0.79	0.76	0.77	0.71	-0.72	0.37	0.31								
U	0.40	0.74	-0.17	-0.49	-0.21	0.31	0.01	0.15	-0.17	-0.52	-0.14	-0.48	-0.60	0.34							
Ni	0.39	0.22	0.94	0.83	0.39	0.50	0.83	0.72	0.96	0.96	-0.24	0.80	0.62	0.79	-0.22						
Cu	-0.41	-0.76	-0.34	-0.01	0.21	-0.77	-0.36	-0.33	-0.36	-0.18	0.71	-0.10	0.06	-0.95	-0.42	-0.40					
Rb	0.25	-0.08	0.77	0.84	0.49	-0.05	0.70	0.66	0.77	0.88	0.39	0.80	0.33	0.16	-0.37	0.68	0.04				
Mo	0.56	0.13	0.97	0.81	0.37	0.38	0.96	0.87	0.95	0.95	-0.22	0.87	0.58	0.81	-0.11	0.91	-0.39	0.68			
Ba	0.52	0.77	0.10	-0.18	0.06	0.43	0.24	0.34	0.12	-0.07	-0.07	-0.20	-0.54	0.42	0.89	0.04	-0.54	-0.08	0.15		
Sr	0.66	0.18	0.95	0.78	0.44	0.36	0.98	0.92	0.92	0.93	-0.06	0.83	0.46	0.75	-0.02	0.84	-0.36	0.71	0.96	0.26	
Discharge	-0.53	-0.47	-0.73	-0.61	-0.62	-0.50	-0.70	-0.62	-0.74	-0.68	0.01	-0.55	-0.18	-0.67	-0.21	-0.67	0.47	-0.48	-0.70	-0.52	-0.81

Table D.2. Spearman's correlation coefficients for samples collected at Prospect. Shaded gray boxes indicate statistically insignificant relationships ($p>0.05$).

	Ca	Mg	Na	K	Si	HCO_3	Cl	SO_4	F	Br	NO_3+NO_2 (as N)	PO_4 (as P)	NH_4 (as N)	Li	U	Ni	Cu	Rb	Mo	Ba	Sr
Ca																					
Mg	0.64																				
Na	0.54	0.52																			
K	-0.22	-0.32	0.39																		
Si	-0.18	-0.17	-0.01	0.43																	
HCO3	0.82	0.73	0.52	-0.27	-0.20																
Cl	0.49	0.50	0.93	0.31	-0.15	0.48															
SO4	0.79	0.74	0.87	0.06	-0.03	0.61	0.79														
F	0.54	0.46	0.92	0.46	0.02	0.51	0.84	0.83													
Br	0.52	0.40	0.91	0.41	0.16	0.53	0.71	0.82	0.86												
NO_3+NO_2 (as N)	-0.61	-0.54	-0.60	0.21	0.47	-0.64	-0.60	-0.59	-0.56	-0.49											
PO_4 (as P)	-0.36	-0.51	0.13	0.85	0.34	-0.42	0.07	-0.18	0.26	0.17	0.28										
NH_4 (as N)	-0.41	-0.59	-0.22	0.42	0.11	-0.37	-0.14	-0.50	-0.13	-0.17	0.29	0.66									
Li	0.78	0.68	0.90	0.19	-0.11	0.77	0.82	0.93	0.87	0.91	-0.67	-0.03	-0.28								
U	0.76	0.78	0.31	-0.58	-0.23	0.67	0.29	0.69	0.26	0.17	-0.49	-0.72	-0.73	0.50							
Ni	0.56	0.51	0.84	0.42	0.28	0.58	0.67	0.79	0.83	0.94	-0.37	0.17	-0.18	0.86	0.29						
Cu	-0.68	-0.73	-0.70	0.15	0.22	-0.77	-0.61	-0.73	-0.62	-0.65	0.78	0.29	0.45	-0.81	-0.62	-0.65					
Rb	-0.09	-0.14	0.58	0.88	0.37	-0.14	0.50	0.28	0.58	0.56	0.12	0.70	0.19	0.34	-0.41	0.51	-0.06				
Mo	0.54	0.48	0.92	0.43	0.10	0.53	0.78	0.82	0.90	0.95	-0.47	0.15	-0.23	0.87	0.29	0.93	-0.67	0.60			
Ba	0.81	0.73	0.50	-0.23	-0.04	0.60	0.40	0.85	0.49	0.44	-0.51	-0.43	-0.61	0.65	0.88	0.54	-0.68	-0.09	0.55		
Sr	0.81	0.71	0.83	0.04	-0.13	0.67	0.77	0.96	0.76	0.75	-0.70	-0.16	-0.43	0.90	0.66	0.73	-0.85	0.24	0.76	0.82	
Discharge	-0.58	-0.69	-0.77	-0.17	-0.22	-0.51	-0.65	-0.84	-0.72	-0.70	0.51	0.10	0.40	-0.73	-0.51	-0.78	0.70	-0.30	-0.74	-0.68	-0.79

Table D.3. Spearman's correlation coefficients for samples collected at Bellepoint. Shaded gray boxes indicate statistically insignificant relationships ($p>0.05$).

	Ca	Mg	Na	K	Si	HCO_3	Cl	SO_4	F	Br	NO_3+NO_2 (as N)	PO_4 (as P)	NH_4 (as N)	Li	U	Ni	Cu	Rb	Mo	Ba	Sr
Ca																					
Mg	0.42																				
Na	0.47	0.67																			
K	-0.07	-0.29	0.03																		
Si	-0.28	-0.48	-0.22	0.65																	
HCO3	0.82	0.72	0.45	-0.34	-0.50																
Cl	0.47	0.62	0.95	-0.12	-0.28	0.43															
SO4	0.49	0.66	0.92	0.23	-0.10	0.43	0.82														
F	0.38	0.61	0.76	0.40	0.02	0.41	0.57	0.88													
Br	0.56	0.72	0.73	0.02	-0.33	0.67	0.56	0.75	0.77												
NO_3+NO_2 (as N)	-0.42	-0.61	-0.81	0.20	0.40	-0.50	-0.70	-0.71	-0.64	-0.79											
PO_4 (as P)	-0.49	-0.81	-0.63	0.51	0.64	-0.75	-0.58	-0.53	-0.49	-0.77	0.78										
NH_4 (as N)	0.08	-0.23	-0.09	0.16	0.29	-0.02	-0.21	-0.09	-0.02	0.06	-0.15	0.17									
Li	0.60	0.81	0.88	0.01	-0.34	0.64	0.78	0.91	0.83	0.86	-0.74	-0.72	-0.08								
U	0.47	0.69	0.52	-0.37	-0.55	0.54	0.64	0.53	0.28	0.34	-0.31	-0.58	-0.56	0.59							
Ni	0.36	0.49	0.55	0.37	0.07	0.37	0.32	0.69	0.82	0.76	-0.51	-0.42	0.13	0.71	0.16						
Cu	-0.44	-0.67	-0.69	-0.06	0.14	-0.56	-0.49	-0.75	-0.83	-0.90	0.76	0.73	-0.07	-0.79	-0.27	-0.82					
Rb	-0.25	-0.32	-0.11	0.82	0.74	-0.45	-0.24	0.06	0.20	-0.15	0.26	0.57	0.32	-0.16	-0.49	0.26	0.09				
Mo	0.33	0.63	0.77	0.38	-0.04	0.38	0.61	0.88	0.93	0.75	-0.61	-0.47	-0.10	0.83	0.37	0.84	-0.77	0.17			
Ba	0.32	0.41	0.60	0.18	-0.05	0.19	0.59	0.71	0.53	0.28	-0.33	-0.19	-0.21	0.57	0.57	0.43	-0.33	0.02	0.63		
Sr	0.46	0.73	0.91	0.19	-0.10	0.46	0.78	0.97	0.87	0.81	-0.73	-0.58	-0.03	0.93	0.48	0.74	-0.80	0.07	0.88	0.67	
Discharge	-0.08	-0.26	-0.32	-0.36	-0.46	-0.12	-0.14	-0.47	-0.58	-0.34	0.26	0.10	-0.19	-0.34	0.09	-0.60	0.54	-0.29	-0.56	-0.41	-0.49

Table D.4. Spearman's correlation coefficients for samples collected at Griggs Reservoir. Shaded gray boxes indicate statistically insignificant relationships ($p>0.05$).

	Ca	Mg	Na	K	Si	HCO_3	Cl	SO_4	F	Br	NO_3+NO_2 (as N)	PO_4 (as P)	NH_4 (as N)	Li	U	Ni	Cu	Rb	Mo	Ba	Sr
Ca																					
Mg	0.31																				
Na	0.39	0.65																			
K	-0.07	-0.25	-0.33																		
Si	-0.23	-0.30	-0.32	0.63																	
HCO3	0.78	0.70	0.45	-0.19	-0.33																
Cl	0.37	0.65	0.96	-0.31	-0.30	0.39															
SO4	0.36	0.70	0.70	-0.02	-0.22	0.45	0.68														
F	0.23	0.61	0.55	0.25	0.12	0.43	0.47	0.78													
Br	0.49	0.63	0.61	-0.26	-0.21	0.71	0.45	0.48	0.62												
NO_3+NO_2 (as N)	-0.28	-0.34	-0.46	0.40	0.28	-0.38	-0.38	-0.48	-0.46	-0.58											
PO_4 (as P)	-0.27	-0.73	-0.69	0.63	0.56	-0.57	-0.61	-0.61	-0.46	-0.63	0.62										
NH_4 (as N)	0.01	-0.44	-0.38	0.12	0.23	-0.07	-0.44	-0.49	-0.39	-0.01	0.00	0.49									
Li	0.50	0.82	0.68	0.05	-0.20	0.72	0.64	0.78	0.75	0.67	-0.38	-0.56	-0.34								
U	0.41	0.73	0.63	-0.32	-0.44	0.48	0.72	0.68	0.31	0.23	-0.09	-0.60	-0.65	0.63							
Ni	0.27	0.32	0.19	0.16	-0.21	0.48	0.03	0.37	0.58	0.48	-0.33	-0.35	-0.07	0.49	0.07						
Cu	-0.26	-0.47	-0.32	-0.08	-0.01	-0.46	-0.23	-0.60	-0.72	-0.62	0.49	0.49	0.23	-0.63	-0.22	-0.63					
Rb	-0.05	-0.39	-0.11	0.52	0.53	-0.22	-0.14	-0.22	0.14	-0.08	-0.10	0.46	0.38	-0.16	-0.61	0.04	0.07				
Mo	0.19	0.41	0.34	0.22	-0.04	0.38	0.24	0.62	0.82	0.49	-0.58	-0.41	-0.20	0.68	0.13	0.80	-0.76	0.19			
Ba	0.29	0.61	0.68	0.17	0.00	0.32	0.68	0.69	0.71	0.35	-0.13	-0.36	-0.55	0.64	0.59	0.34	-0.38	0.01	0.43		
Sr	0.30	0.74	0.62	-0.19	-0.41	0.51	0.62	0.84	0.67	0.47	-0.37	-0.68	-0.54	0.72	0.72	0.45	-0.50	-0.37	0.55	0.62	
Discharge	-0.21	-0.41	-0.51	-0.39	-0.24	-0.22	-0.43	-0.56	-0.74	-0.39	0.16	0.20	0.36	-0.58	-0.25	-0.41	0.55	-0.20	-0.52	-0.83	-0.31

Table D.5. Spearman's correlation coefficients for samples collected in downtown Columbus. Shaded gray boxes indicate statistically insignificant relationships ($p>0.05$).

	Ca	Mg	Na	K	Si	HCO_3	Cl	SO_4	F	Br	NO_3+NO_2 (as N)	PO_4 (as P)	NH_4 (as N)	Li	U	Ni	Cu	Rb	Mo	Ba	Sr
Ca																					
Mg	0.05																				
Na	0.42	0.34																			
K	0.42	-0.01	0.79																		
Si	0.26	-0.34	0.53	0.75																	
HCO3	0.88	0.25	0.21	0.04	-0.14																
Cl	0.30	0.54	0.94	0.65	0.32	0.21															
SO4	0.42	0.39	0.89	0.90	0.54	0.14	0.85														
F	0.41	0.29	0.90	0.91	0.68	0.11	0.84	0.96													
Br	0.69	0.23	0.81	0.74	0.57	0.46	0.75	0.79	0.77												
NO_3+NO_2 (as N)	0.45	0.19	0.76	0.77	0.69	0.16	0.63	0.75	0.83	0.62											
PO_4 (as P)	0.46	-0.31	0.64	0.90	0.89	0.02	0.41	0.71	0.78	0.65	0.68										
NH_4 (as N)	-0.19	-0.73	-0.31	-0.34	-0.10	-0.18	-0.40	-0.56	-0.50	-0.28	-0.41	-0.15									
Li	0.47	0.38	0.92	0.83	0.47	0.26	0.85	0.94	0.90	0.74	0.70	0.68	-0.54								
U	0.02	0.81	0.20	-0.05	-0.32	0.28	0.40	0.22	0.19	0.00	0.21	-0.32	-0.73	0.32							
Ni	0.56	-0.25	0.50	0.72	0.81	0.16	0.27	0.57	0.59	0.77	0.55	0.84	-0.08	0.46	-0.45						
Cu	-0.17	-0.19	-0.64	-0.75	-0.54	0.09	-0.51	-0.74	-0.67	-0.55	-0.49	-0.67	0.48	-0.76	-0.12	-0.57					
Rb	0.19	-0.13	0.73	0.92	0.83	-0.24	0.58	0.82	0.85	0.65	0.67	0.90	-0.20	0.71	-0.26	0.74	-0.68				
Mo	0.24	0.14	0.72	0.89	0.74	-0.13	0.65	0.88	0.87	0.75	0.65	0.78	-0.46	0.74	-0.05	0.73	-0.72	0.93			
Ba	0.30	0.66	0.34	0.24	-0.05	0.45	0.47	0.41	0.37	0.28	0.36	-0.01	-0.80	0.51	0.89	-0.12	-0.32	-0.03	0.22		
Sr	0.28	0.79	0.57	0.37	-0.11	0.37	0.72	0.65	0.55	0.41	0.38	0.06	-0.79	0.73	0.82	-0.09	-0.44	0.16	0.37	0.88	
Discharge	-0.45	-0.15	-0.82	-0.93	-0.73	-0.11	-0.74	-0.93	-0.95	-0.79	-0.75	-0.84	0.49	-0.87	-0.07	-0.68	0.68	-0.90	-0.93	-0.36	-0.51

Table D.6. Spearman's correlation coefficients for samples collected at Circleville. Shaded gray boxes indicate statistically insignificant relationships ($p>0.05$).

APPENDIX E: AUXILIARY EXISTING DATA

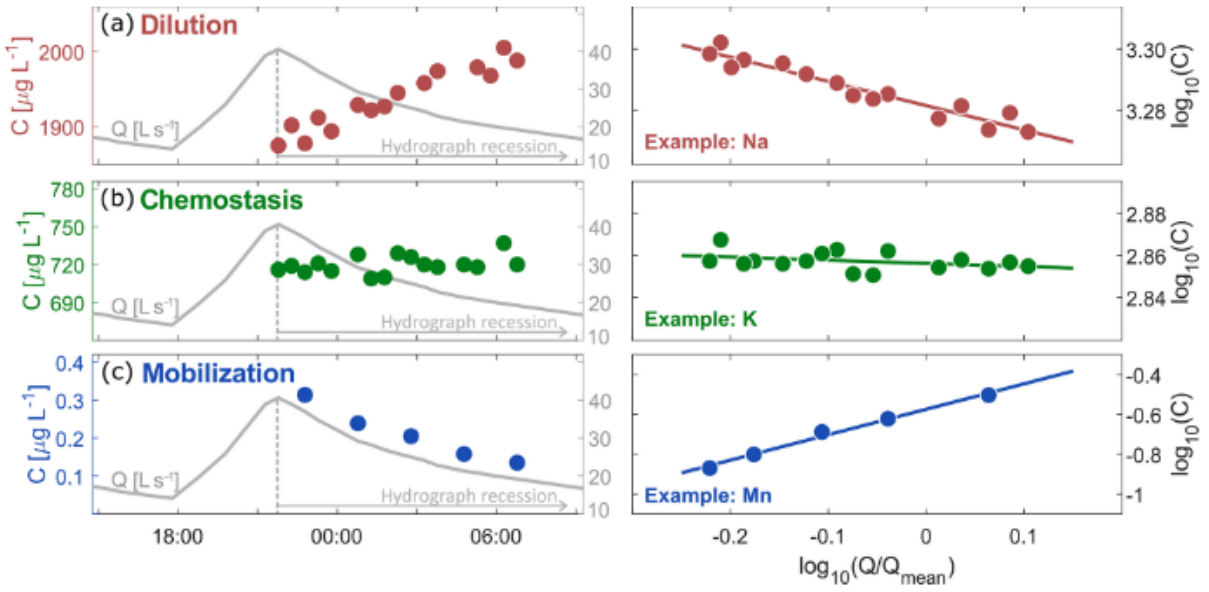

Figure E.1. Concentration-discharge (C – Q) relationships from Knapp et al. (2020). Left panels show analyte concentrations over time plotted with hydrograph representing a high flow event. Right panels show log C – log Q relationships relative to corresponding behavior in left panel.